STUDIES OF ELECTRICAL RESISTIVITY

IN THIN METALLIC FILMS AT LOW TEMPERATURES

A Thesis Submitted by

DAVID GODFREY VINCENT

for the Degree of

Doctor of Philosophy

of the

University of London.

Imperial College of Science and Technology,
London.

July 1966.

ABSTRACT

The work described in this Thesis is centred on the measurement of the electrical resistivity of epitaxial thin films of silver. The epitaxial (single crystal) films are obtained by evaporation on to a hot substrate, and have a better crystal structure than films evaporated on to a cold substrate, i.e. they have fewer dislocations. The dislocations cannot be ignored, however, as they appear to provide the main contribution to the bulk residual resistivity of the films.

The films range in thickness from ~ 500 to ~ 60,000Å. The resistance measurements were made over the temperature range 4.2°K to room temperature. As the surfaces play an important part in size effect resistivity, the surfaces of some specimens were modified by the addition of thin layers of aluminium or extra silver.

The resistivity results are analysed in terms of Fuchs' free electron theory of thin film resistivity. Two important parameters of the theory are the bulk resistivity and the fraction of electrons specularly scattered at the film surface. The bulk resistivity at 4.2°K is estimated to lie in the range 0.01 to 0.02 $\mu\,\Omega$ cm. The surface specularity, estimated from both high and low temperature results, is found to be greater than 0.5 for most of the thicker films.

It is shown that the bulk resistivity at higher temperatures cannot be obtained simply by adding the residual resistivity to the ideal lattice resistivity, as the dislocations contribute a temperature dependent term. A method for estimating the dislocation contribution is described. The experimental results are compared with Fuchs' theory

over the whole temperature range, and good agreement is obtained down to quite low temperature.

The final chapter is devoted to an extension of the theory, by a numerical method, to allow for low angle scattering, as this type of scattering is expected from phonons at low temperatures.

Acknowledgements

I wish to thank the following:

Dr. J.G. Park, for suggesting the subject of this research and for his advice and encouragement during the course of the investigation.

Dr. B.R. Coles and members of Metal Physics group, for providing a congenial atmosphere in which to work.

Professor M. Blackman, Dr. N.D. Lisgarten and Dr. A.E. Curzon of Electron Diffraction group, for the use of some of their apparatus and for advice on the preparation and examination of the films.

Mr. C. Gonzales of Electron Diffraction group, for making and examining the replicas, and for the use of the photographs obtained.

Standard Telecommunication Laboratories Ltd., Harlow, Essex, for their help in making the masks.

The D.S.I.R. (later S.R.C.) and the U.K.A.E.A. for financial support.

My wife, for her willing acceptance of many inconveniences.

CONTENTS

Introduction

It was recognized early in this century that the electrical resistivity of a metal can depend on the size of the specimen measured, if it is sufficiently small. In this context sufficiently small means that at least one dimension of the specimen must be comparable with the mean free path of the current carrying electrons.

The theory of the size dependent resistivity of thin films of a free electron metal was developed by Fuchs in 1938. He used a simple model of surface scattering of electrons which covers the range from fully diffuse to fully specular scattering. This theory remains the basis for the interpretation of experimental results, as any extension is both difficult, and not clearly demanded by the experimental results available.

Experimental observation of resistivity size effects requires thin films or long electronic mean free paths. The thin films are usually prepared by evaporation or sputtering and long mean free paths are obtained by lowering the temperature of measurement. Very thin evaporated or sputtered films can be prepared, but they usually have highly defective structures, making comparison with the bulk material difficult.

The structural disadvantages of evaporated films have been reduced in recent years by the advent of a method for producing single crystal films of silver and gold. Such films have far fewer defects than normal films. They can be prepared thin enough to have a significant size effect at room temperature, and the lattice is sufficiently free from defects to allow long mean free paths at low temperatures.

The disentangling of the processes contributing to the resistivity of thin films is not at all easy. This is largely because there are too many unknown factors; the structure of the bulk, the structure of the surface and the way in which electrons interact with the surface. Ideally the films should have a structure identical to that of the bulk metal from which they are made. The single crystal films of silver and gold approach this ideal more closely than any other films. They have fairly simple electronic structures so comparison with the free electron theory is not too unreasonable. There is, therefore, some hope of understanding the resistivities of these films and thereby providing a basis for the understanding of less simple films. Some steps in this direction are presented in the following chapters.

CHAPTER I

ELECTRONS IN METALS

Introduction

The theory of electrons in metals involves the quantum mechanical treatment of many electrons interacting with each other and with the atomic nuclei. In all simple models these complex interactions are replaced by a periodic potential function. Solutions are sought for a single electron moving in a potential resulting from the nuclei and the other electrons. The electrons in a metal are divided into two groups, (i) the core electrons which are tightly bound to particular nuclei and (ii) the conduction electrons which are free to move throughout the volume of the metal. Only the conduction electrons are considered in the theory, the core electrons merely contribute to the potential. The theory is discussed in texts on solid state physics[1,2,3], and only some of the results obtained are given here.

Models which consider single electrons moving in a fixed potential are referred to as one electron models and the solutions of the Schrödinger equation obtained as one electron states.

The free electron model

This model assumes the simplest possible potential. The conduction electrons are treated as being in a potential well with its walls at the surface of the metal and a constant potential inside. The solutions of the Schrödinger equation for an electron in a constant potential are of

the form exp (i $\underline{k}.\underline{r}$), where $|\underline{k}|$ is proportional to the momentum of the electron. The boundary condition, that the wave function must be zero at the surface, restricts the solutions to particular values of $\underline{k}$, so electron states can be represented by points in $\underline{k}$-space . The states are distributed in $\underline{k}$-space with uniform density. The energy of an electron in a particular $\underline{k}$-state is proportional to $|\underline{k}|^2$, so the surfaces of constant energy in $\underline{k}$-space are spherical.

Each one electron state can be occupied by only two electrons, one for each spin direction. The fraction of states occupied at $\underline{k}$ is given by the distribution function $f(\underline{k})$ which, therefore, represents the state of the conduction electrons as a whole. Fermi-Dirac statistics apply to a system of electrons, and in the absence of an electric field the distribution function is the Fermi function $F(\varepsilon)$, a function of energy alone. At zero temperature $F(\varepsilon)$ has the value one up to the Fermi energy ε_o and zero above. The surface in $\underline{k}$-space at ε_o is called the Fermi surface. At finite temperatures the change from one to zero takes place over an energy range $\sim 3\kappa T$, which for normal temperatures is small compared with the Fermi energy. The Fermi surface is then no longer a true surface, but has a finite width. The Fermi function is shown in Figure 1.1 for a number of temperatures.

The periodic potential.

Any reasonable potential function must reflect the periodicity of the crystal lattice in which the electrons move. This periodicity alone leads to striking consequences. Solutions of Schrödinger's equation $\psi(\underline{r})$ for an electron in a periodic potential must have the form exp (i $\underline{k}.\underline{r}$) $u_k(r)$,

where $u_k(\underline{r})$ is a function with the same periodicity as the lattice. The wave vector $\underline{k}$ takes the same values as in the free electron model, but it is not uniquely defined for a given state. If $\psi(r)$ has the above form it has equivalent forms with k replaced by $\underline{k}+\underline{K}$, where $\underline{K}$ is any vector of the reciprocal lattice derived from the crystal lattice. The planes which bisect the reciprocal lattice vectors divide $\underline{k}$-space into regions called Brillouin zones.. Within each Brillouin zone $\underline{k}$ is uniquely defined and there is one electron state per atom of the metal.

The energy function $E(\underline{k})$ is no longer proportional to $|\underline{k}|^2$. The most important changes occur at the boundaries of the Brillouin zones where E(k) is discontinuous. The detailed shapes of the constant energy surfaces in k-space depend on the form of the periodic potential function. The kind of changes that are produced by a weak periodic potential in the case of a two dimensional lattice are shown in Figure 1.2. The energy surfaces well away from the zone boundaries have the free electron form. Near the zone boundaries the surfaces tend to bulge towards them, and if close to make contact.

The distribution of electrons among the one-electron states is given by the Fermi function which is a function of energy, so to obtain the distribution function in terms of $\underline{k}$ the energy function $E(\underline{k})$ must be known.

Real Metals.

In order to obtain detailed information on the electronic structure of real metals it is necessary to appeal to experiment. A review of the experimental methods used has been given by Pippard[4]. The results

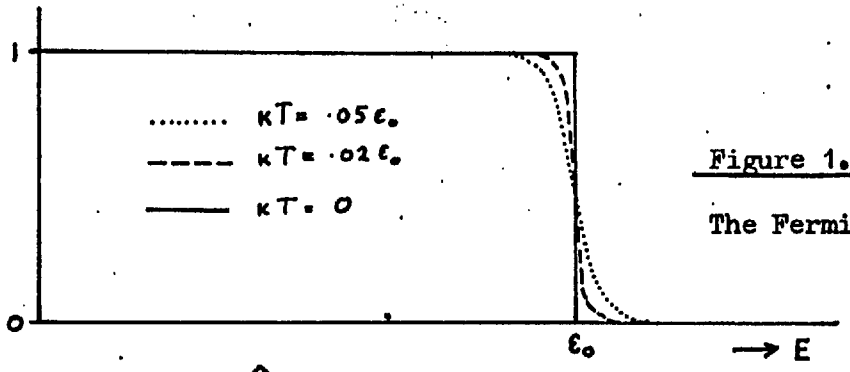

Figure 1.1

The Fermi function.

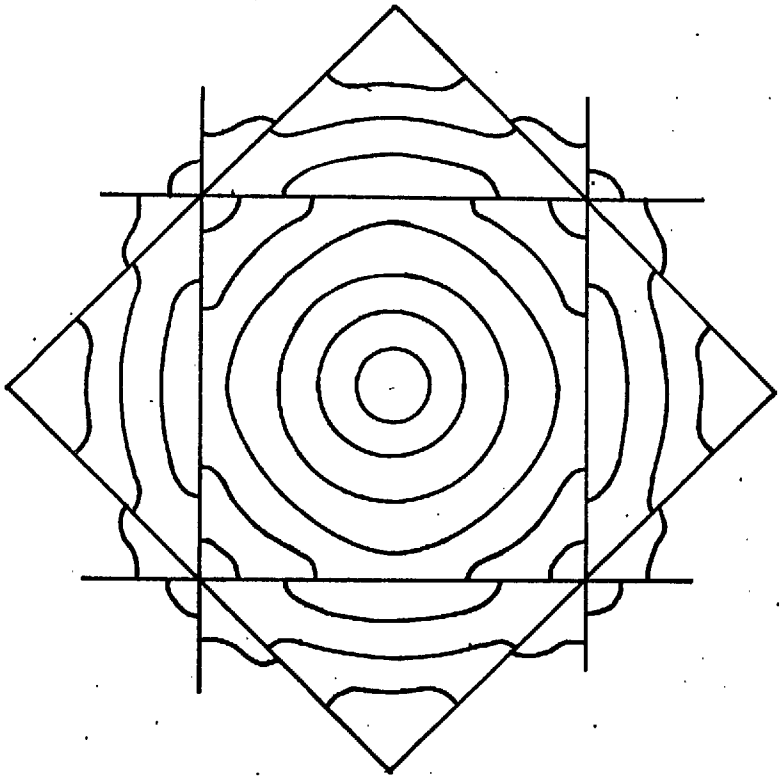

Figure 1.2

Energy contours in two dimensions.

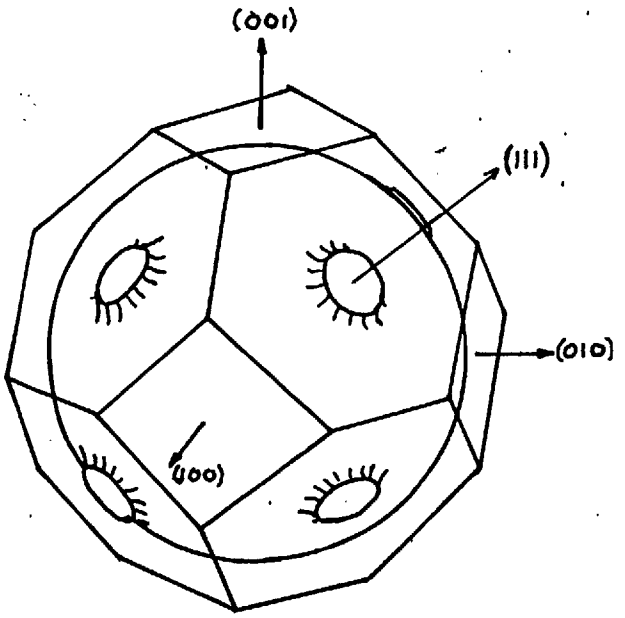

Figure 1.3

The Fermi surface of silver.

obtained are in agreement with the general picture given by the one-electron theory.

As this thesis is concerned with silver films, this chapter will be concluded with a description of the electronic structure of silver.

Silver has a close packed cubic lattice, and has one conduction electron per atom. The free electron Fermi surface for one electron per atom lies completely within the first Brillouin zone, but passes fairly close to the [111] zone boundaries. The theory shows that the constant energy surfaces tend to bulge towards zone boundaries, so the possibility arises that the Fermi surface may make contact with the [111] boundaries. That this is the case in silver has been shown by Shoenberg (5) using the de Haas-Van Alphen effect. The Fermi surface of silver is shown in Figure 1.3. It is roughly a sphere with necks to the [111] zone boundaries. Shoenberg showed that the cross section area away from the necks is within a few per cent of that of the equivalent free electron sphere. The neck distortions occupy only a small fraction of the Fermi surface, i.e. 2% if the diameter of the region involved is twice the contact diameter of the neck. These results suggest that it would be reasonable in many circumstances to treat silver as a free electron metal.

CHAPTER II

THE THEORY OF ELECTRICAL CONDUCTIVITY.

1) The Boltzmann Equation.

The conduction electrons are so named because they are the ones which, by being free to move throughout the volume of the metal, are able to carry an electric current. These alone are considered in the theory of conductivity.

The mechanism by which the current is established and maintained is best approached from the point of view of the distribution function and the Boltzmann equation. The theory is introduced in a general way, and simplifying assumptions are made when they are needed, so their significance can be readily seen. Simpler methods, such as the mean free path method, start with the assumptions built in, and their reliability can only be assessed by seeing how closely the results obtained agree with those from the Boltzmann equation approach.

The theory of conductivity is dealt with in many standard texts(e.g.1,2,6), so detailed references will not be given in the following account.

The Boltzmann equation can be obtained for any collection of particles that can be described by a distribution function, and of which the dynamics are known. Here electrons in metals will be specifically treated, and the distribution function in terms of $\underline{k}$ used, i.e. $f(k)$, or if variation with position is included $f(\underline{k},\underline{r})$.

The theory of electrical conductivity is concerned with finding the current produced in a metal by an electric field. The current density is obtained from the distribution function by a generalization of the simple relationship $j = nev$, i.e.

$$\underline{j} = e \int \underline{v}(\underline{k})\, f(\underline{k})\, d\underline{k} , \qquad (2.1)$$

where $d\underline{k}$ is a volume element in k-space and $\underline{v}(\underline{k})$ is the velocity of electrons with wave vector $\underline{k}$. All integrals are assumed to be over the whole physically meaningful range of each variable, unless otherwise stated. The discussion starts with a metal carrying zero current, as this is the normal state of an isolated piece of metal. The distribution function is then $f_o(\underline{k})$ which must satisfy 2.1 with $\underline{j} = 0$. The temperature will be assumed constant unless otherwise stated.

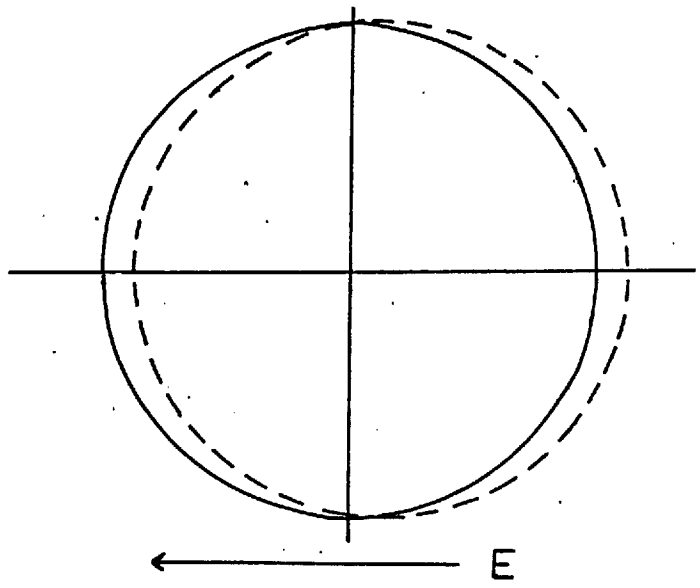

Figure 2.1 Displacement of distribution function by an electric field.

When an electric field is established in the metal the distribution function changes. It tends to move bodily through $\underline{k}$-space in the direction of -E (Figure 2.1). This process is immediately opposed by scattering processes which tend to return the distribution to f_o. The scattering processes must always occur, but leave the zero current distribution unchanged. The two processes achieve a dynamic equilibrium when the distribution is slightly displaced from f_o, and a current flows.

To obtain the equilibrium distribution function in the presence of an electric field, and hence the current, more detailed consideration of the ways in which f changes is required. If variation of f with $\underline{r}$ is allowed, there are three factors which tend to change it.

(a) External fields.

In the presence of electric and magnetic fields an electron moves through $\underline{k}$ - space with a velocity given by:

$$\dot{\underline{k}} = \frac{e}{\hbar}\left(\underline{E} + \frac{1}{e}\, v(\underline{k}) \wedge \underline{H}\right). \qquad (2.2)$$

This movement means that $f(\underline{k})$ at time t is replaced by $f(\underline{k}-\delta\underline{k})$ at time $(t + \delta t)$, where $\underline{\delta k} = \dot{\underline{k}}\, \delta t$.

$$f(\underline{k} - \underline{\delta k}) = f(\underline{k}) - \nabla_k f(\underline{k}).\, \underline{\delta k}\ . \qquad (2.3)$$

The rate of change of f due to fields is, therefore,

$$\left.\frac{\partial f(\underline{k})}{\partial t}\right]_{\text{fields}} = -\dot{\underline{k}}.\nabla_k f(\underline{k})\ . \qquad (2.4)$$

If an electric field only is considered, $\dot{\underline{k}}$ is independent of $\underline{k}$, and the bodily movement of the distribution through k-space mentioned earlier occurs. Then:

$$\left.\frac{\partial f(\underline{k})}{\partial t}\right]_{field} = -\frac{e}{\hbar}\,\underline{E}.\nabla_{\underline{k}}\, f(k). \qquad (2.5)$$

(b) Diffusion.

The electrons in a metal have real-space velocities, so the distribution at a given point is formed from a continuously changing collection of electrons, and is thus influenced by the distributions at surrounding points. The situation is formally similar to that of the the previous section. Electrons from an element in $\underline{k}$-space at $\underline{k}$, which are at $\underline{r}$ at time t, were at $\underline{r} - \delta\underline{r}$ at time $t - \delta t$, where $+\,\delta\underline{r} = \underline{v}(\underline{k})\,\delta t$. The change in $f(\underline{k},\underline{r})$ caused by this movement is $-\nabla_{\underline{r}}\, f(\underline{k},\underline{r})\;\delta\underline{r}$, i.e. $\underline{v}(\underline{k}).\,\nabla_{\underline{r}} f(\underline{k},\underline{r})\,\delta t$, so the rate of change of the distribution function owing to diffusion is:

$$\left.\frac{\partial f}{\partial t}\right]_{diff.} = -\,\underline{v}(\underline{k}).\,\nabla_{\underline{r}}\, f(\underline{k},\underline{r}). \qquad (2.6)$$

(c) Scattering.

The one-electron states of a metal are obtained on the assumption of a perfect periodic potential. In a real metal there are departures from perfection, in the form of impurities, structural defects and phonons, which induce transitions between the one-electron states of the perfect lattice. In the zero external field situation these

processes must produce no change in the distribution function.

$$\dot{f}_o\Big]_{\text{scatt.}} = 0 \qquad (2.7)$$

The rate of change of the distribution function in general is complicated, and discussion will be left until later, apart from the comment that scattering tends to return the distribution to f_o.

The Boltzmann equation in zero magnetic field.

To obtain the D.C. electrical resistance, the constant current produced by a constant electric field is required. The distribution function is, therefore, constant, and its total rate of change is zero.

$$\dot{f}\Big]_{\text{fields}} + \dot{f}\Big]_{\text{diff.}} + \dot{f}\Big]_{\text{scatt.}} = 0 \qquad (2.8)$$

Replacing the first two terms by the expressions already obtained:

$$+\frac{e}{\hbar}\,\underline{E}\cdot\nabla_k f + \underline{v}\cdot\nabla_r f = \dot{f}\Big]_{\text{scatt.}} \qquad (2.9)$$

This is the general Boltzmann equation in the absence of a magnetic field.

Linearization.

A simplification which is immediately available on considering the magnitude of the displacement of the distribution, when a current is flowing, is the replacement of f by fo in $\nabla_k f$. Taking f as fo+g, Figure 2.2 shows that g and $\nabla_k g$ are small if $\delta\underline{k}$ is small compared with

the width of the Fermi surface in $\underline{k}$ space.

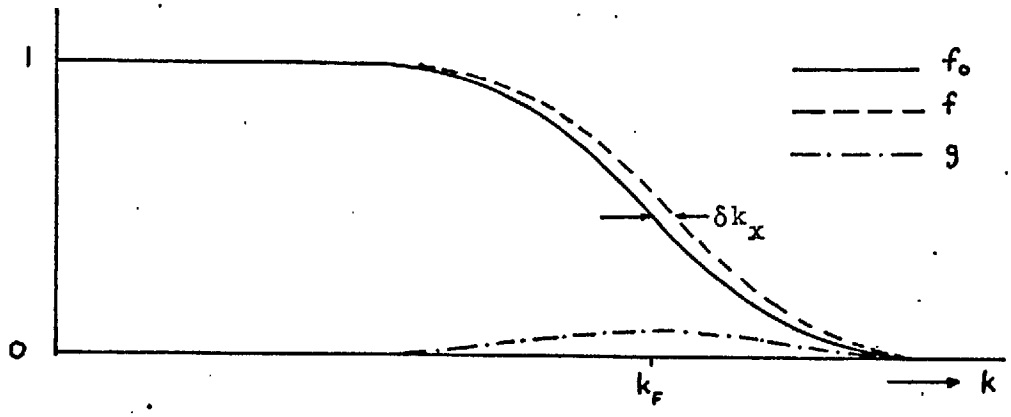

Figure 2.2 f and g at the Fermi surface.

A rough estimate of δk can be obtained on the basis of the free electron model. The current density is:

$$j = nev_F , \qquad (2.10)$$

where v_F = the velocity of electrons at the Fermi surface.
and n = the number of electrons contributing to the current.
These lie in a layer at the Fermi surface of average thickness $\sim \delta k_x$.

$\therefore$ $n = \delta k_x$ x(Surface area of Fermi sphere)
x(Density of states in k-space)

The value of δk_x obtained in this way for a reasonable current density (10^4 amp/cm^2) is the same as the Fermi surface width produced by a temperature of 10^{-3} °K. Thus $\nabla_k g$ is negligible and $\nabla_k f_o$ can replace $\nabla_k f$ in equation 2.9, giving the linearized Boltzmann equation:

$$+\frac{e}{\hbar}\,\underline{E}\cdot\nabla_k f_o + \underline{v}\cdot\nabla_r f = +\dot{f}\Big]_{scatt.} \qquad (2.11)$$

The solutions of this equation are linear in E in agreement with Ohm's law. This provides a justification for the linearization, as metals usually obey Ohm's law.

Spatial variations of f.

The second term in 2.11 involves real space variations of f, and it is of interest to see how these can arise. In a specimen with no external fields f_o might be determined by gradients of composition (i.e. in an alloy) or of temperature. These will not be considered here, although the variation with temperature is of importance in the theory of electronic thermal conductivity.

When f_o is constant throughout the specimen, variations of f with $\underline{r}$ can still occur as a result of the influence of an electric field if the specimen is small enough for the presence of the surfaces to be important. This is the situation which is of interest in the discussion of the resistivity of thin films.

The distribution function f may be expressed as

$$f(\underline{k},\underline{r}) = f_o(\underline{k}) + g(\underline{k},\underline{r}) \qquad (2.12)$$

where g is the change in the distribution function caused by the electric field. f_o is to be assumed independent of $\underline{r}$ in this work, so the real-space term becomes $\underline{v}\cdot\nabla_r\, g(\underline{k}\,\underline{r})$, and the Boltzmann equation becomes:

$$\frac{e}{\hbar}\ \underline{E}\cdot\nabla_k f_o(\underline{k}) + \underline{v}\cdot\nabla_r g(\underline{k},\underline{r}) = \dot{f}(\underline{k},\underline{r})\Big]_{scatt.} \qquad (2.13)$$

The scattering term.

The ease of solution of the Boltzmann equation depends largely on the form of the scattering term, which will now be considered. Complete discussion would involve the details of the interactions between the conduction electrons and the lattice, imperfections and other electrons. The conduction electrons are assumed to occupy one-electron states and interactions to result in transitions between these states, so the total effect of all types of interactions can be represented by a function $Q(\underline{k},\underline{k}')$, which gives the intrinsic transition probability from a state $\underline{k}$ to a state $\underline{k}'$. This means that the probability of an electron in a state $\underline{k}$ being scattered into a totally unoccupied element of $\underline{k}$-space $\delta\underline{k}'$ at $\underline{k}'$ is $Q(\underline{k},\underline{k}')\delta\,\underline{k}'$ per unit time.

In order to calculate transition rates we must take account of the occupation of the initial and final states. The number of electrons per second being scattered out of an element of k-space $d\underline{k}$ at $\underline{k}$ is proportional to the number of electrons in the element, i.e. $f(\underline{k})\,\delta\underline{k}$. The probability of an electron being scattered into an element $\delta\underline{k}'$ at $\underline{k}'$ is proportional to the number of unoccupied states in the element, i.e. $(1 - f(\underline{k}'))\ d\underline{k}'$. The rate of scatter from $\delta\underline{k}$ to $\delta\underline{k}'$ is, therefore;

$$f(\underline{k})\ \ (1 - f(\underline{k}'))\ \ Q(\underline{k},\underline{k}')\ d\underline{k}\ \ d\underline{k}'. \qquad (2.14)$$

Electrons are also scattered from $\underline{k}'$ to $\underline{k}$, at a rate of;

$$f(\underline{k}')\,(1 - f(\underline{k}))\;\; Q(\underline{k}',\underline{k})\; d\underline{k}\; d\underline{k}'. \qquad (2.15)$$

The intrinsic transition probability is the same in both directions, i.e. $Q(\underline{k},\underline{k}') = Q(\underline{k}',\underline{k})$, so the net rate of electron transfer from $\delta\underline{k}$ to $\delta\underline{k}'$ is given by the difference between 2.14 and 2.15, which, when simplified, is:

$$(f(\underline{k}) - f(\underline{k}'))\;\; Q(\underline{k},\underline{k}')\; d\underline{k}\;\; d\underline{k}'\,. \qquad (2.16)$$

The total rate of scattering of electrons out of an element $\delta\underline{k}$ at $\underline{k}$, regardless of their final states, is obtained by integrating 2.16 over all final states;

$$\dot{f}(\underline{k},\underline{r})\Big]_{\text{soatt}} = \int \Big(f(\underline{k},\underline{r}) - f(\underline{k}',\underline{r})\Big)\; Q(\underline{k},\underline{k}')\; d\underline{k}' \qquad (2.17)$$

If $f(\underline{k},\underline{r})$ is replaced by $fo(\underline{k}) + g(\underline{k},\underline{r})$ the scattering term becomes;

$$\dot{f}\Big]_{\text{scatt}} = \int \Big(g(\underline{k},\underline{r}) - g(\underline{k}',\underline{r})\Big)\; Q(\underline{k},\underline{k}')\; d\underline{k}'\,. \qquad (2.18)$$

The Boltzmann equation can now be written:

$$\frac{e}{\hbar}\; \underline{E}\cdot \nabla_k f_o(\underline{k}) + \underline{v}(k)\cdot \nabla_r g(\underline{k},\underline{r}) = \int \Big(g(\underline{k},\underline{r}) - g(\underline{k}',\underline{r})\Big)\, Q(\underline{k},\underline{k}')\; dk' \qquad (2.19)$$

If f_o and Q are given this equation can, in principle, be solved for g. The current density at point $\underline{r}$ is

$$\underline{j}(\underline{r}) = e\int \underline{v}(\underline{k})\, f(\underline{k},\underline{r})\, d\underline{k} = e\int \underline{v}(\underline{k})\, g(\underline{k},\underline{r})\, d\underline{k} + e\int \underline{v}(\underline{k})\, f_o(\underline{k})\, d\underline{k} . \tag{2.20}$$

The final term is zero, as f_o is defined as the zero current distribution, so

$$\underline{j}(\underline{r}) = \frac{e}{4\pi^3}\int \underline{v}(\underline{k})\, g(\underline{k},\underline{r})\, d\underline{k} . \tag{2.21}$$

The foregoing integrals are taken over all $\underline{k}$-space.

2) Some Solutions Of The Boltzmann Equation

The Boltzmann equation 2.19 is very general, being restricted only by constancy of temperature. It is, however, only of formal interest as it stands, because solving it for arbitrary functions f_o and Q would be prohibitively difficult. Some restriction on the forms of these functions is required if solutions are to be obtained, and the following assumptions are made.

1) The energy surfaces in $\underline{k}$-space are spherical. This is slightly more general than the free electron model, as it does not require that the electron energy is proportional to k^2. The distribution function as a function of energy is the Fermi function $F(\epsilon)$. When the energy surfaces are spherical ϵ is a function of $|\underline{k}|$ (or k) only, so f_o is a function of k only.

2) The conduction electrons are scattered elastically, so energy is conserved. It is reasonable to make this assumption when the scattering is by impurity atoms, but less so when scattering is by phonons. The energy change caused by phonons is small compared with the total energy of the electrons, but comparable with the thermal width of the Fermi surface.

3a) The intrinsic scattering probability on a given energy surface depends only on the angle of scatter, ψ, and not at all on the initial or final values of $\underline{k}$.

The function Q may then be re-written as follows.

$$Q(\underline{k},\underline{k}')\, d\underline{k}' \longrightarrow Q(\psi,k)\, k^2\, d\Omega'\, dk' \,.$$

where $d\Omega$ is an element of solid angle.

Before considering whether solutions can be obtained with Q in this form, the consequences of a further simplification will be discussed.

3b) The intrinsic scattering probability on a given energy surface is independent of ψ,

$$\text{i.e.} \quad Q(\underline{k},\underline{k}') \begin{cases} = & Q(k) \text{ if } k = k' \\ = & 0 \quad \text{if } k \neq k' \end{cases}$$

$$\text{or} \quad Q(\underline{k},\underline{k}') = Q(k)\delta(k-k') \qquad (2.22)$$

It is now possible to simplify the scattering term in the Boltzmann equation, but before doing so a property of the function $g(\underline{k},\underline{r})$ must be established.

Re-writing the Boltzmann equation 2.19 with polar coordinates in $\underline{k}$-space we have :

$$\frac{e}{\hbar}\ E.\nabla_{\underline{k}}\ f_o(\underline{k}) + \underline{v}\ \nabla_r g\ (\theta,\phi,k,r)$$

$$= + \int \Big(g(\theta,\phi,k,r) - g(\theta',\phi',k',r)\Big)\ Q(k)\ \delta(k-k')\ k'^2 \sin\theta'\, d\theta'\, d\phi'\, dk' \ .$$

(2.23)

Integration of the right hand side over k' has the effect of replacing the k' by k in the second g. The equation can then be solved for each value of k independently. Now, the number of electrons in $\underline{k}$-space is conserved under the influence of a field, and this places a constraint on g, the change in the distribution function caused by the field, i.e.

$$\int g\ d\underline{k} = 0$$

$$\text{or} \qquad \int g(\theta,\phi,\ k,r)\ k^2 \sin\theta\ d\theta\ d\phi\ dk = 0 \ . \tag{2.24}$$

But Q(k) is arbitrary, and g depends on Q(k), so the integral in equation 2.24 must be zero for each value of k.

$$\text{i.e.} \quad \int g(\theta,\phi,k,r)k^2 \sin\theta\ d\theta\ d\phi = 0 \ . \tag{2.25}$$

The scattering term from equation 2.23, with the k integration done, is :

$$\dot{g}\Big]_s = -\int \big(g(\theta,\phi,k) - g(\theta',\phi',k)\big)\, Q(k)\, k^2 \sin\theta'\, d\theta'\, d\phi'$$

$$= -Q(k)\, k^2 \Big\{ g(\theta,\phi,k) \int \sin\theta'\, d\theta'\, d\phi' - \int g(\theta',\phi',k) \sin\theta' d\theta'\, d\phi' \Big\} .$$

(2.26)

The first integral = 4π and the second, as is shown above, is zero.

$$\therefore \dot{g}\Big]_s = -4\pi k^2 Q(k)\, g(\theta,\phi,k) \quad . \tag{2.27}$$

The rate of change of g due to scattering at a particular point in $\underline{k}$-space is now proportional to the value of g at that point only, so, in the absence of other disturbing influences, g decays exponentially to zero with a time constant, or relaxation time, $\tau(k) = 1/4\pi k^2 Q(k)$. This tremendous simplification has been bought at the price of the assumptions made earlier, but it leaves an equation which can be solved for each combination of θ,ϕ and k independently.

The Boltzmann equation, with the assumption (1) applied to the first term, is now:

$$\frac{e}{\hbar} \frac{df(k)}{dk} \underline{E} \cdot \hat{\underline{k}} + \underline{v} \cdot \nabla_r g(\theta,\phi,k,\underline{r}) = -\frac{g(\theta,\phi,k,\underline{r})}{\tau(k)} , \tag{2.28}$$

where $\hat{\underline{k}}$ is a unit vector in the direction of $\underline{k}$.

The simple relaxation time form of the scattering term is frequently taken as an assumption when elementary solutions of the

Boltzmann equation are required (e.g. 6, 7). Here, the restrictions on $Q(\underline{k},\underline{k}')$ required to justify this assumption have been given explicitly, and are summarized below:

1. Spherical energy surfaces .
2. Energy conserved on scattering .
3. Q depending only on k, i.e $Q = Q(k)\ \delta(k-k')$.

It will be shown in the next section that some relaxation of the last condition is possible, while still obtaining an analytical solution when bulk material only is being considered.

The Bulk Case.

In bulk material, i.e. specimens large compared with the distances an electron travels between collisions, there is no variation of g with $\underline{r}$, so the second term in 2.28 is zero. The solution is then immediately available. If $\underline{E}$ is directed along the polar axis;

$$g = \frac{Ee}{\hbar}\ \tau(k)\ \frac{df_o(k)}{dk}\ \cos\ \theta. \qquad (2.29)$$

The current is obtained from this with equation 2.21. Symmetry ensures that the current density $\underline{j}$ is in the same direction as $\underline{E}$.

$$j = e \int v(k)\ \cos\theta\ g(k,\theta)\ k^2\ \sin\theta d\theta d\phi\ dk$$

$$= \frac{Ee^2}{\hbar} \int \tau(k)\ v(k)\ k^2\ \frac{df_o(k)}{dk}\ \cos^2\theta\ \sin\theta\ d\theta\ d\phi\ dk. \qquad (2.30)$$

For metals $\frac{df_o(k)}{dk}$ is finite only in a small range of k at the Fermi

surface. If $\underline{v}(k)$ and $\tau(k)$ are relatively slowly varying functions of k, it behaves as a δ-function. τ, v and k take their values at the Fermi surface, τ_F, v_F k_F, and

$$\int \frac{df_o}{dk}\, dk = 1. \qquad (2.31)$$

leaving

$$j = \frac{Ee^2}{4\hbar\pi^2}\, \tau_F\, v_F\, k_F^2 \int d\phi \int \cos^2\theta \sin\theta\, d\theta . \qquad (2.32)$$

The ϕ integration gives 2π and the θ integration 2/3,

$$\therefore \quad j = E\, \frac{4\pi}{3\pi^2} \frac{v_F\, k_F^2}{\hbar}\, e^2\, \tau_F . \qquad (2.33)$$

$$\sigma = \frac{4\pi}{3\pi^2} \frac{v_F\, k_F^2}{\hbar}\, e^2\, \tau_F . \qquad (2.34)$$

The value of k_F depends solely on the number density of conduction electrons, but v_F depends on the rate of change of energy with k at the Fermi surface, and cannot be obtained without some assumption about this. If the free electron model is chosen the expression for σ reduces to

$$\sigma = \frac{ne^2 \tau_F}{m} , \qquad (2.35)$$

n = no. of electrons/cc and m = electronic mass.

It may seem that a rather elaborate procedure has been adopted to obtain a formula which can also be obtained by the simple mean free path approach[e.g. 6,7]. The success of the mean free path approach depends on the simplicity of the angular dependence of g in the bulk case, and cannot be reliably extended to size effect problems.

The simplicity of the angular dependence of g in the bulk case also allows a relaxation of the restriction on Q, in that the assumption 3(b) (page 24) can be shown to be unnecessary, i.e. Q may depend on ψ. We assume that g has the form $G(k) \cos\theta$, and evaluate the scattering term using $Q(\psi,k)$. The result obtained is;

$$\dot{g}\Big]_{\text{scatt.}} = \frac{G(k)\cos\theta}{\tau(k)} \quad , \tag{2.36}$$

where $\tau(k) = 1/2\pi\, k^2 \int (1-\cos\psi)\, Q(\psi,k) \sin\psi\, d\psi.$ (2.37)

Thus if $G(k) = \frac{Ee}{\hbar}\, \tau(k)\, \frac{df_o(k)}{dk}$, $G(k)\cos\theta$ is a solution of the Boltzmann equation, and the relaxation time concept is still applicable. The details of this argument are given in Appendix 1.

Ziman[1] states that it should be possible to define a relaxation time in the bulk case with fewer restrictions on Q than have been assumed so far. The only requirement is that scattering should be elastic, then the relaxation time should have a form similar to 2.37, but with a more complicated function of direction weighting Q.

The Mean Free Path.

If electrons are scattered isotropically, the relaxation time τ is

the mean time between scatterings, where the probability of scattering is p per unit time and $\tau = 1/p$. Only electrons at the Fermi surface are important for conduction, and their velocity is v_F, so the mean distance travelled by electrons between scatterings is $\tau v_F = l$, the mean free path. The simple conductivity formula (2.35) may be re-written in terms of l,

$$\sigma = \frac{ne^2 l}{mv_F} \quad . \tag{2.38}$$

If scattering is not isotropic l defined as above is no longer the distance between scatterings. Several low angle scatterings are required to produce the same effect as one large angle one, and l is then a measure of the average distance travelled by an electron before it 'forgets' its initial direction.

3) The Intrinsic Scattering Function $Q(k,k')$ in Practice.

So far $Q(\underline{k},\underline{k})$ has been taken as given. In practice it is neither 'given' nor is it easy to obtain. Only some general aspects of its form under certain conditions will be discussed.

Crystal Imperfections.

Two basic types of scattering agent will be mentioned - imperfections and phonons. The term 'imperfection' is used to cover such static departures from the ideal lattice as impurities, vacancies and dislocations. An imperfection involves a departure from the potential of the ideal lattice. Electrons are scattered from the perturbing potential with unchanged energy and an angular distribution which depends on its shape. If the potential is spherically symmetric the probability of scattering depends only on the angle of scatter, and Q has the form $Q(\psi,k)$. Thus the condition imposed to obtain the last solution of the Boltzmann equation discussed may be approached in practice by metals of simple electronic structure at low temperatures, when only imperfection scattering is of importance. As a spherically symmetric perturbing potential is required, the imperfections should be mainly impurity atoms.

Phonons.

Important departures from the ideal lattice of a solid result from the thermal motions of the ion cores. The thermal excitation of an ideal lattice may be resolved into a set of independent modes. These are plane waves which are specified by their wave vectors (q), which lie on a rectangular lattice in $\underline{q}$-space just as do the electron states in $\underline{k}$-space. The energy of a mode of frequency w_q is quantized in units of

$\hbar w_q$ called phonons. The mean energy in a given mode depends on the temperature, and is given by $\hbar w/(\exp(\hbar w/kT)-1)$. At low temperature, only phonons of low w and q are excited in significant numbers.

The simplest treatment of the vibrational modes is that of Debye. The crystal is treated as a continuum, and the modes ennumerated by applying suitable boundary conditions to the accoustic wave equation. The frequency of each mode is proportional to q, and the energy of the quantum to q^2. A crystal differs from a continuum in having a maximum frequency of vibration when the wavelength is twice the interatomic distance. A cut-off is included in the Debye model by limiting the total number of modes to 3N, the number of degrees of freedom of a lattice of N atoms.

The application of the perturbation theory of scattering to the lattice deformation of a phonon shows that interactions only occur when the following condition is satisfied;

$$\underline{k}' + \underline{K} = \underline{k} \pm \underline{q}\,, \qquad (2.39)$$

where $\underline{k}$ and $\underline{k}'$ are the initial and final states of the electron and $\underline{K}$ is a reciprocal lattice vector. When $\underline{K} = 0$, the interaction is called a normal process, and is illustrated in $\underline{k}$-space in Figure 2.3.

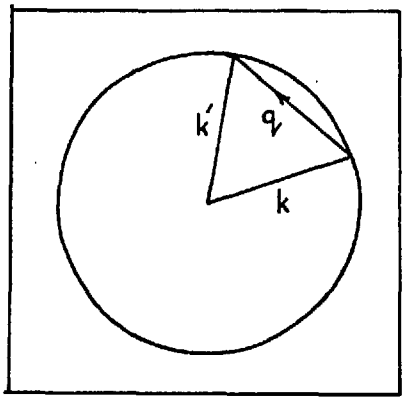

Figure 2.3 Normal Processes.

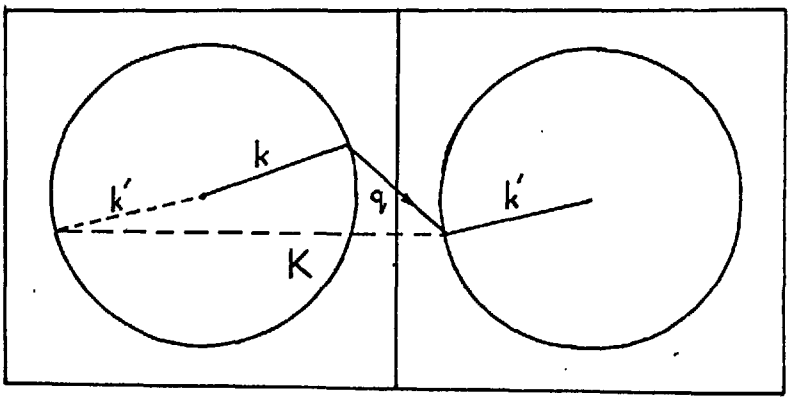

Figure 2.4 Umklapp Processes.

The angle through which the electron is scattered is determined by the value of $\underline{q}$. The maximum angle through which an electron can be scattered by a normal process depends on the maximum value of q, and is about 79° for the free electron model. When $\underline{K} \neq 0$ the change of state is equivalent to scattering into another zone of the repeated zone scheme (Figure 2.4). When returned to the equivalent point in the original zone it is seen that the angle of scattering is not so simply related to $\underline{q}$, and that large angles of scatter can result from

small values of $\underline{q}$, especially if the Fermi surface is close to, or touches, the zone boundary. These are called Umklapp processes.

The energy condition on the interaction between an electron and a phonon is;

$$E(\underline{k}') = E(\underline{k}) \pm E(\underline{q}) , \qquad (2.40)$$

as the phonons may be created or annhilated. This means that the solutions of the Boltzmann equation obtained assuming that scattering takes place on a constant energy surface in k-space are not applicable when scattering is by phonons.

The temperature dependence of the electrical resistivity has been calculated by Grüneisen (1933) and Wilson (1937) assuming the free electron model and the Debye vibrational spectrum, and ignoring Umklapp processes. The results predict a lattice resistivity proportional to T^5 at low temperatures and to T at high temperatures. This is borne out in practice in most cases, particularly for metals of simple electronic structure such as the alkalie metals and the noble metals.

The discussion of bulk resistivity has already been taken well beyond what can be extended to thin films, so it will not be taken further.

CHAPTER III

THE THEORY OF SIZE EFFECT RESISTANCE

1) Introduction.

This chapter is concerned with the way in which the electrical resistance of a specimen depends on its size and shape. The shape of a large specimen is only of importance in determining its resistance for a given resistivity of the material from which it is made. The resistivity is constant for a given material, provided that the specimen under consideration is sufficiently large. The relationship between the resistance and resistivity is simple if the specimen is in the form of a bar of uniform cross section, and the resistance is measured between the ends of the bar. The resistance, R, is then :

$$R = \rho \frac{b}{a} \quad . \quad , \qquad (3.1)$$

where ρ is the resistivity, b the length of the bar and a the cross section area.

When one or both of the transverse dimensions is small, equation 3.1 is no longer valid with ρ as the normal bulk resistivity, though the material remains unchanged. In small specimens the surface influences the resistance, and equation 3.1 is used to define an effective resistivity, which depends on the small dimensions of the specimen, and is the resistivity that would give the measured resistance if the effect of the surface could be ignored.

From the size-effect point of view there are three classes of specimens:

(a) Bulk specimens.

(b) Specimens with one small dimension - films.

(c) Specimens with two small dimensions - wires.

The purpose of this chapter is to give an account of the basic theoretical treatment of the resistance of small specimens. The discussion is concerned mainly with thin films, as these are the subject of the experimental part of this work. The extension to thin wires is briefly discussed for purposes of completeness and comparison.

The electronic mean free path.

The concept of mean free path, which was introduced near the end of the previous chapter, is of considerable importance in the understanding of size effect phenomena. Roughly speaking it is a measure of the distance travelled by an electron before it 'forgets' about the distribution from which it originally came. Thus a disturbance of the distribution at a given point only influences the surrounding distributions to distances of a few mean free paths at most. Applying these ideas to electrical resistivity, it is seen that the surface will only have a significant effect if at least one dimension of the specimen is comparable with the bulk mean free path of the electrons at the Fermi surface.

2) Simple Methods.

Mean free path concepts have been used by a number of workers to obtain expressions for the resistivity of thin films and wires[8,9,10].

To illustrate these methods formulae for the effective resistivity of small specimens will be obtained for the two extreme cases, (a) when the mean free path is much less than the smallest dimension, and (b) when the mean free path is much longer than the smallest dimension. Both methods can be applied to films and wires.

(a) Small mean free path.

Consider a specimen of arbitrary cross section (Figure 3.1). The effect of the surface is confined to a thin layer of thickness proportional to l, the mean free path. It is assumed that in this layer the average current is reduced to a fraction β of its value in the bulk. If S is the cross section area, P the length of the perimeter and j the bulk current density the total current through the wire is $jS - \beta\, j\, l\, P$. If the surface had no effect the total current would be jS, so the ratio of specimen conductivity to bulk conductivity is

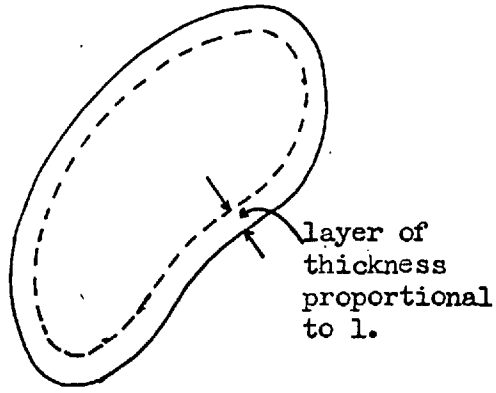

Figure 3.1

$$\frac{\sigma_s}{\sigma_b} = \frac{j\,S - \beta\, j\, l\, P}{j\,S}$$

$$= 1 - \beta \frac{lp}{S} \qquad (3.2)$$

As the second term is small the resistivity ratio is

$$\frac{\rho_s}{\rho_b} = 1 + \frac{\beta l p}{S} , \qquad (3.3)$$

where subscripts s and b refer to specimen and bulk material respectively. For films of thickness t this becomes

$$\frac{\rho_s}{\rho_b} = 1 + 2\beta \frac{l}{t} , \qquad (3.4)$$

and for wires of diameter d

$$\frac{\rho_s}{\rho_b} = 1 + 4\beta \frac{l}{d} . \qquad (3.5)$$

Nordheim obtained a value of 1/4 for β by considering the probability of an electron hitting the surface. The value of β will be discussed later in the light of more reliable treatment of films and wires, (page 64).

b) Large mean free paths.

The method used by Lovell[10] is based on the bulk formula for resistivity

$$\rho = \frac{mv}{ne^2 l} \qquad (3.6)$$

It is assumed that the bulk mean free path can be replaced by an average which allows for the shortening of some paths by the surface.

The following assumptions are also made:

(i) All free paths start at the surface.

(ii) All paths not terminated at the surface are of length l.

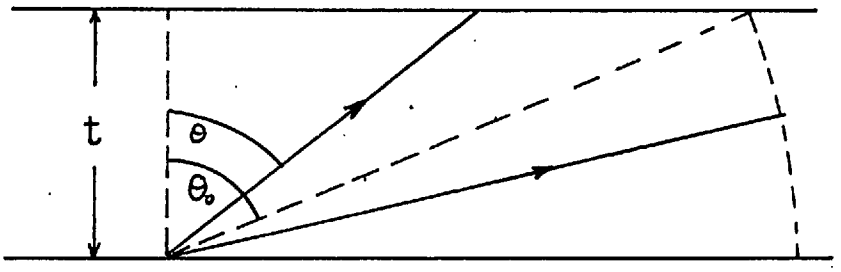

if d is electron path and $l = t/\cos\theta_o$

$$d = t/\cos\theta \qquad \theta < \theta_o$$
$$d = l \qquad \theta > \theta_o$$

Figure 3.2

Electron paths are of two types. (Figure 3.2). Those terminating at the surface when the distance to the surface is less than l, and those terminating in the bulk; all of length l. The average of the free paths in all directions is taken (l_{eff}) and the ratio of the effective resistivity to the bulk resistivity assumed to be l/l_{eff}. Lovell's result for films is:

$$\frac{\rho_f}{\rho_b} = 1/K(\log \frac{1}{K} + 1) , \qquad (3.7)$$

where K is t/l and ρ_f is the effective film resistivity.

J.J. Thomson[8] obtained a similar formula by considering only free paths which start in the bulk, giving

$$\frac{\rho_f}{\rho_b} = 2/K(\log \frac{1}{K} + \frac{3}{2}) \qquad (3.8)$$

These two expressions differ mainly by a factor $\frac{1}{2}$.

Lovell's method is open to the following criticisms. (Fuchs).

(i) All paths do not start at the surface.

(ii) The free paths in the bulk are exponentially distributed about l, not of fixed length.

(iii) The simple average over all directions is not the correct way to obtain the current. The simple resistivity formula is a result of the simplicity of the bulk situation for which it is valid. It cannot be expanded again to apply to a more general case merely by averaging the electron paths.

These criticisms apply equally well to Thomson's method if (i) is reversed.

Lovell's and Thomson's results are plotted in Figure 3.3 with Fuchs' results from the Boltzmann equation approach.

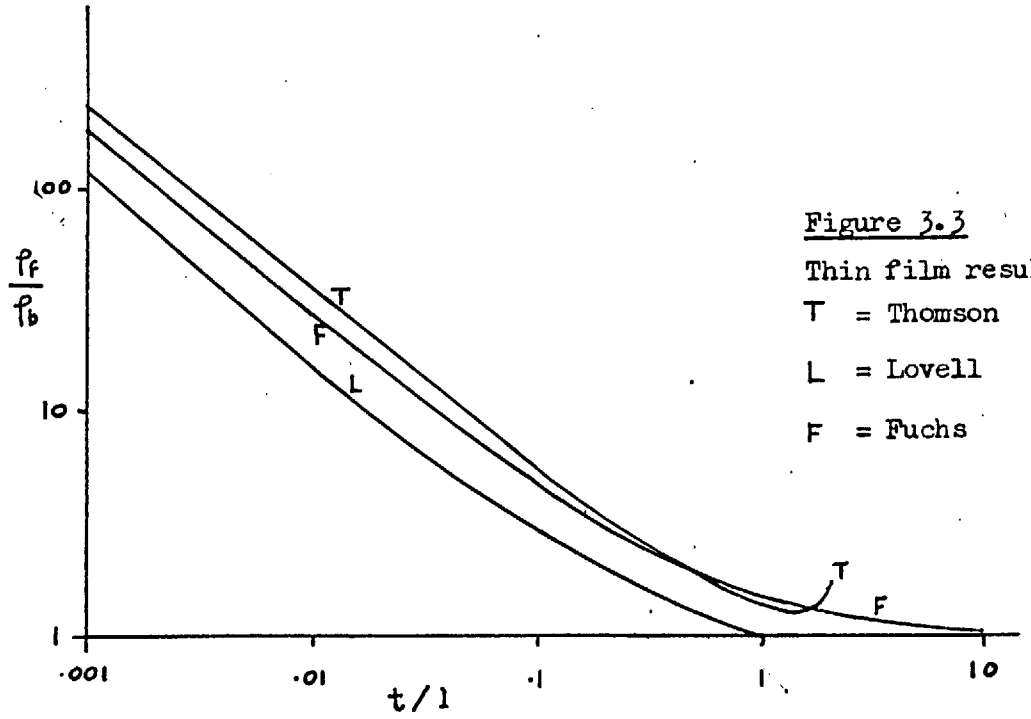

Figure 3.3
Thin film results
T = Thomson
L = Lovell
F = Fuchs

3) Size-Effect Resistivity From the Boltzmann Equation.

It is impossible to be confident of the reliability of results obtained by the mean free path methods without being able to compare them with a more rigorous treatment. Such a treatment has been provided by Fuchs[11]. The mean free path methods require two types of assumption. The first concerns the nature of the films, in that they are made from a free electron metal and that electrons behave in a specified way on reaching the surface. The second concerns the method used to evaluate the resistivity which is assumed to be proportional to the reciprocal of an effective mean free path, obtained by averaging over possible mean free paths. Fuchs makes only the first type of assumption and obtains the resistivity rigorously from the Boltzmann equation. Thus, differences between theory and experiment must be explained in terms of failure of the assumptions about the nature of the films, and cannot be attributed to an incorrect method of estimating the resistivity.

The discussion of the resistivity of thin films given below is essentially that given by Fuchs.

Solutions of the Boltzmann equation are required in the presence of surfaces, but at constant temperature. The groundwork has been laid in the previous chapter. The appropriate equation is (2.13) :

$$\frac{e}{\hbar}\ \underline{E}\cdot\nabla_k f_o(\underline{k}) + \underline{v}\cdot\nabla_r g(\underline{k},\underline{r}) = \dot{g}(\underline{k},\underline{r})\Big]_s \qquad (3.9)$$

The second term must now be retained, as variations of g over the specimen

are expected. This equation can only be easily solved if the scattering term at a given point can be reduced to the simple form where it is proportional to the value of g at that point only. The possibility of doing this was shown to depend in turn on the three assumptions discussed on page 24 .

In brief: 1) Spherical energy surfaces in k-space.

2) Electrons scattered elastically.

3) The intrinsic scattering probability is constant on any energy surface.

The equation to be solved is then:

$$+ \frac{e}{\hbar} \underline{E} \cdot \nabla_k f_o(\underline{k}) + \underline{v} \cdot \nabla_r g(\underline{k},\underline{r}) = - \frac{g(\underline{k},\underline{r})}{\tau(k)} \quad , \qquad (3.10)$$

from 2.28, where $\tau(k) = 1/4\pi k^2 Q(k)$.

The general solution to this equation was found by Chambers[12], and is established below using his approach, which shows clearly the way in which the surface influences the distribution function in the presence of a field.

Consider the electrons in an element of $\underline{k}$-space at $\underline{k}$, with velocities $v(\underline{k})$. In Figure 3.4 a line with direction $\underline{v}(\underline{k})$ is drawn from a point on the surface (S) to somewhere in the bulk (B).

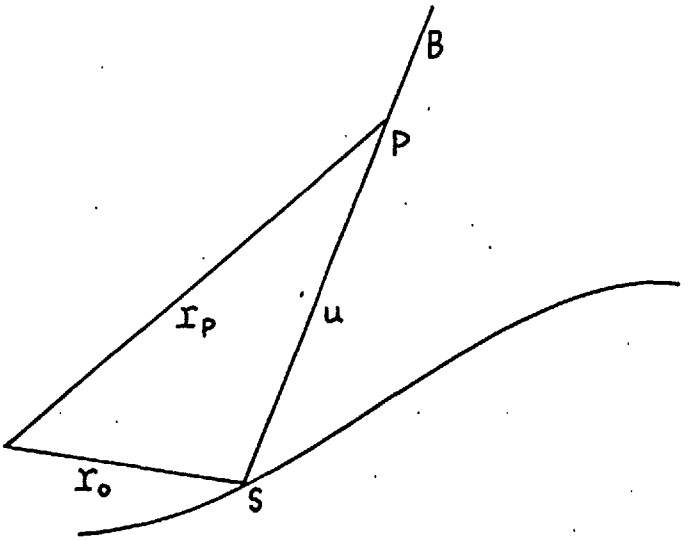

Figure 3.4

A general point P on SB is $\underline{r}_p$. If $\underline{k}$ is fixed in equation 3.10 the first term is a constant scalar (A) and the second is the product of v and the rate of change of g along SB, so the equation refers only to values of g on SB, which can therefore be solved for independently of the values of g for other positions and other directions. The only coordinate that need be considered is the distance along SB, i.e. $u = \underline{r}_p - \underline{r}_o$. Equation 3.10 may now be written for a fixed value of $\underline{k}$,

$$v \frac{dg(u)}{du} + \frac{g(u)}{\tau} = -A \qquad (3.11)$$

The solution of this equation is

$$g(u) = \tau A(1 - C e^{-u/\tau v}) , \qquad (3.12)$$

where C is a constant for particular values of $\underline{k}$ and $\underline{r}_S$. The full general solution of 3.10 may now be written:

$$g(\underline{k},\underline{r}) = \frac{-\tau(k)e}{\hbar}\ \underline{E}\cdot\nabla_k f_o(k)\left(1 - C(\underline{k},\underline{r}_s)\ e^{-|\underline{r}-\underline{r}_s|/\tau v}\right).$$

(3.13)

$C(\underline{k},\underline{r}_s)$ is an arbitrary function which cannot be determined without some information about the nature of the surface. It represents the disturbance of the function g from its bulk value, caused by the surface. On moving into the metal the disturbance dies away exponentially.

Equation 3.13 applies to a specimen of arbitrary, but constant, cross section. It is made much more manageable by restricting it to the case of a thin film. The z axis is taken perpendicular to the film, with the surfaces at z = 0 and z = t. The electric field direction is along the x axis. The surfaces are assumed uniform in properties, so $g(\underline{k})$ depends only on z, and C depends only on $\underline{k}$. The general solution of the Boltzmann equation is then :

$$g(\underline{k},z) = \frac{-\tau(k)e}{\hbar}\ E.\nabla_k f_o(\underline{k})\left(1 - C(\underline{k})\ e^{-z/l\cos\theta}\right),$$

(3.14)

where spherical polar coordinates are used in $\underline{k}$-space, i.e. θ is the angle from the z axis, and ϕ the angle of rotation about the z axis, with $\phi=0$ in the x direction. The bulk mean free path l replaces τv. No further progress can be made until something has been said about the nature of the scattering processes at the surface.

Surface Scattering.

The scattering of electrons at a surface may be represented by a function $S(\underline{k}',\underline{k})$, similar to the bulk scattering function $Q(\underline{k}',\underline{k})$. $S(\underline{k}',\underline{k})$ gives the probability that an electron in state $\underline{k}'$ on arriving at the surface will be in state $\underline{k}$ on leaving. If the distribution function of electrons approaching the surface is $f_a(\underline{k})$, and that of those leaving is $f_b(\underline{k})$, the latter is related to the former by :

$$f_b(\underline{k}) = \int S(\underline{k}',\underline{k})\, f_a(\underline{k}')\, d\underline{k}' \quad . \qquad (3.15)$$

If zero current flows both f_a and f_b equal f_o, so replacement of f by $f_o + g$ in 3.15 gives:

$$g_b(\underline{k}) = \int S(\underline{k}',\underline{k})\; g_a(\underline{k}')\, d\underline{k}' \quad . \qquad (3.16)$$

This represents a boundary condition which must be applied to 3.14 to obtain a particular solution. Solutions can be fairly readily obtained with two simple forms of the surface scattering function, one for diffuse scattering and one for partially specular scattering.

Diffuse Scattering

This is the simplest form of scattering. It assumes that the scattering is elastic and that all directions are equally probable. Most surfaces have irregularities larger than the wavelength of conduction electrons, so this is quite a reasonable assumption. The irregularities must, however, be small compared with the mean free path, or the specimen could no longer be treated as a plane surfaced film.

The surface scattering function becomes:

$$S(\underline{k}',\underline{k}) = S_o \, \delta(k-k') \qquad (3.17)$$

where S_o = constant. In 3.16 this gives:

$$g_b(\underline{k}) = \int S_o \, \delta(k-k') \; g_a(\underline{k}') \, d\underline{k}' \,,$$

$$= 0 \qquad (3.18)$$

using the result obtained on page 26. The electrons leaving the surface have the zero current distribution f_o. This boundary condition must be put into the general solution for films, 3.14, to obtain $C(\underline{k})$. The function $g(\underline{k},z)$ is considered in two parts:

$$\left.\begin{array}{ll} g_+(\underline{k},z) & k_z > 0 \\ g_-(\underline{k},z) & k_z < 0 \end{array}\right\} . \qquad (3.19)$$

At $z = 0$ g_+ refers to electrons which have just been scattered, and is zero for all $\underline{k}$. From the general solution, reverting to an earlier abbreviation, and using C_+ and C_- to correspond with g_+ and g_-,

$$g_+(\underline{k}, 0) = \tau A (1 - C_+(\underline{k})) = 0 \qquad (3.20)$$

i.e. $C_+(\underline{k}) = 1.$

At z = t:

$$g_-(\underline{k},t) = \tau A (1 - C(k)\, e^{-t/l \cos\theta}) = 0 \qquad (3.21)$$

i.e. $$C_-(k) = e^{t/l \cos\theta}$$

So the solution to the Boltzmann equation for a film with diffuse scattering of the electrons at its surfaces is:

$$\left.\begin{aligned} g_+(\underline{k},\underline{r}) &= \tau A (1 - e^{-z/l \cos\theta}) \\ g_-(\underline{k},\underline{r}) &= \tau A (1 - e^{(t-z)/l \cos\theta}) \end{aligned}\right\} \qquad (3.22)$$

These functions are completely symmetrical about the mid-plane of the film. Figure 3.5 shows some examples of their form with respect to variation of z.

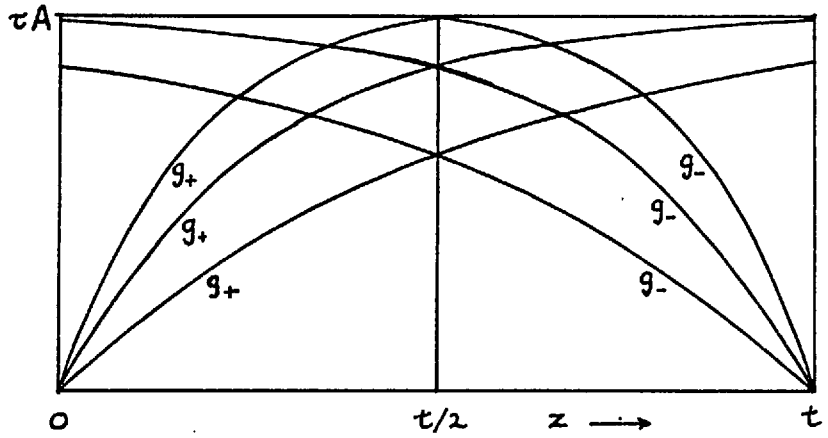

Figure 3.5. Examples of g vs. z.

The variation of g with direction, especially for films with K(=t/l) below 1, shows a sharp singularity at $\theta = 90^\circ$, i.e. the direction

parallel to the surface of the film. This is illustrated in Figure 3.6 where g v. θ plots are given for a film with K = 0.2 at three values of z. The ϕ dependence of g is as for the bulk case, proportional to cos θ.

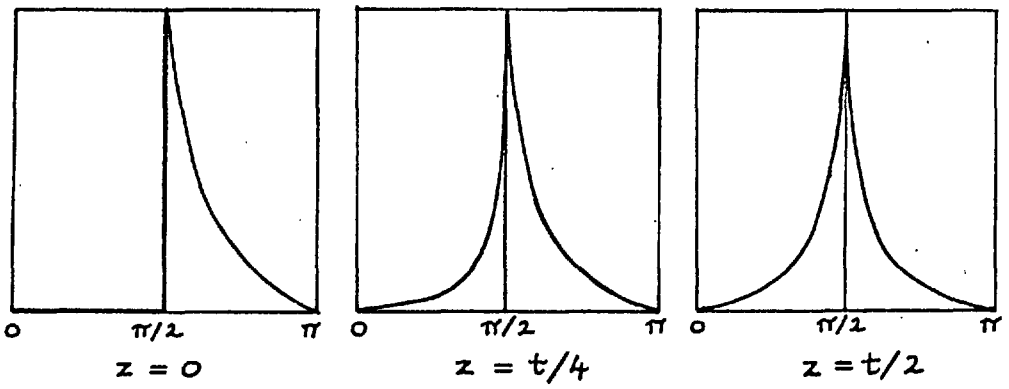

Figure 3.6 g vs. θ for three values of z.

The Current

The current density at each value of z is given by :

$$j_x(z) = e\int v_x\, g(\underline{k},z)\, d\underline{k} \quad . \tag{3.23}$$

The current measured is the total current:

$$J = \int_0^t j(z)\, dz \quad . \tag{3.24}$$

The effective resistivity is calculated allowing for the size and shape of the specimen, and assuming the current to be uniform across the film.

$$\rho_f = E/\left(\frac{1}{t}\int_0^t j(z)\, dz\right) \quad . \tag{3.25}$$

The two parts of g are symmetrical about the mid-plane of the film, so the current can be obtained from just one of them. e.g.

$$J = \frac{2e}{2\pi^3}\int_0^t v_x\, g_+ (\underline{k},z)\, d\underline{k} \qquad (3.26)$$

i.e. $$J = \frac{2e}{2\pi^3}\int v(k) \sin\theta \cos\phi \left(\frac{-\tau(k)\, e}{\hbar}\right) E \frac{df_o}{dk} \sin\theta \cos\phi \,(1-e^{-z/l\cos\theta})$$

$$k^2 \sin\theta\, d\theta\, d\phi \ . \qquad (3.27)$$

$$= \frac{2E}{h}\frac{e^2 v}{2\pi}, \int_0^{\pi/2} d\theta \sin^2\theta \int_0^t dz(1 - e^{-z/l\cos\theta}) \int_0^{2\pi} d\phi \cos^2\phi$$

$$\int dk\, k^2\, v(k)\, \tau(k) \frac{df_o}{dk} \ . \qquad (3.28)$$

The pseudo delta function $\frac{df_o}{dk}$ replaces the final integral by $k_F^2\, \tau_F v_F$.
The constant term outside the remaining integrals is

$$\frac{3}{2} \cdot \frac{4\pi}{3\pi^2} \frac{e^2\, v_F\, \tau_F\, k_F^2}{h} \quad E \quad = \quad \frac{3}{2}\, \sigma_b \ E \ , \qquad (3.29)$$

where σ_b is the conductivity of the bulk material, (page 29). The effective conductivity may now be written in terms of J,

$$\sigma_f \ = \ \frac{J}{tE} \ = \ \frac{3}{2}\, \sigma_b \int_0^{\pi} d\theta \sin^3\theta \int dz \frac{1}{t}\,(1-e^{-z/l\cos\theta}) \qquad (3.30)$$

The integration may be taken a little further analytically, but numerical methods must eventually be used. Before giving the results for the diffusecase the extension to partially specular scattering will be discussed.

Partially Specular Scattering at the Surface.

The assumption that scattering is diffuse may often be justified, but if a surface is a crystalline plane the possibility of specular or near specular scattering may need to be considered. This possibility was allowed for by Fuchs by assuming a simple one-parameter model for the scattering. A fraction p of the electrons arriving at the surface are assumed to be specularly scattered, and the remainder to be diffusely scattered. The scattering function S for this model is

$$S(\underline{k}',\underline{k}) = S_o\big((1-p) + p\ \delta(\theta' + \theta)\ \delta(\phi'-\phi)\big)\delta(k'-k) \quad , \qquad (3.31)$$

where S_o is a constant. The effect on the boundary conditions of this type of scattering can be seen without explicitly putting $S(\underline{k}',\underline{k})$ in the boundary condition equation 3.16. The diffuse part contributes nothing to the g of the outgoing electrons. The specular part involves transitions of the type shown in Figure 3.7 for a fraction p of the electrons, so the g for the outgoing electrons has the same form as the g for the ingoing electrons, but scaled down by the factor p, and with k_z replaced by $-k_z$.

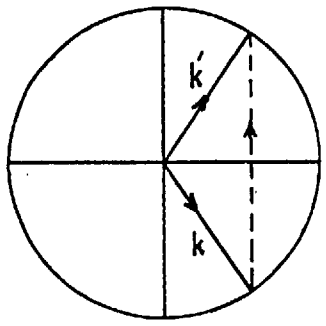

Figure 3.7

i.e. at $z = 0$ $\quad g_+(k_z) = p\, g_-(-k_z)$, (3.32)

and at $z = t$ $\quad g_-(-k_z) = p\, g_+(k_z)$. (3.33)

Replacing the 'g's in these equations by the general solution of the Boltzmann equation for films (3.14) gives two equations for the two functions $C(\underline{k})$, C_+ and C_-, which aresolvable by simple substitution.

The particular solution thus obtained for partially specular scattering is:

$$g_+ = \tau A \left(1 - \frac{1 - p}{1-p \exp(-t/l \cos\theta)} \exp(-z/l \cos\theta)\right),$$

$$g_- = \tau A \left(1 - \frac{(1-p) \exp(t/l \cos\theta)}{1 - p \exp(-t/l \cos\theta)} \exp(-z/l \cos\theta)\right).$$

(3.34)

Examples of g_+ and g_- plotted against z and θ are given in Figure 3.8 The solution for diffuse scattering is now a special case, obtained when $p = 0$.

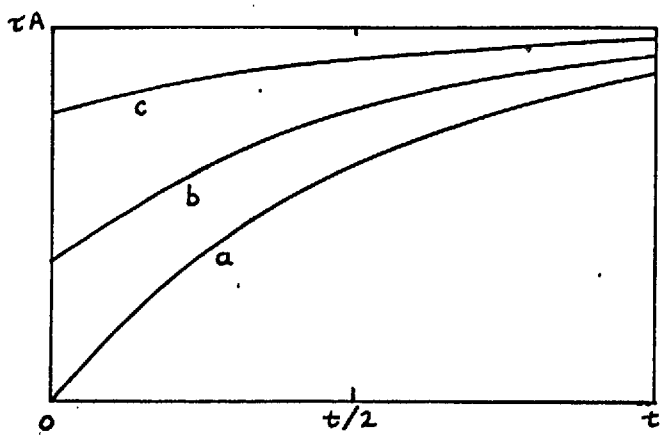

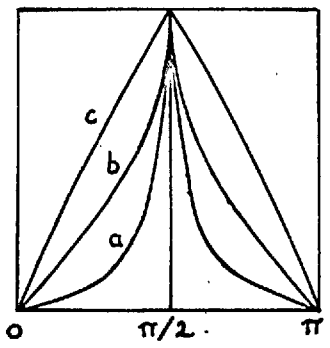

g_+ vs. t.

g vs. θ

a: p=0, b: p=0.4, c: p=0.8

z= t/2

Figure 3.8

The effective conductivity.

The expression obtained for the conductivity in the diffuse scattering case (3.30) can be immediately extended to the case of partially specular scattering as $C(\underline{k})$ depends only on θ, and the θ integration has not been done.

$$\sigma_f = \frac{3}{2}\,\sigma_b \int_0^{\pi/2} d\theta\, \sin^3\theta \int_0^t dz\, \frac{1}{t}\left(1 - C(\theta)\, e^{-z/l\cos\theta}\right). \tag{3.35}$$

The integration with respect to z is quite straightforward, and gives:

$$\frac{\sigma_f}{\sigma_b} = \frac{3}{2}\int_0^{\pi/2} \left(1 - C(\theta)\,\frac{(1-\exp(-K/\cos\theta))}{K}\right) \sin^3\theta\, d\theta\,, \tag{3.36}$$

where $K = t/l$. The $C(\theta)$ required is:

$$C_+ = \frac{1 - p}{1 - p \exp(-K/\cos\theta)} \qquad (3.37)$$

from g_+ on page 52. If $p = 0$, the special case of diffuse scattering is recovered.

The final integration must be done numerically. Fuchs gave an expression for it in the form of a series, and Sondheiner[13] tabulated the results for some values of p.

The function σ_f/σ_b depends on p and K only. The ratio of the effective resistivity to the bulk resistivity (ρ_f/ρ_b) is the reciprocal of σ_f/σ_b, and will sometimes be written as $F(K,p)$.

Program to calculate ρ_f/ρ_b.

In order to allow detailed comparison with the experimental results presented later in this work, a computer program was written which obtains ρ_f/ρ_b ($= \sigma_b/\sigma_f$) from the expression given by Fuchs:

$$\frac{\rho_b}{\rho_f} = \frac{\sigma_f}{\sigma_b} = 1 - \frac{3(1-p)}{8K} + \frac{3}{4K}(1-p)^2 \sum_{n=1}^{\infty} e^{n-1} \left\{ B(Kn) \left(K^2n^2 - \frac{K^4n^4}{12} \right) + e^{-Kn} \left(\frac{1}{2} - \frac{5}{6} Kn - \frac{K^2n^2}{12} + \frac{K^3n^3}{12} \right) \right\}, \qquad (3.38)$$

where $B(x) = \int_x^\infty \frac{e^{-t}}{t}\, dt$ (3.39)

The program was written in Fortran, and run on the I.B.M. 7090 computer at Imperial College. The results are plotted in Figure 3.9 as $F(K,p)$ v. K for a number of values of p.

Simple formulae in extreme cases.

The complex formula used to cover the full range of K can be reduced to simple forms at high and low K (Fuchs[11], Sondheimer[13])

At high K:

$$\frac{\rho_f}{\rho_b} = 1 + \frac{3}{8}\frac{(1-p)}{K} \quad . \tag{3.40}$$

This is of the form obtained from the simple approaches to film resistivity discussed at the beginning of this chapter.

At low K:

$$\frac{\rho_f}{\rho_b} = \frac{1}{K \log\frac{1}{K}} \quad . \tag{3.41}$$

This formula is applicable only at very low K (< 0.01). A slightly modified version is useful up to $K = 0.1$ (Mayer[14]):

$$\frac{\rho_f}{\rho_b} = \frac{1}{K(\log(\frac{1}{K}) + .423)} \quad . \tag{3.42}$$

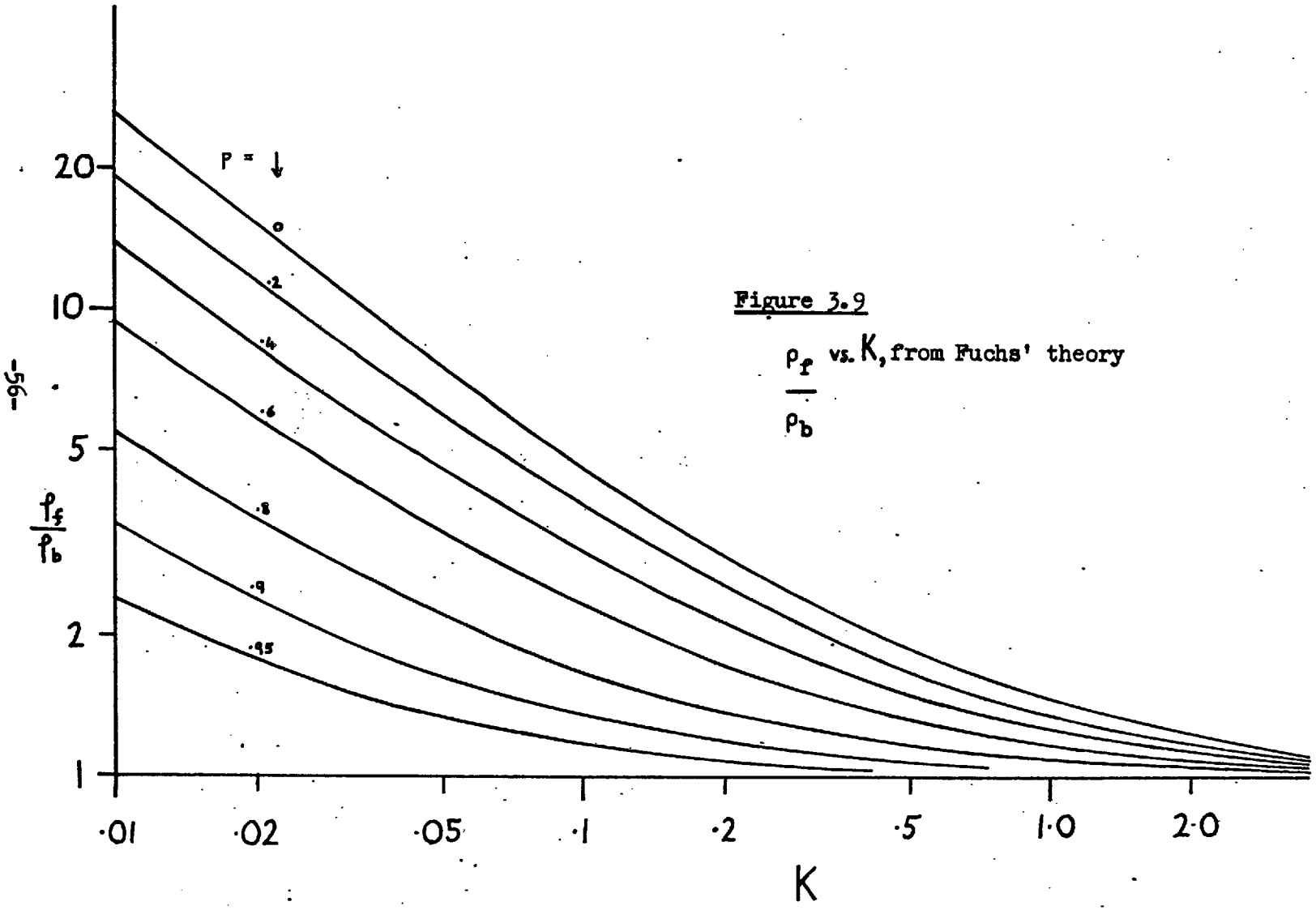

Figure 3.9

$\frac{\rho_f}{\rho_b}$ vs. K, from Fuchs' theory

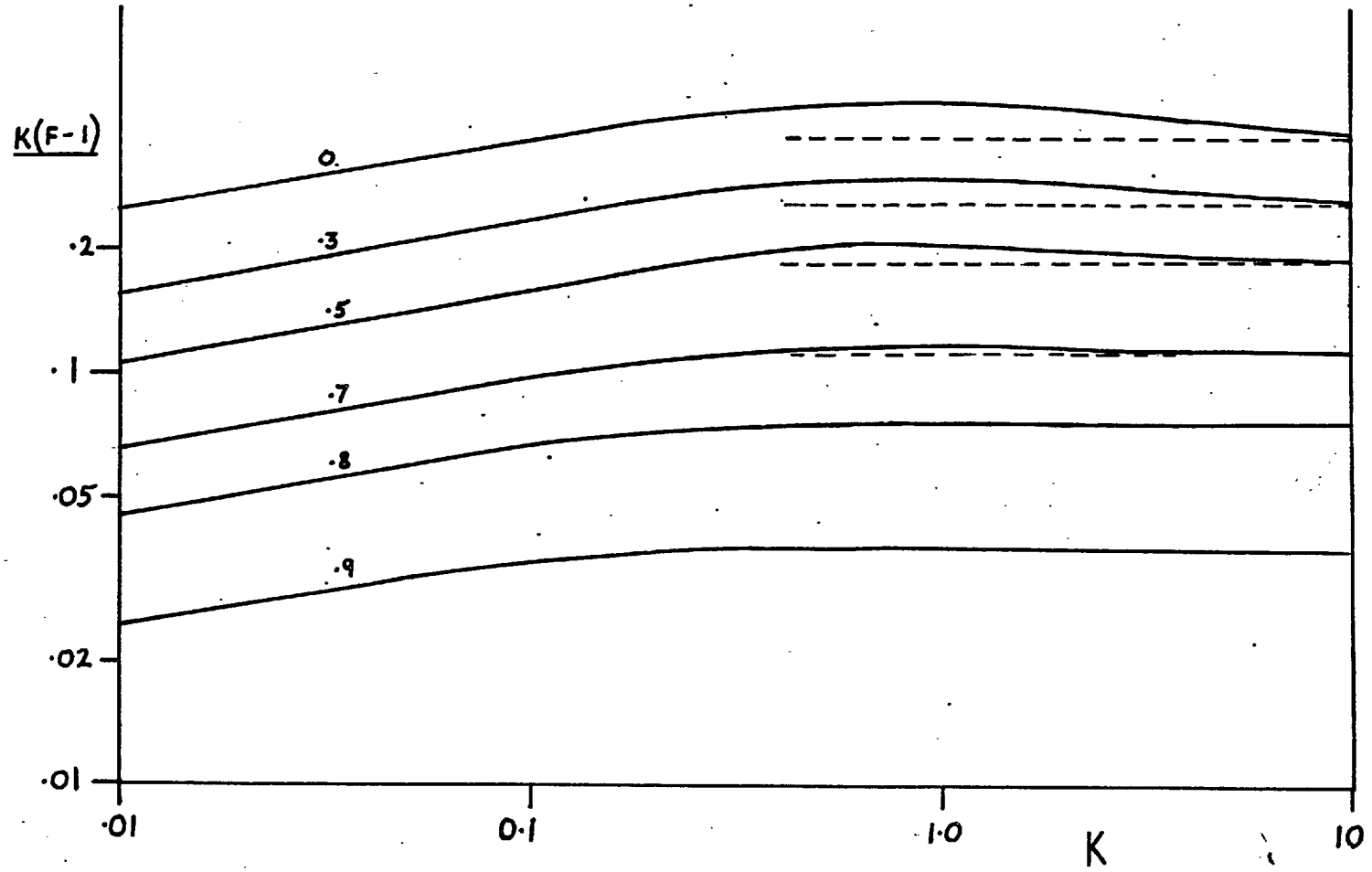

Figure 3.10 K(F-1) vs. K from Fuchs' theory.

Matthiessen Rule.

The concept of the surface as just another independent scattering mechanism leads to an extra term in the familiar form of Matthiessen's rule which applies to impurity and phonon scattering in bulk[6,14].

$$\left.\begin{aligned} \rho_f &= \rho_i + \rho_{ph} + \rho_s \\ \text{or} \quad \rho_f &= \rho_b + \rho_s \end{aligned}\right\} \qquad (3.43)$$

where subscripts i, ph and s refer to impurity, phonon and surface scattering respectively. This formula is supported by the thick film limit of Fuchs' theory;

$$\rho_f = \rho_b + \frac{3}{8t}(1 - p)\rho_b l . \qquad (3.44)$$

as $\rho_b l$ is a constant for a given metal or range of dilute alloys.

It is of interest to see to what extent Matthiessen's rule can be applied when the condition $K >> 1$ does not hold. This is best shown by the form of $(\rho_f - \rho_b)$, which should be constant if Matthiessen's rule holds. The result expected on the basis of Fuchs' theory is given below.

$$\begin{aligned} \Delta\rho_m &= \rho_f - \rho_b \\ &= \rho_b F(K,p) - \rho_b \\ &= \rho_b(F(K,p) - 1) . \end{aligned} \qquad (3.45)$$

Expressing ρ_b in terms of K:

$$\Delta\rho_m = \frac{C}{t} K(F(K,p) - 1) , \quad (C = \rho_b l) . \qquad (3.46)$$

For a film of given thickness $\Delta\rho_m$ is proportional to $K(F(K,p)-1)$. This expression is plotted in Figure 3.10 for a number of values of p. The curves show that $\Delta\rho_m$ is fairly constant down to about $K = 0.4$, when it begins to fall steadily with K. There is a rise above the high K value at about $K = 1$, which is largest at low p, when it is about 10% of $K(F-1)$.

Theory for a film with non-identical surfaces.

The possibility that the two surfaces of a film may be different can be dealt with within the framework of Fuchs' theory by assuming that the surfaces have different values of p, p_1 and p_2 say. As only a change in the boundary conditions is involved only a change in the function $C(\underline{k})$ is expected. The boundary conditions are determined by the two equations (cf page 52).

$$\left.\begin{aligned} g_+(k_z) &= p_1\, g_-(-k_z) \qquad (z = 0) \\ g_-(-k_z) &= p_2\, g_+(k_z) \qquad (z = t) \end{aligned}\right\} \qquad (3.47)$$

The functions g_+ and g_- are replaced by the general form (equation 3.14) and the equation solved for C_+ and C_-, giving :

$$C_+ = \frac{(1-p_1) + (1-p_2)\, p_1 \exp(-K/\cos\theta)}{1 - p_1\, p_2 \exp(-2K/\cos\theta)} ,$$

$$C_- = \frac{(1-p_2) + (1-p_1)\, p_2 \exp(-K/\cos\theta)}{1 - p_1 p_2 \exp(-2K/\cos\theta)} \qquad (3.48)$$

C_+ and C_- can be inserted directly into the conductivity equation (3.36), but now g_+ and g_- are no longer symmetrical about the mid-plane, so both must be used. $C(\theta)$ in equation 3.36 is replaced by $(C_+(\theta) + C_-(\theta))/2$.

$$\frac{\sigma_f}{\sigma_b} = \frac{3}{2} \int \left(1 - \frac{C_+(\theta) + C_-(\theta)}{2K} \cos\theta \,(1-e^{-K/\cos\theta})\right) \sin^3\theta \, d\theta \qquad (3.49)$$

It would be quite straightforward to evaluate this integral numerically, but no attempt has been made to do so. Instead the consequences of assuming a one -p form, when the two-p form should be used, are discussed for two extreme cases.

(a) $\underline{K >> 1}$. The exponentials can be taken as zero .

$$\frac{C_+(\theta) + C_-(\theta)}{2} = \frac{(1-p_1) + (1-p_2)}{2} = \left(1 - \frac{p_1 + p_2}{2}\right) \qquad (3.50)$$

Compare this with the single p form which gives:

$$C_+ = C_- = 1 - p \qquad (3.51)$$

Thus, at high K, the two-p form is the same as the one-p form with the mean of p_1 and p_2 ($\bar{p}$) used instead of p.

This result is not surprising for thick films, as the effect produced by one surface does not extend far enough to influence the other.

(b) Films with one surface specular.

In this case the effective conductivity (or resistivity) can be obtained over the whole range of K from the one-p results for the p on the non-specular surface. If $p_2 = 1$ the film is equivalent to half a film with p_1 on both surfaces. Putting $p_1 = p$:

$$\left.\begin{aligned} C_+(\theta) &= \frac{1 - p}{1 - \exp(-2t/l\cos\theta)} \\ C_-(\theta) &= \frac{(1-p)\exp(-2t/l\cos\theta)}{1 - \exp(2t/l\cos\theta)} \end{aligned}\right\}, \qquad (3.52)$$

which are as for the one-p case, but with t replaced by 2t. If ρ_f/ρ_b in the two-p case is written as $F(K,p_1,p_2)$ then $F(K,1,p) = F(2K,p)$.

$F(K,1,p)$ was obtained in this way for a number of values of p, and the result compared with the one-p result for the mean of the two values of $p(\bar{p} = (1+p)/2)$, to see whether the use of the mean could be extended to low values of K.

The difference between $F(K,1,p)$ and $F(K,\bar{p})$ is plotted in Figure 3.11 as a percentage of the latter. As the situation considered here is an extreme one, these curves indicate the maximum error that would arise from using $\bar{p}$ in the one-p theory instead of p_1 and p_2 in the 2-p theory. The resistivity with p_1 and p_2 different is always greater than for the one-p case with $p=\bar{p}$.

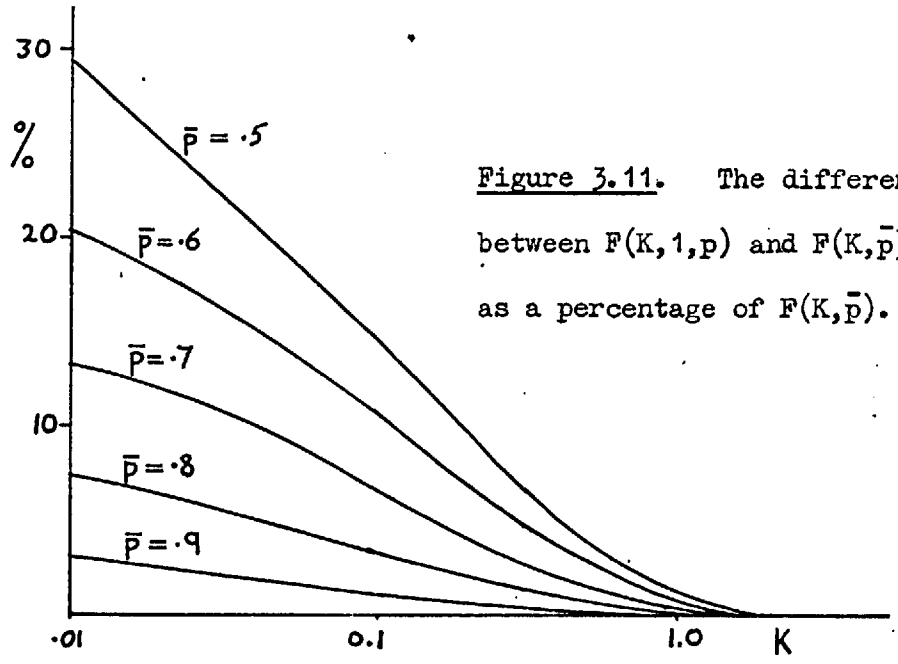

Figure 3.11. The difference between $F(K,1,p)$ and $F(K,\bar{p})$ as a percentage of $F(K,\bar{p})$.

4) Thin Wires.

The application of the simple theories of size effect resistance to wires has already been discussed (pages 38).

A rigorous treatment of the problem by the solution of the Boltzmann equation has been given by Dingle[15]. The same assumptions are made as for films, and the argument is identical up to the general solution of the Boltzmann equation (3.13). The same surface scattering model is also used to obtaining the function $C(\underline{k})$. Finding $C(\underline{k})$ and integrating to get the current is more complicated for wires than for films, and will not be discussed in detail here. The results obtained by Dingle for wires with $p = 0$ and $p = 0.5$ are given in Figure 3.12. For wires K is d/l where d is the diameter.

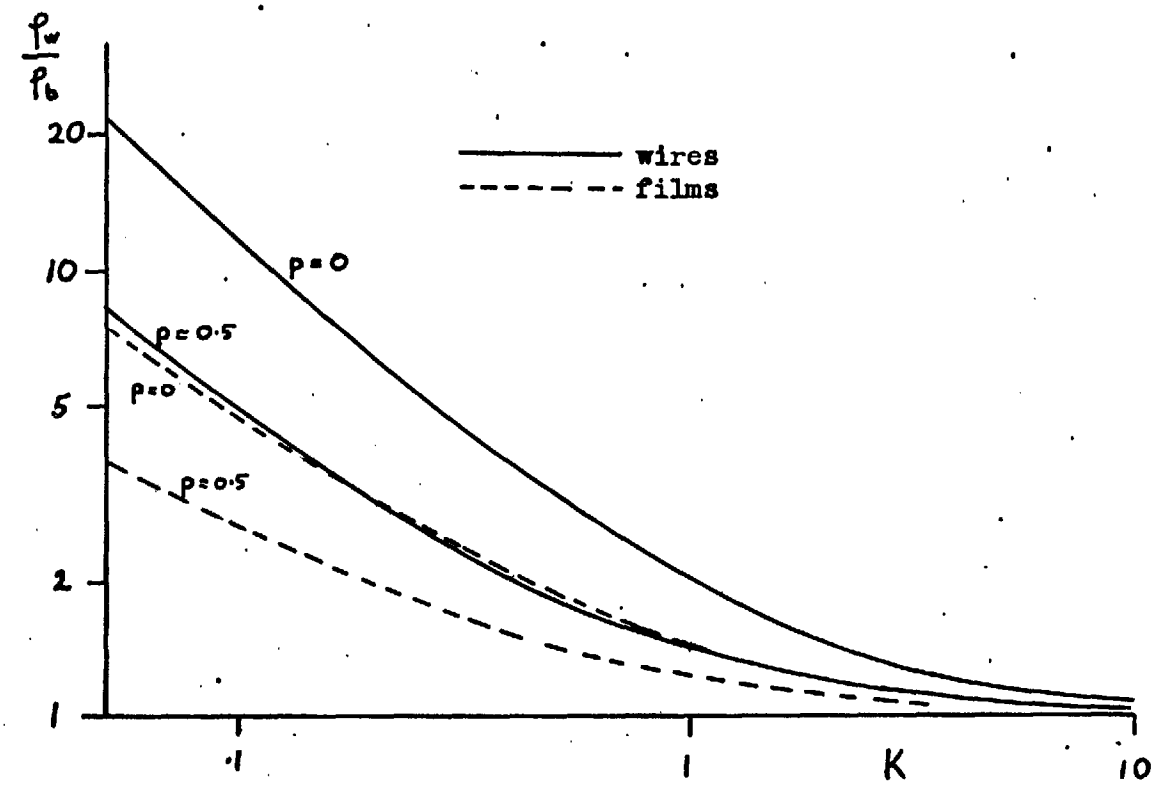

Figure 3.12 ρ/ρ_b for wires and films.

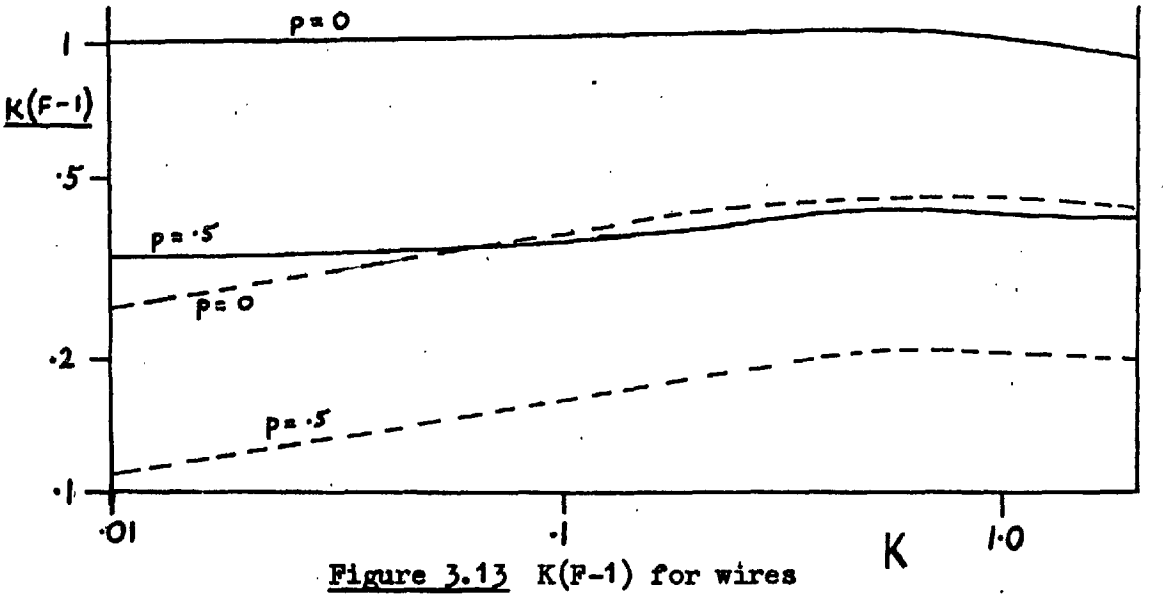

Figure 3.13 K(F-1) for wires and films compared.

Comparing Wires and Films

An instructive comparison of wires and films can be made by considering how well each obeys Matthiessens rule. It was shown for films that $K(F(K,p) -1)$ is proportional to the difference between the film resistivity and the bulk resistivity, and should be constant if Matthiessens rule is obeyed. This applies equally well to wires. The function given above is plotted in Figure 3.13 for both films and wires. The two are similar at high K, down to about K=1. Below this there is a marked difference. The wire curves remain more nearly constant than the film curves. Wires obey Matthiessens rule much better than do films at low K.

The high K limit.

The similarity between wires and films at high K is shown in their high K forms.

Films: $$\frac{\rho_f}{\rho_b} = 1 + \frac{3}{8}(1-p)\frac{1}{t} \quad . \qquad (3.53)$$

Wires: $$\frac{\rho_w}{\rho_b} = 1 + \frac{3}{4}(1-p)\frac{1}{d} \quad . \qquad (3.54)$$

If these are compared with the general formula for the small mean free path case (page 39),

$$\frac{\rho}{\rho_b} = 1 + \beta \frac{C\,p}{S} \quad , \qquad (3.55)$$

it can be seen that a β of 3/16 gives both the wire and the films results.

The low K limit

The differences between wires and films at low K are shown by the low K limits of Fuchs' and Dingle's theories:

$$\text{Films} \qquad \frac{\rho_f}{\rho_b} = \frac{1}{K \log \frac{1}{K}} \,, \qquad K \ll 1 \qquad (3.56)$$

$$\text{Wires} \qquad \frac{\rho_w}{\rho_b} = \frac{1}{K} \,. \qquad K \ll 1 \qquad (3.57)$$

As $\rho_o \propto K$ in both cases, the resistivity of the wire is constant at low K, while that of the film falls as $1/\log (1/K)$.

If an effective mean free path is defined, after Sondheimer[13], by

$$\rho_f = \frac{m v}{n e^2 l_{eff}} \,, \qquad (3.58)$$

we get for films in the low K limit,

$$l_{eff} = t \log \frac{l}{t} \qquad (3.59)$$

and for wires

$$l_{eff} = d \,. \qquad (3.60)$$

The effective mean free path increases indefinitely with l in films, though more slowly, while in wires it reaches a maximum equal to the diameter of the wire. The difference lies in the number of electrons

attaining the full mean free path. In wires such electrons occupy a spot on the 'front' of the Fermi surface of area $\sim (d/l)^2$, (where the total area of the Fermi surface is $\sim 4\pi$). The electrons over the rest of the Fermi surface have mean free paths $\sim d$. If the current is j

$$j \propto 4\pi d + \left(\frac{d}{l}\right)^2 l = 4\pi d \left(1 + \frac{d}{4\pi l}\right) \qquad (3.61)$$

i.e. the electrons in the 'front spot' contribute less as the wire become thinner. In films the electrons attaining the full mean free paths lie in a band around the 'equator' of the Fermi surface. Treated as above the current in a film is

$$j \propto 4\pi d + \frac{d}{l} \cdot l \qquad (3.62)$$

i.e. the contribution from the band round the 'equator' is of the same order as that from the rest of Fermi sphere. This approach is too crude to resolve the log term obtained by Fuchs.

CHAPTER IV

THIN FILMS FOR SIZE EFFECT STUDIES.

1) Introduction.

The theory of resistance size effects given in the previous chapter shows that the effect is only significant if K is small (~ 1 or less), where $K = t/l$, t being the film thickness and l the mean free path of the electrons in bulk material. The value of K may be reduced by decreasing t, increasing l, or both.

Specimens of small thickness have been produced by rolling bulk material (Andrew[16]), and by evaporation or sputtering methods. The latter two have been most often used, as much thinner films can be produced by these methods. The thinnest films obtained by Andrew by rolling were about 30,000Å thick, whereas evaporated films may be obtained less than 100Å thick.

The mean free path of electrons in a metal may be increased by reducing its temperature. The limit is set by the defects and impurities in the metal which determine its residual resistivity. Thus, for low temperature work, the film structure is of considerable importance.

Thin films of many metals can be prepared by evaporation and sputtering[(17)]. In the evaporation method the metal is heated strongly in a vacuum, and the metal vapour allowed to condense on the substrate. The sputtering method also involves condensation of the metal vapour, but in this case it is produced by making the metal the cathode of a glow discharge in an inert gas at low pressure. Unfortunately films prepared by these

methods usually have highly defective structures,[18,25] resulting in high bulk residual resistivities and making comparison with the normal bulk material difficult. Under some circumstances, however, it is possible to obtain single crystal films with far fewer defects. Such films are the subject of much previous work, and also of the experimental part of this work. The remainder of this chapter is devoted to a discussion of single crystal films, their preparation and their structures.

Epitaxial thin films.

When crystalline materials are grown on crystalline substrates, it is frequently observed that the axes of the overgrowth crystal are oriented in a definite way with respect to those of the substrate. This phenomenon, known as epitaxy, is observed for a wide variety of overgrowth-substrate combinations, and methods of growth. A review of the occurrences of epitaxy is given by Pashley[19].

In particular, epitaxial films of silver may be obtained by evaporation on to cleavage surfaces of various crystals, e.g. mica, rocksalt and molybdenum bisulphide[46,47,25]. It is necessary to heat the substrate to about 300°C during evaporation for good epitaxy to occur. Silver grows on mica and molybdenum bisulphide with the [111] planes parallel to the surface, but on rocksalt with the [100] planes parallel to the surface. The details of the preparation of the epitaxial silver films used in the experimental part are given in Chapter VI. Epitaxial gold films on mica are best produced by sputtering[35]. The resulting films have [111] planes parallel to the surface, as in silver films on mica.

2) Methods for the Study of the Structure of Thin Films.

The structure of thin films is examined mainly by two complementary but related techniques; electron diffraction and electron microscopy. Brief descriptions of these techniques are given below, followed by an account of the information obtained by using them. Electron diffraction is used to check the epitaxy of the specimen films used in the experimental part, and details of the experimental procedure are given in Chapter VI.

Electron diffraction.

When a beam of electrons is incident on a crystal there are diffraction maxima for only certain combinations of incident and scattering directions. The directions of the diffraction maxima are determined by the requirement that the scattered electron waves from the atoms of the crystal should reinforce each other. The Bragg approach to diffraction by crystals will first be described, then a construction which allows the diffraction directions for any incident beam direction to be determined. The details of the theory are given in the standard texts(e.g. 20).

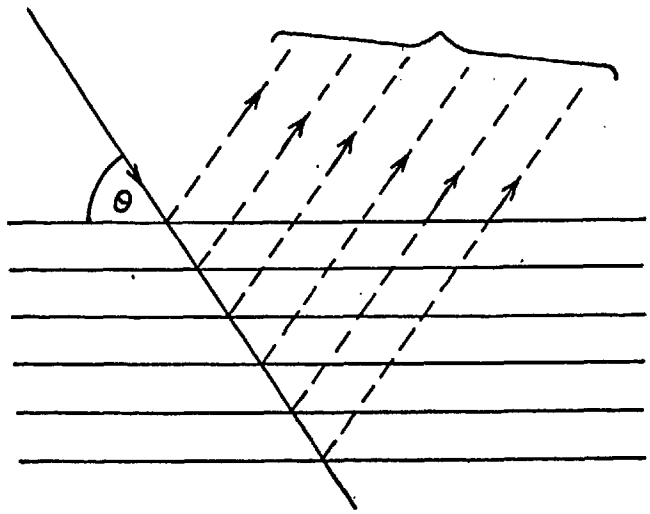

Figure 4.1

A set of crystal planes are considered (Figure 4.1). The scattered waves from a single plane are in phase when the angle of incidence equals the angle of reflection, but the waves from different planes only reinforce each other if the following condition is also satisfied:

$$n\lambda = 2d \sin\theta, \qquad (4.1)$$

where d is the separation of the planes, λ is the wavelength of the electrons and n is an integer. This is Bragg's law.

The construction mentioned above involves the reciprocal lattice (base vectors $\underline{b}_1$, $\underline{b}_2$, and $\underline{b}_3$), which is related to the direct crystal lattice (base vectors $\underline{a}_1$, $\underline{a}_2$ and $\underline{a}_3$) by:

$$\underline{b}_1 = \frac{\underline{a}_2 \wedge \underline{a}_3}{\underline{a}_1 \cdot (\underline{a}_2 \wedge \underline{a}_3)} \qquad \text{etc.} \qquad (4.2)$$

The line joining the origin to the reciprocal lattice point (h,k,l) is perpendicular to the planes in the direct lattice with Miller indices (hkl), and its length is 1/d, where d is the separation of the (hkl) planes. A line is drawn from the origin in the direction opposed to the incident beam and of length $1/\lambda$, (OC in Figure 4.2). The sphere of radius $1/\lambda$ with centre at C is the Ewald sphere (the wavelength of the electrons used is small compared with interatomic distances, i.e. $\sim 0.06\text{Å}$, so the radius of the Ewald sphere is large compared with the reciprocal lattice spacing). If the Ewald sphere passes through any point of the reciprocal lattice, P, there will be a diffraction maximum in the direction CP.

The relationship between the Ewald sphere construction and Bragg's law is also illustrated in Figure 4.2, $OP = 1/d = 2 \sin\theta/\lambda$. The

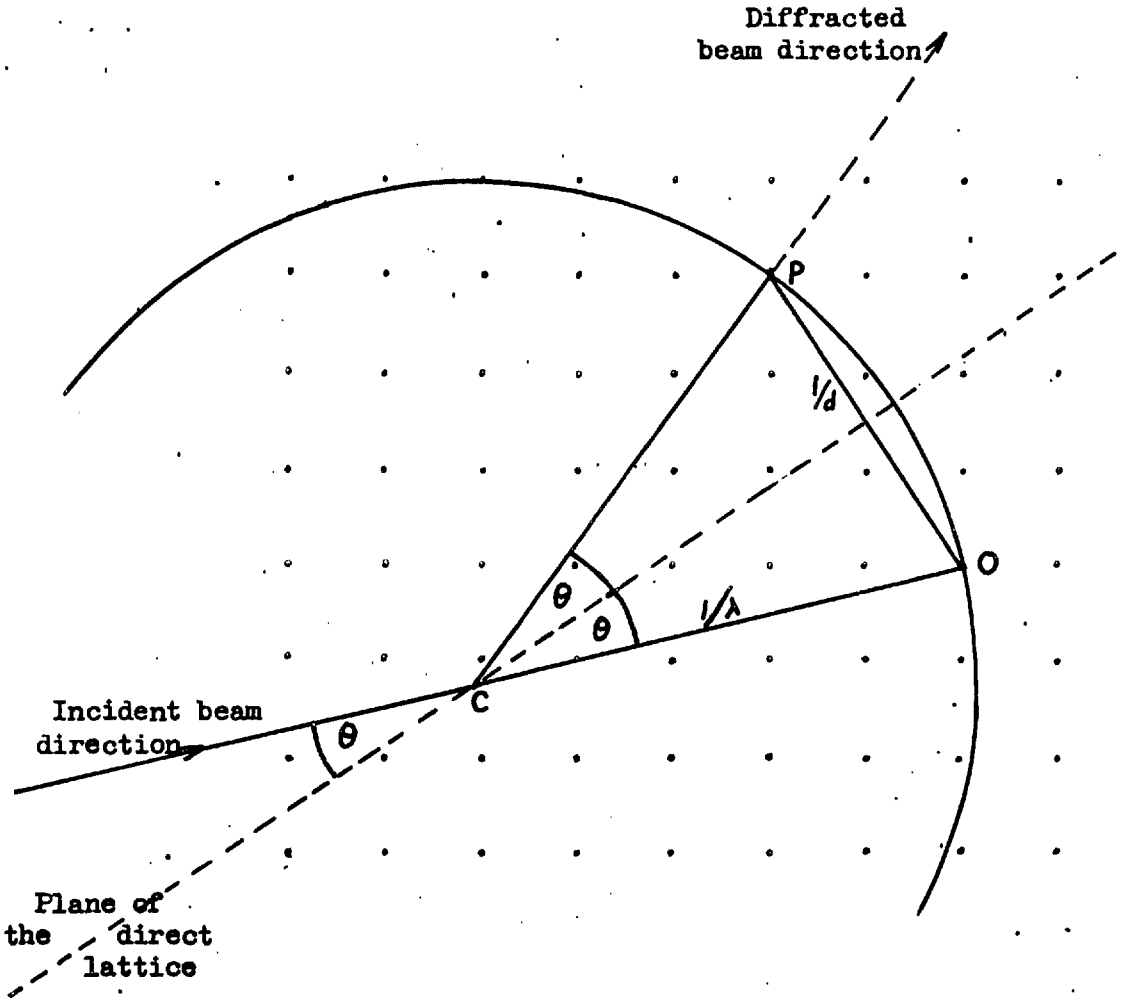

Figure 4.2 The Ewald Sphere Construction.

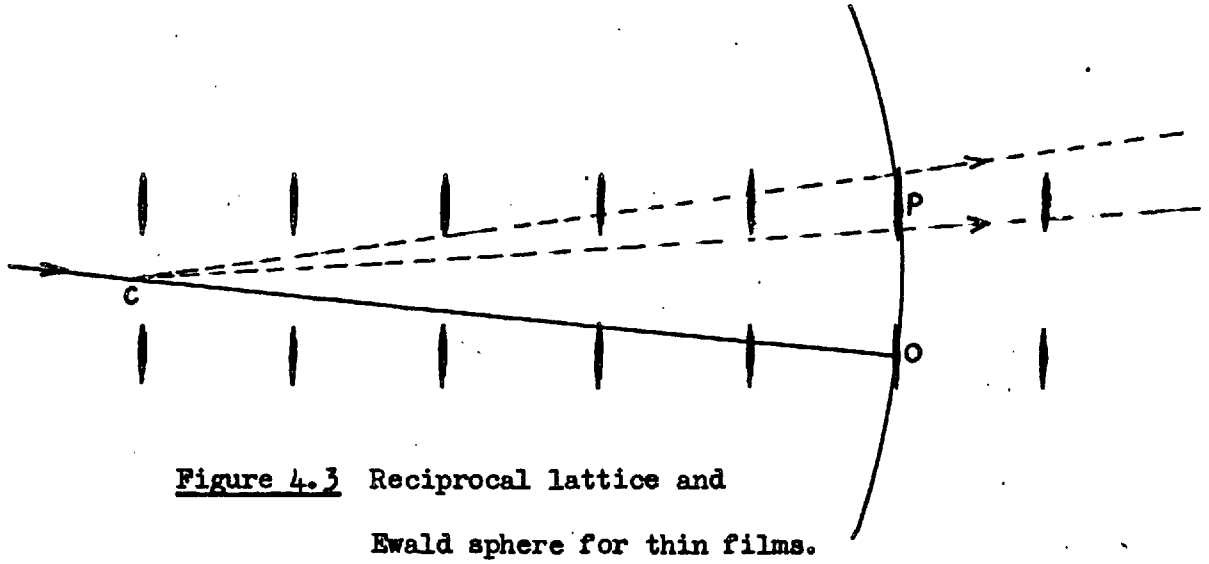

Figure 4.3 Reciprocal lattice and Ewald sphere for thin films.

diffraction maximum indicated by P is equivalent to a Bragg reflection from the corresponding set of planes in the direct lattice.

The Ewald sphere would only be required to pass through the precise reciprocal lattice point for diffraction if the crystal were perfect and of infinite extent. In the case of real crystals a diffraction maximum is obtained if the Ewald sphere passes through a region around the point. The shape and size of this region is influenced by the shape and size of the crystal. If the crystal is very thin, a few atomic layers, the region is elongated in the thin direction. This situation is illustrated in Figure 4.3.

Electron diffraction observations of films are usually made with the electron beam at a small angle to the film surface (Figure 4.4). Electrons are only scattered through small angles by atoms, so diffracted beams are only found at small angles to the incident beam. The Ewald construction shown in Figure 4.3 is for this situation. The nature of the diffraction pattern obtained depends on the degree of elongation of the regions around the reciprocal lattice points, which depends in turn on the effective thickness of the film. The effective thickness is the number of crystalline layers which contribute to the diffraction

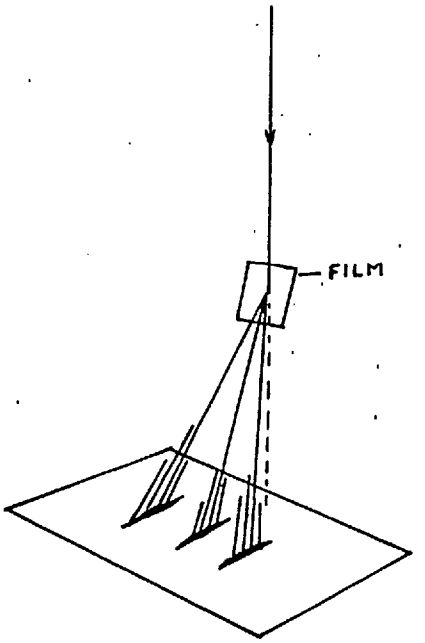

Figure 4.4

pattern. While an electron is in the film it may be scattered inelastically, after which it cannot contribute to the diffraction pattern. A measure of the possible path lengths inside the film is given by the mean free path for inelastic collisions of the beam electrons. The way in which the nature of the surface influences the effective thickness is shown in Figure 4.5. Films with flat surfaces have small effective thicknesses and the diffraction directions are spread out perpendicular to the film surface (Figure 4.3).

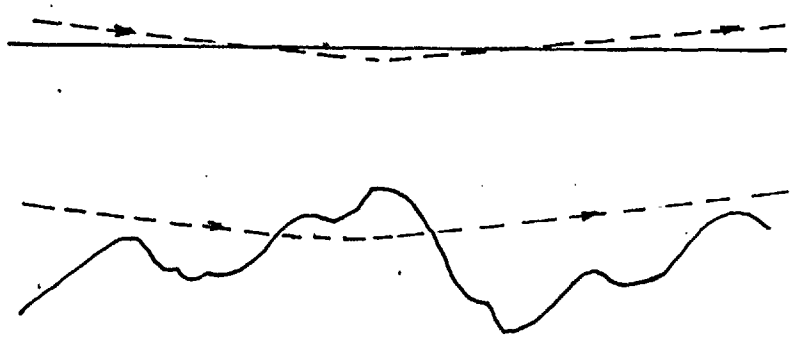

Figure 4.5. Electron penetration.

Some electron diffraction patterns for silver films are shown in Plates 1 and 2 (page 117). Plate 1 is from an epitaxial film, and the vertical streakiness indicates surface flatness. Plate 2 is from a film evaporated on to a cold mica substrate. The greater resolution of the spots suggests a rougher surface.

Electron diffraction observations show clearly the presence of epitaxy in thin films, and can be used to estimate lattice constants. They also give an indication of the smoothness of the surface of the film. The electron beam is wide on the atomic scale so all information obtained

is averaged over a relatively large area. For the detailed study of film structure the electron microscope must be used.

Electron microscopy.

The electron microscope is a most valuable instrument for the study of the structure of thin films. A small region of the film is observed, and details can be seen which are entirely lost in the averaging process of electron diffraction.

The use of the electron microscope for the study of thin films has been reviewed by Bassett, Menter and Pashley[21] and by Thun[22]. The films are usually observed by transmission techniques after removing them from their substrates. There are two basic methods for obtaining images of crystalline objects. In the first method, known as diffraction contrast, the aperture of the objective lens is restricted so that no diffracted beams are allowed to pass. Variation in contrast then occurs if there is variation in the intensity of the diffracted beam from one part of the specimen to another. In the second method, at least one diffracted beam is allowed to contribute to the image, and a periodic fringe pattern is obtained which is related to the periodicity of the crystal lattice. This is known as the lattice resolution method. The resolution of electron microscopes limits the direct application of this method to crystals with lattice spacings greater than about 5Å, so the lattices of elements and simple compounds cannot be resolved. However, the Moiré patterns that are obtained when two lattices are superimposed can be resolved. The misorientations of growing crystallites and the presence of dislocations in films can both be studied by this method.

The surface topology of films may be studied by the replica technique[23]. A layer of carbon is evaporated onto the specimen surface and reproduces the surface features. A little chromium is then evaporated on to the carbon replica from a small angle to the film surface. The specimen film material is dissolved away, and the shadowed replica observed in an electron microscope. Shadowing is used as the image contrast from an unshadowed carbon replica is poor.

3) The Growth and Structure of Epitaxially Evaporated Thin Films.

Growth

Electron diffraction and electron microscope work have yielded a clear picture of the way in which epitaxial films grow[19,25]. The first detectable stage of the deposition is the formation of three dimensional crystalline nuclei scattered over the surface of the substrate. These nuclei are mainly well oriented with respect to the substrate[26,27]. The nuclei grow with the arrival of more material, becoming island crystallites. When two crystallites grow close together they coalesce very quickly in a liquid-like fashion. The crystallites eventually link up over the whole surface leaving only holes. Further deposition fills in the holes and thickens the film.

The above details of the initial stages of film growth can be observed directly in the electron microscope. A recent study of the growth of gold and silver films on molybdenum bisulphide by Pashley, Stowell, Jacobs and Law[24] brings out many details of the growth of evaporated thin films. The films were evaporated inside an electron microscope on to a flake of substrate thin enough to allow the transmission of the electron beam. The growth of the films could then be observed continuously. The Moiré

patterns obtained between the substrate lattice and the metal lattice were interpreted to reveal the following orientational aspects of film growth. The small crystallites found in the early stages of growth are not perfectly oriented with respect to the substrate. Misorientations are typically one or two degrees. When the crystallites are still small the misorientation between a coalescing pair is eliminated by the rotation of one or both, presumably by recrystallization. Misorientations between larger coalescing crystallites are not eliminated, and must be taken up by dislocations. The defects produced in this way become permanent features of the film.

The substrates on which epitaxial deposits are formed usually have lattice spacings significantly different from those of the overgrowth materials. Electron diffraction work has shown that, in spite of this, the overgrowth has its normal bulk lattice spacing even at the earliest detectable stage[26,27,28]

Defects in epitaxial thin films.

The presence of structural defects in films is clearly observable by electron microscopy[21,29,31]. Dislocations and stacking faults are shown up by the diffraction contrast technique, and dislocations by the Moire pattern technique. Bassett et al.[21] describe the methods used, and present some results for [111] gold films evaporated on to epitaxial silver films, and separated by dissolving the silver in nitric acid. Dislocation lines are present in large numbers, estimated at between 10^{10} and 10^{11} cm/cm^3. They are inclined to the plane of the film at ~70°, i.e. they lie in [111] planes, and extend from surface to surface.

Similar results were obtained by Matthews[29], who used [100] silver

films which had been evaporated on to rocksalt. He estimated that the dislocation density lies between 1.10^{11} and 3.10^{11} cm/cm^3. It is interesting to note that the above values for dislocation densities are similar to the value obtained by Baily[30] for cold worked silver. Rolling to 95% reduction resulted in a dislocation density of about 5.10^{11} cm/cm^3.

The origin of defects in thin films.

Several mechanisms have been suggested for introducing imperfections into epitaxial thin films. These are listed by Pashley[25] who considers that the most important are the presence of misorientations in the early stages of growth, which have already been mentioned, and displacement misfits. Displacement misfits arise between two growing crystallites as a result of the difference in lattice spacing between the film material and the substrate. The extended lattices defined by the two initial nuclei do not, in general, coincide. The difference must be taken up by defects when the crystallites coalesce.

The electron microscopy work described has been mainly on very thin films, usually little thicker than required for complete coverage of the substrate. It is to be expected, however, that the dislocation structure will largely persist, as the substrate for subsequent layers is the highly defective initial layer.

Film surfaces.

The electron diffraction patterns obtained from epitaxial silver films have streaks rather than spots, indicating that the surface is flat on a near atomic scale over much of its area. The streakiness of the diffraction spots shows that the depth of penetration of the electrons

is only a few atomic layers, perhaps only one or two as suggested by Newman and Pashley[46].

Further information about the surfaces of the epitaxial silver films used in the experimental part of the present work is provided by the replica technique. Carbon replicas of some of the specimens used were prepared and examined by C. Gonzales[32] and they show that the surfaces have large flat areas with occasional steps of a few tens of angstroms and occasional pits. These results are discussed in greater detail in Chapter IX.

Summary

The results described in this chapter provide a picture of epitaxial thin films of silver and gold which may be summarized as follows:

(a) The films are well oriented with respect to their substrates.

(b) The lattice spacing is as for the normal bulk material.

(c) They have large numbers of dislocations, comparable with the numbers found in heavily worked bulk material.

(d) The free surface of a film is nearly atomically flat over most of its area.

CHAPTER V

PREVIOUS EXPERIMENTAL WORK ON RESISTANCE SIZE EFFECTS.

In this chapter some previous measurements of the electrical resistance of small specimens are described. The emphasis is mainly on films of the noble metals, particularly single crystal films, as these are most relevant to the present work. Other types of film, and wires, are also discussed in an attempt to provide a wider picture. The work is grouped according to the type of specimen involved.

Rolled foils.

Specimens produced by rolling have thicknesses much greater than the mean free path of electrons at room temperature, so size effects can only be obtained at low temperatures. Andrew[16] measured the resistivity of foils of tin with thicknesses down to 3.3μ, and obtained size effects at temperatures below about 20°K. At each temperature the resistivities of the thicker foils were independent of thickness, giving a value which could be taken as the bulk resistivity, while those of the thinner foils increased with decreasing thickness. The results could be roughly fitted to Fuchs' theory with p = 0, giving a value for the mean free path. The resistivities of the thinner foils were a factor of ten greater than the bulk value at 3.8°K, indicating a K (= thickness/ mean free path) of less than 0.1. The values obtained for the mean free path at the three temperatures were 0.1 mm. at 3.8°K, .005 mm. at 14°K and .002 m m. at 20°K.

Alkali Metals.

Mayer[14] has shown that it is possible to obtain films of alkali

metals which have reproducible electrical properties. The films are prepared by evaporating the metals ontoa glass substrate cooled to about 90°K. Lovell[10,33] also evaporated films onto a cooled substrate and observed changes in the film resistance after evaporation was complete. Mayer avoided these effects by the use of a very high vacuum (10^{-9} torr) and a very pure source metal.

The resistivities of caesium, potassium and rubidium films in the thickness range ~ 100Å to ~ 5000Å were measured. The bulk resistivity (ρ_b) was obtained from the results for the thicker films, and the reduced resistivities (ρ_f/ρ_b) fitted to Fuchs' theory with p = 0. Although the films were quite thin the lowest value of K reported was 0.15. The agreement with Fuchs' theory was quite good and values for the mean free path at 60°K and 90°K were obtained.

Films deposited at low temperatures can be expected to have a highly defective structure. This is shown up in Mayer's films by the values obtained for the bulk resistivity, which are significantly higher than for the normal bulk material. The bulk resistivities estimated for potassium films were 1.3μΩ-cm at 60°K and 2.1μ Ω-cm at 90°K. The corresponding ideal lattice bulk values are 0.6 and 1.2 respectively. (MacDonald[34]).

Silver and gold films.

It was shown in the previous chapter that evaporated or sputtered films, in the early stages of their growth, are a collection of isolated crystallites. In this condition the film resistivity is very high and remains so until there is a substantial amount of interconnection of the crystallites. The change from the high resistivity, characteristic of the 'island' state, to the much lower value, characteristic of a

continuous film, occurs for quite a small increase in the average thickness of the deposit. The point at which this rapid change occurs varies considerably with the method of preparation.

Chopra, Bobb and Francombe[35] give results of resistivity measurements on gold films which show the onset of conductivity. This occurred at ~160Å for single crystal films sputtered on to heated mica. When the measuring voltage was applied during the sputtering process, the onset of conductivity did not occur until 300Å. Results given by Ennos[36] for gold films evaporated on to an evaporated layer of bismuth oxide on glass show a much earlier onset of conductivity, at about 40Å.

If evaporated or sputtered films are to be used for size effect studies, they must be thick enough to be outside the range of the structural effects associated with the early stages of growth.

The resistivities of continuous films vary considerably with the method of preparation. Reynolds and Stillwell[37] showed that, when films are evaporated on to a room temperature substrate, the rate of evaporation and the pressure of the residual gas in the evaporation chamber are important parameters. The lowest film resistivities were obtained using a high rate of evaporation and low residual gas pressure. An increase in film resistivity by a factor of five could be obtained by lowering the evaporation rate or raising the pressure. The results for silver films of the low resistance type in the thickness range 100 - 1500Å, measured at room temperature, gave a mean free path of about 500Å when compared with Fuchs' theory for p=0. This value is in good agreement with that obtained from the free electron model assuming one conduction electron per atom.

As films evaporated on to a cold substrate have many defects, it is reasonable to attempt to reduce the bulk resistivity by annealing. This approach was successfully adopted by Gillham, Preston and Williams[38,39] who used sputtered bismuth oxide on glass as a substrate. Gold was sputtered on to the substrate while it was at room temperature, then the film was annealed at 450°C. Films only 50Å thick, prepared by this method, had low resistivities. A further reduction in resistivity was obtained by coating the free surface of the gold film with sputtered bismuth oxide before annealing. The resistivity of the bulk material was estimated from the results for the thicker films (400 - 800Å), and was found to be significantly higher than the accepted value for pure gold, i.e. 3.6μ Ω-cm compared with 2.48μ Ω-cm. This shows that many defects must have remained after annealing.

The most striking feature of this work is the low resistivity of the very thin films. At room temperature a film of thickness 55Å had a resistivity of 4.8μ Ω cm. A reasonable value for the bulk mean free path is over 200 Å, making $K \sim 0.25$. In order to explain the small size effect on the basis of Fuchs' theory it is necessary to assume that p lies between 0.8 and 0.9.

The resistivity of gold films is also the subject of a paper by Chopra, Bobb and Francombe[35]. They measured the room temperature resistivity of films obtained both by sputtering and by evaporation on to freshly cleaved mica substrates. A polycrystalline film was obtained with the substrate at room temperature, and an oriented single crystal film obtained when the substrate was heated to about 300°C during deposition. The thickness range covered was 100 to 1000Å. The results were similar to

those obtained by Gillham et al. in that the resistivities of the unannealed (polycrystalline) films were considerably higher than those of annealed (single crystal) films. The results for the polycrystalline films could be fitted reasonably well to Fuchs' theory with p=0. The single crystal sputtered films had constant resistivity, about 6% above the value for pure bulk gold, down to 250Å. This is only 100Å above the thickness of the onset of conductivity. Both polycrystalline and single crystal evaporated films had higher resistivities than the corresponding sputtered films. The thick film resistivity of evaporated epitaxial films was 20% above the pure bulk value.

It is of interest to see what extra resistivity might result from the dislocation density estimated by Pashley for gold films discussed in Chapter 4. The effect of dislocations on resistivity is reviewed by Bamzinski, Dugdale and Howie, [40] who give values for the increased resistivity per cm. of dislocation in various metals. The value for gold, taken with the limits on the dislocation density given by Pashley, results in an increased resistivity of between 0.003 and 0.03μ Ω-cm. The larger value is still a factor of five too small to explain the increase found in the best of Chopra's films. This comparison must be treated with caution, however, as the films were prepared in different ways

The curves obtained by Chopra et al. and Gillham et al. for gold films are given in Figure 5.1. Some room temperature results for silver films, obtained in the course of the present work, are included in this figure. To allow comparison of the gold and silver results the curves are plotted in a reduced form, i,e. as ρ_f/ρ_1 against thickness, where ρ_1 is the ideal lattice resistivity of the metal at room temperature.

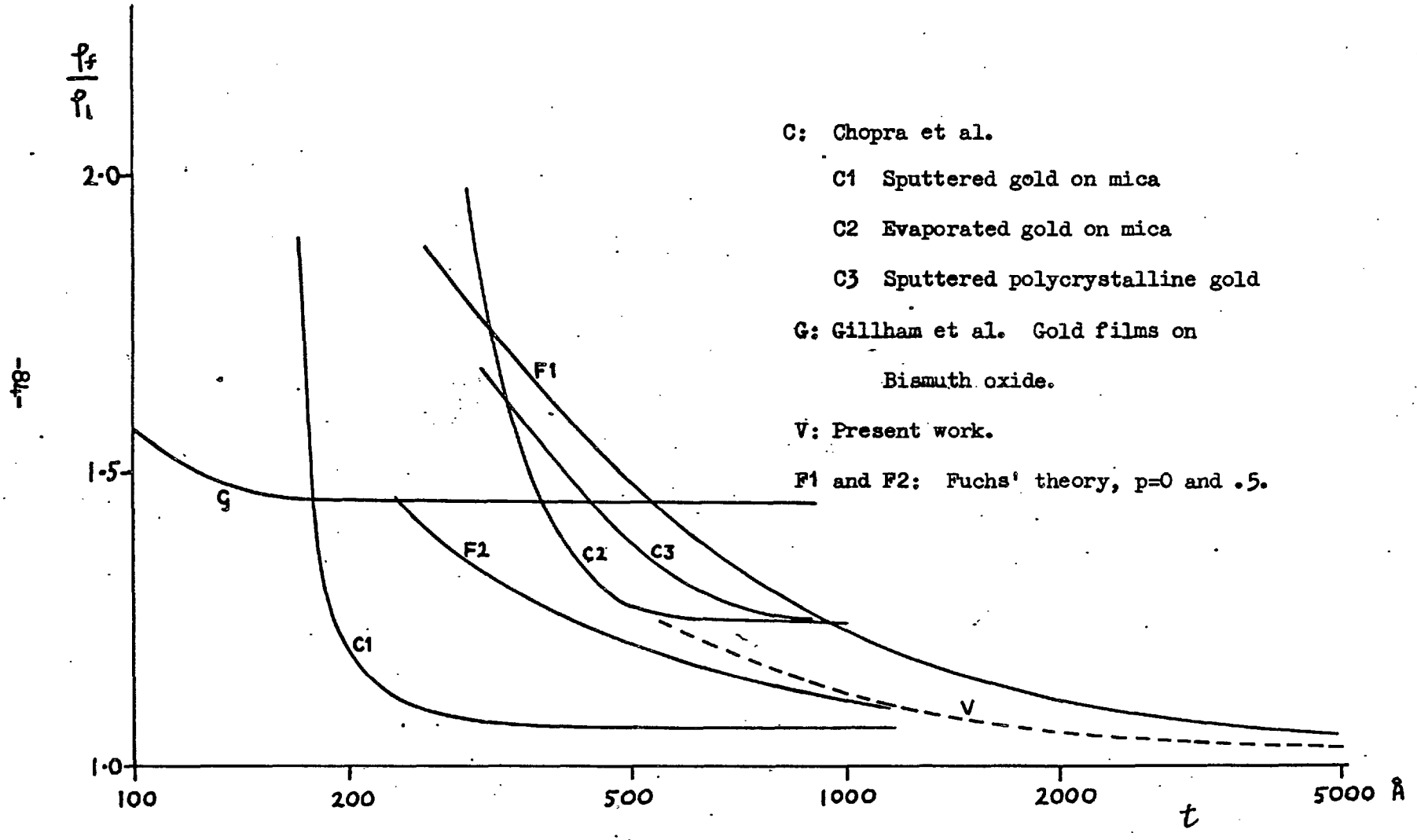

Figure 5.1 Reduced room temperature film resistivities.

The work on gold films on mica was extended to lower temperature and thicker films by Chopra and Bobb[41]. They showed that the temperature coefficient of resistivity of single crystal sputtered gold films, down to 78°K, is consistent with Fuchs' theory with p = 0.8. The films used were up to 5000Å thick.

An interesting demonstration of the presence of partially specular scattering at the surface of gold films evaporated on to bismuth oxide was given by Lucas[43]. Taking annealed films as a starting point he evaporated a further layer of gold on top, while recording the resistance continuously. The resistance went up, at first, even though the film was getting thicker. This effect was interpreted as being caused by the lower value of p at the new, unannealed, surface.

Low temperature resistance measurements on epitaxial silver films have been reported by Larson and Boiko[44]. The films were prepared in the usual way, but with a very high vacuum (5×10^{-8} torr). The film resistivities were measured at room temperature and 4.2°K, and the thickness range covered was 600 to 13000Å. The thicker films had resistivity ratios ($\rho_{300}/\rho_{4.2}$) as high as 175. No low temperature measurements of epitaxial gold films have been reported, but the high bulk values found by Chopra et al. at room temperature indicate that the resistivity ratios would be no more than 17. The low temperature silver results were found to fit reasonably well to Fuchs' theory with p = 0.5.

Chopra[42] measured the variation of resistivity with temperature of silver films at low temperatures. The films he used were quite thick, 15,000 to 60,000Å, both epitaxial and polycrystalline. The epitaxial films showed a twofold increase in resistivity in the temperature range

8 - 10°K (Figure 8 page 164) a smaller increase in the same range was found for polycrystalline films. In order to explain this effect Chopra took up a suggestion made by Olsen[45]. This was that the low angle scattering of electrons by phonons of small wave number, which predominate at low temperatures, should be more effective in promoting resistivity in the presence of a diffusely scattering surface. This subject will be considered again in later chapters, and will be referred to as the phonon-surface effect.

Thin wires

As wires cannot be made very thin the size effect can only be observed by using very pure metals and making measurements at low temperatures. Measurements on pure mercury wires were made by Andrew[16] and the results evaluated by Dingle[15] in the light of his theoretical treatment of resistance size effects in wires. The results were in agreement with the theory with p=0, though the accuracy was not good enough for this value to be certain. The thinner wires did not obey Matthiessen's rule, whereas the theory indicated that they should.

The failure of Mattiessen's rule for thin wires was also observed by Olsen[45] using pure indium wires. This result was the reason for his suggestion that the phonon-surface effect mentioned above might be important.

Conclusion.

The work described in this chapter shows that resistance size effects occur quite generally in small specimens, and that the results obtained can often be explained in terms of Fuchs' theory. The existence of surfaces from which electrons are partially specularly

scattered has also been demonstrated.

The work of Olsen and Chopra has raised the question: what part does low angle phonon scattering play in resistance size effects at low temperatures?

CHAPTER VI

EXPERIMENTAL METHODS

This chapter describes the various experimental methods, used in the course of this work, for the preparation, examination and measurement of thin silver films.

1) Preparation of Specimens.

The thin film specimens were prepared by evaporating, in a vacuum, pure silver from a basket shaped tungsten filament on to a heated mica substrate. The silver used was Johnson Matthey 'spec-pure' (99.999%). A diagram of the evaporation set up is given in Figure 6.1. It is based on an Edwards evaporating unit which has a 4 inch oil diffusion pump to evacuate the evaporation chamber.

The filament is wound from 0.5 mm. tungsten wire, and is heated by passing a current of about 20 amp through it. Before a new filament is used for evaporation, it is outgassed by heating it in a vacuum for a few minutes at a current higher than that used for evaporation.

The hot stage.

The stage on which the substrate rests during evaporation is constructed from 'spec-pure' copper, as normal commercial copper contains impurities which may evaporate when the stage is hot and contaminate the film. (Pashley[47]). The stage is heated electrically by a constantin heater, insulated by mica and sandwiched between two pieces of copper. The temperature of the stage is measured using a copper-constantin

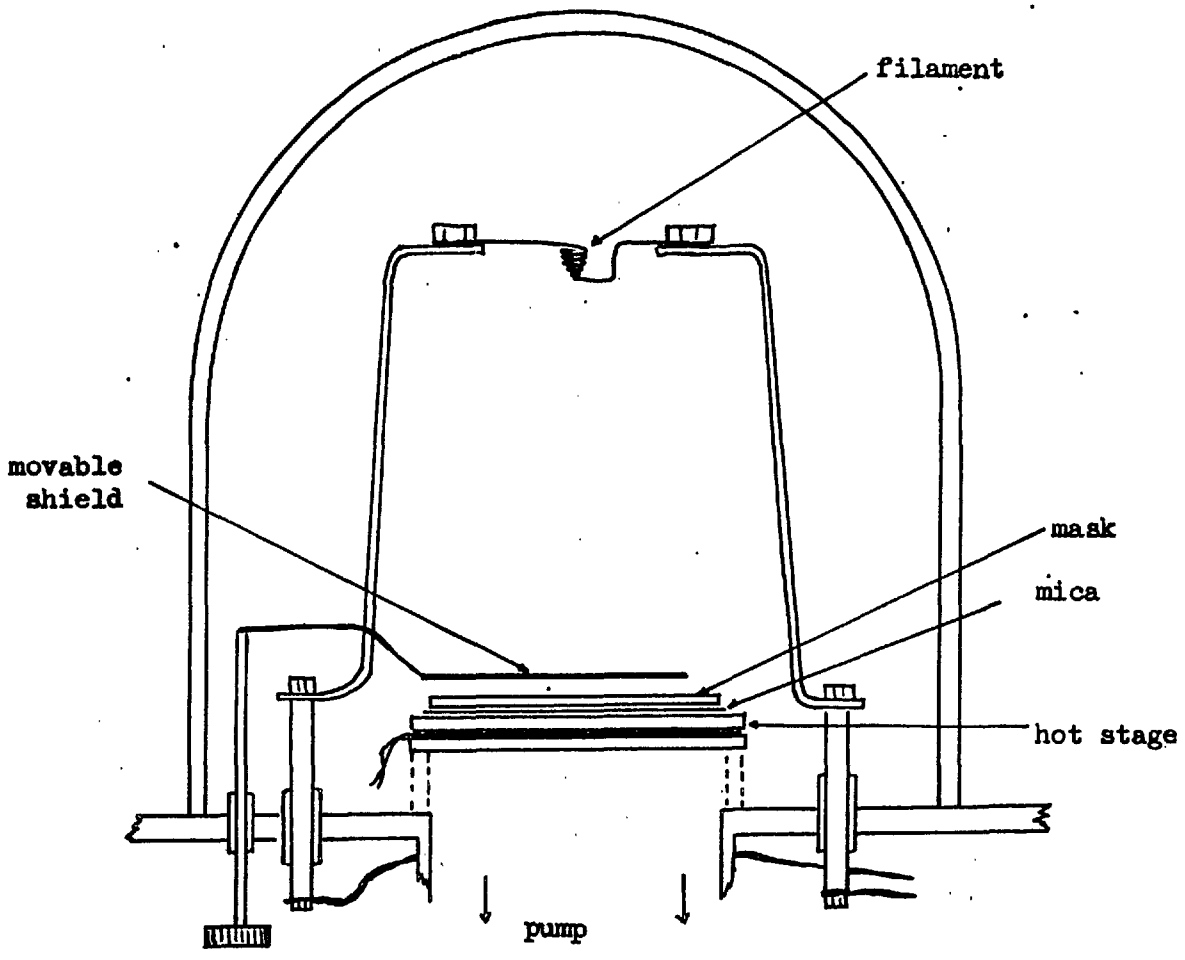

Figure 6.1 Evaporation chamber.

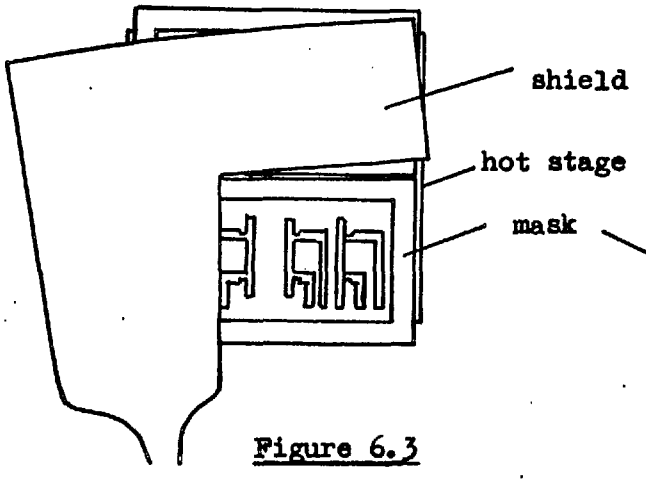

Figure 6.3

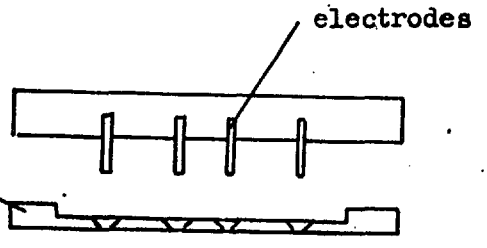

Figure 6.2

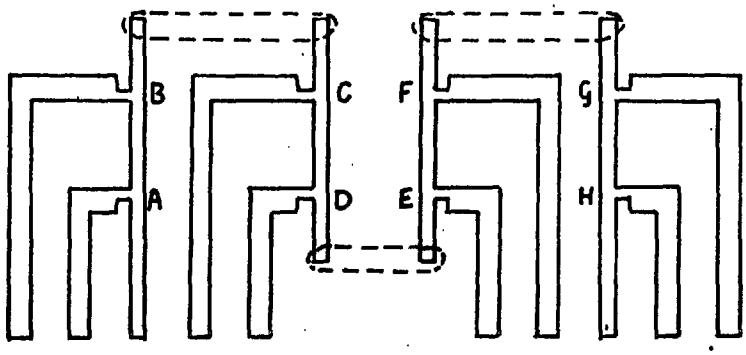

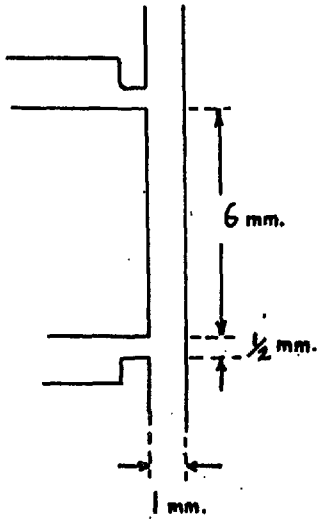

Figure 6.4

Arrangement of specimen set.

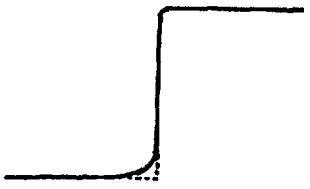

Figure 6.5 Specimen edge.

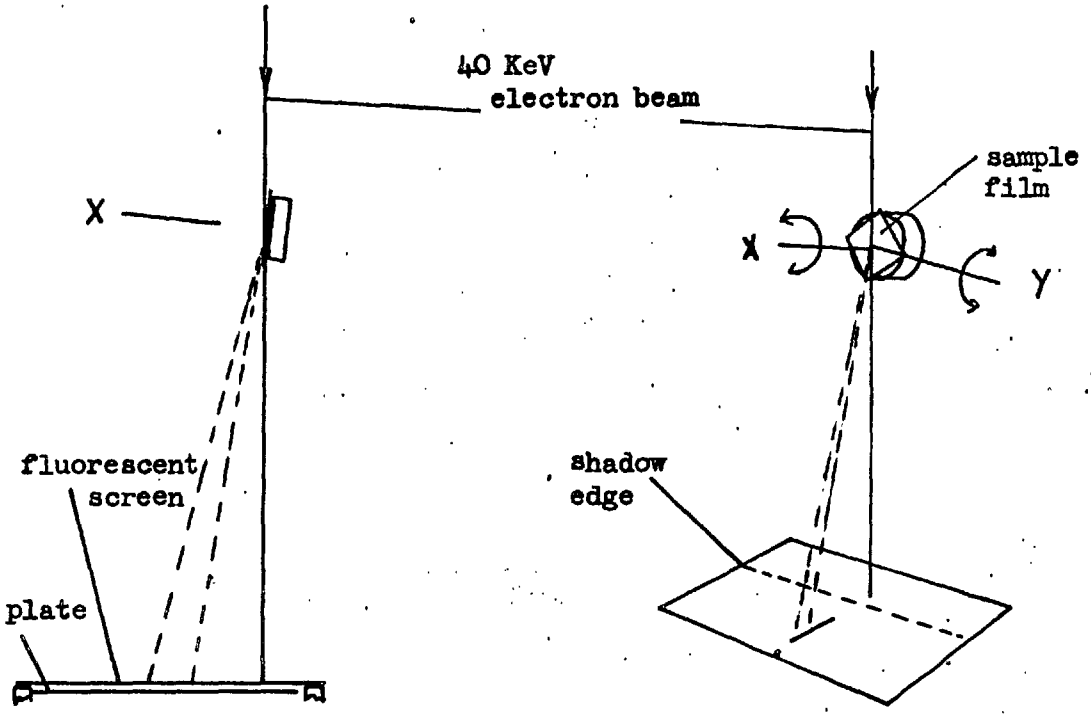

Figure 6.6 Electron diffraction.

thermocouple attached to the upper copper plate.

The Masks.

In order to obtain thin film specimens of a shape suitable for resistance measurements, a mask is placed over the mica substrate during evaporation. It is required that the edges of the specimens should be sharp, so the edges of the mask must be thin and lie close to the surface of the mica. A mask of thin material satisfies the former condition, but cannot be kept flat enough to be close to the mica at all points.

The problem was solved by making the masks from thick material and thinning the regions near the specimen apertures. The starting material was 3 m.m. thick 'spec-pure' copper sheet. A central rectangle was milled down to 1mm. thick leaving a border of the full thickness for rigidity. The apertures were made in the central region by spark etching, with the help of Standard Telecommunications Laboratories Ltd. When an arc discharge occurs between two metal electrodes immersed in a dielectric liquid, such as paraffin, some material is removed from the electrodes, mainly from the anode. This process is exploited in the spark etching method of shaping intricate pieces of metal. A suitably shaped cathode is lowered on to the workpiece (the anode) and etches its way through by repeated arc discharges. The breakdown through the paraffin occurs when the separation between the electrodes is very small (~0.001"), and the result obtained closely follows the shape of the cathode. Sections through a mask and one of the electrodes used in producing it are shown in Figure 6.2. The electrodes were made from 'Elkonite', an alloy made by Johnson Matthey Ltd.

The Substrate

Mica has been used throughout this work as a substrate for the evaporated silver films as it has two important advantages, i) Silver film evaporated on it are epitaxial. ii) It can be cleaved to give large fault free areas, which are essential for resistance measurements. The mica is freshly cleaved before use to minimize surface contamination. Pieces suitable for substrates are obtained as follows. A sheet of mica about 2 inches square is carefully cleaved using a fine needle. The quality of the cleavage surfaces is checked by joining the two surfaces again, but slightly displaced from their original position, and looking at the white light fringes formed between them. Fault free areas join very closely and show no fringes. A fault produces two close steps in the thickness of the air films between the surfaces, and these are shown up very clearly by the white light fringes. Although the white light fringes cannot be expected to show steps less than about 2500Å, the method appears to give good results. No faults have been observed on specimen films during the course of the interferometric thickness measurements described later in this chapter. The two pieces of mica are left in contact until required for evaporation, not more than an hour later.

The Evaporation.

Each mask produces four specimens on a single sheet of mica. The four specimens on one sheet will be referred to as a 'specimen set'. Two specimen sets are evaporated together. The sheets of mica are placed on the stage with the masks over them. A smaller piece of

freshly cleaved mica is placed on the masks to provide a sample for electron diffraction observations. A length of 2mm. silver wire (between about $\frac{1}{2}$ cm. and 3cm. depending on the specimen thickness required) is placed in the tungsten basket. The evaporation chamber is pumped down to below 10^{-4} mm Hg and the current to the stage heater is switched on. The evaporation is performed when the temperature of the stage is between 320 and 330°C.

There is a movable shield which is controlled from outside the evaporation chamber and can be moved above the masks (Figure 6.3). With the shield fully covering the specimen apertures the filament is heated just sufficiently to melt the silver, so the silver can outgas without contaminating the surface of the mica. The masks are then fully exposed and evaporation commenced. Variation in the thickness of the specimens is achieved by moving the shield stepwise across the masks. The shape of the shield is such that one mask can be exposed alone if required. After evaporation is complete, the stage is allowed to cool to near room temperature before air is admitted to the chamber.

If the surface of a specimen set is to be modified this can be done by means of a second evaporation, using only a small amount of material to produce a thin additional layer.

The Specimens.

The shape and size of films obtained through the masks in shown in Figure 6.4. There are four specimens AB, CD, EF and GH, each with a pair of potential leads which go to the edge of the mica sheet. The current circuit A to H is completed by painting on a silver suspension ('Dag' silver

in M.I.B.K, manufactured by Acheson Colloids Ltd.) as indicated by the dotted lines. This dries to give a conducting layer.

In order to obtain the thickness of the film from the high temperature resistance measurements, the ratio of the distance between the mid-points of the potential leads (d) and the width (w) is required. These dimensions are obtained for each specimen using a travelling microscope and viewing the specimens in reflected light, when the edges can be clearly seen. The edges of the specimens are not so clear when viewed in transmitted light, as some silver spreads a little way under the edge of the mask, giving a section of the type shown in Figure 6.5.

The accuracy of the ratio d/w depends mainly on w, the smaller of the two distances. The width is measured at at least two points and these rarely differ by more than 1%. The mean is taken for w. The error in d contributes at most 0.3% to the error in d/w.

Storage of Specimens.

Between preparation and measurement, a period of a few days, the specimens are kept in dry air is a dessicator, with silica gel as the drying agent. Specimens stored in this way show no visible signs of change even after several months, while any left in the open air soon become discoloured.

2) Electron Diffraction.

The electron diffraction patterns from the surface of a thin film provide a useful check on the epitaxy, and to some extent on the surface flatness, of the film. In this work the electron diffraction observations were usually made on the sample film produced with the specimens for this purpose.

A diagram of the arrangement of the electron diffraction camera is given in Figure 6.6. A piece of the sample about 5mm. square is attached to a flat metal support with 'Aquadag' which also provides a conducting path from the film, to prevent it becoming charged by the electron beam. The specimen support is clamped on a mounting which allows the specimen to be rotated in its plane and also about an axis perpendicular to the beam and in the plane of the film (Figure 6.6 axes X and Y respectively).

With the specimen in position the electron diffraction camera is evacuated to a pressure of about 10^{-3}mm Hg and the beam switched on. The diffraction pattern is visible on the fluorescent screen. The specimen is rotated about the Y axis to bring the shadow edge to a suitable position, roughly as in Figure 6.6. It is then rotated about X until the spot or line pattern appears. This is recorded on the photographic plate by raising the fluorescent screen for a few seconds.

Examples of diffraction patterns from epitaxial silver films are shown in Plates 1 and 2, page 117.

3) The Low Temperature Apparatus.

The thin film resistance measuring apparatus was built to fit into an existing glass cryostat. The general arrangement of the apparatus is shown in Figure 6.7. The outer dewar is for liquid nitrogen and the inner one for liquid helium.

A two can system is used to cover the temperature range between 4.2°K and about 300°K. The outer can is cooled by liquid helium or liquid nitrogen and the space between the cans evacuated. The inner

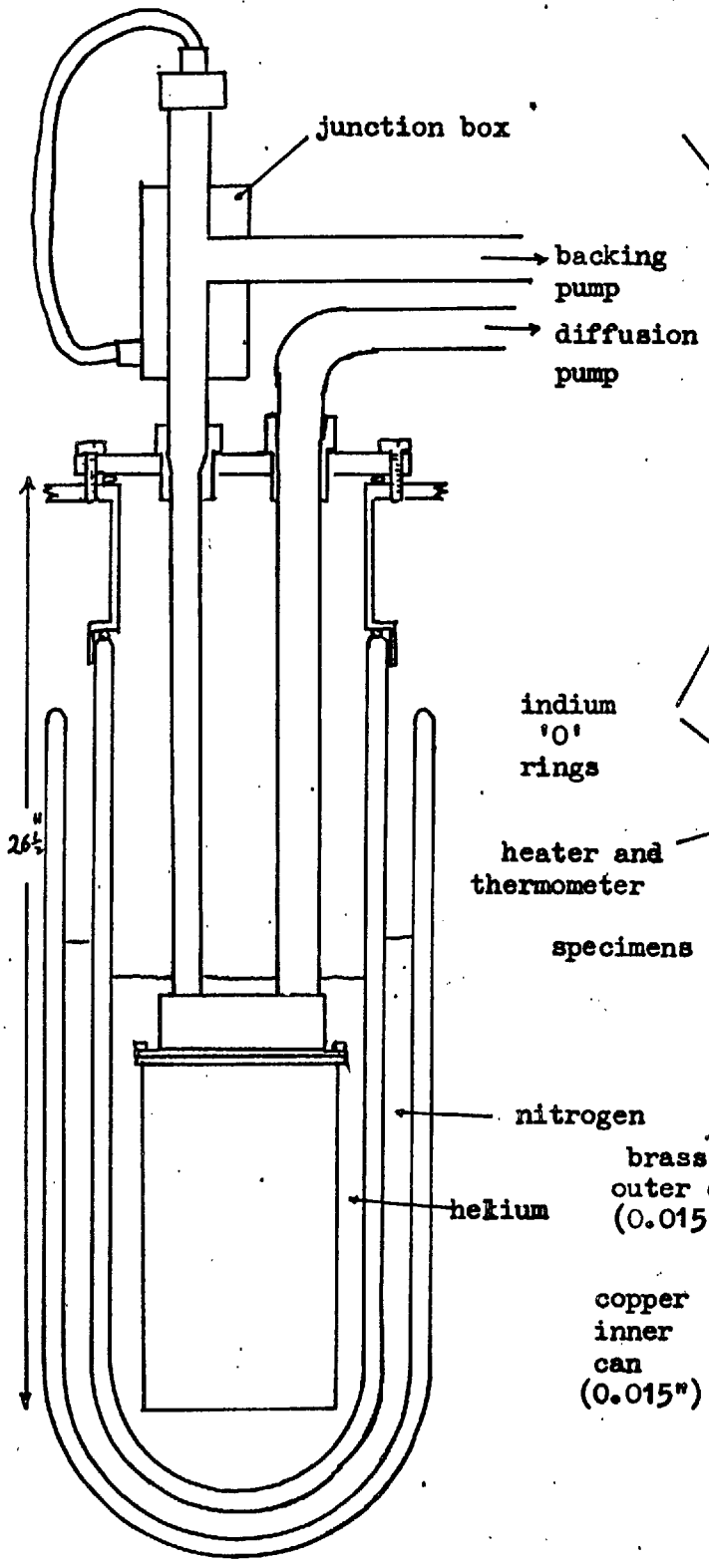

Figure 6.7

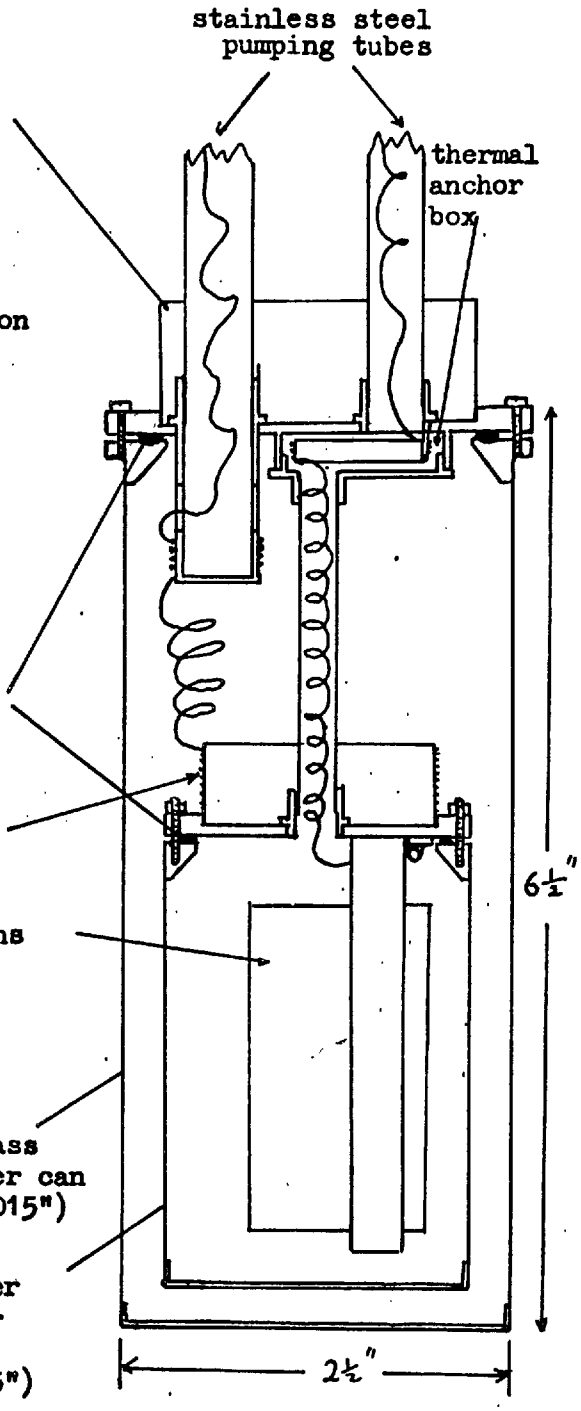

Figure 6.8

can may then be maintained at some temperature above that of the outer can by supplying just sufficient heat to balance the losses.

The arrangement of the cans is shown in Figure 6.8. They are supported from the brass top plate by two thin walled (.006") stainless steel pumping tubes. The $\frac{1}{2}$" diameter tube is connected at its top end to an oil diffusion pump and leads directly to the inter-can space. The smaller tube ($^3/_{16}$" diameter) is connected to a backing pump, and leads to the inner can via the inner cans support tube.

Both cans must be vacuum tight so some form of demountable vacuum joint is required. Indium 'O' rings are used as they are both convenient in use and avoid the heating required by solder joints with the attendant risk of damage to films, wires and other permanent solder joints. The 'O' rings are freshly made each time from 1/16" indium wire. The ends of the wire are overlapped and the ring compressed by a set of 12 6BA screws between a flat surface and a shallow 'V' groove, as shown in the detail of Figure 6.8.

The brass outer can has on top a 1 inch high container made from sheet copper. This holds liquid nitrogen to cool the cans to about 78°K.

The inner can.

The inner can is supported from the thermal anchor box in the top plate of the outer can by a $\frac{1}{4}$" diameter thin walled stainless steel tube. This can is constructed mainly of copper to ensure uniformity of temperature. A sheet copper cylinder soldered to the top of the can has wound on it a 200 Ω heater of 42 S.W.G. constantin wire, and also a copper resistance thermometer of 46 S.W.G. enamelled copper wire which has a room temperature resistance of about 185 Ω. The wires connecting

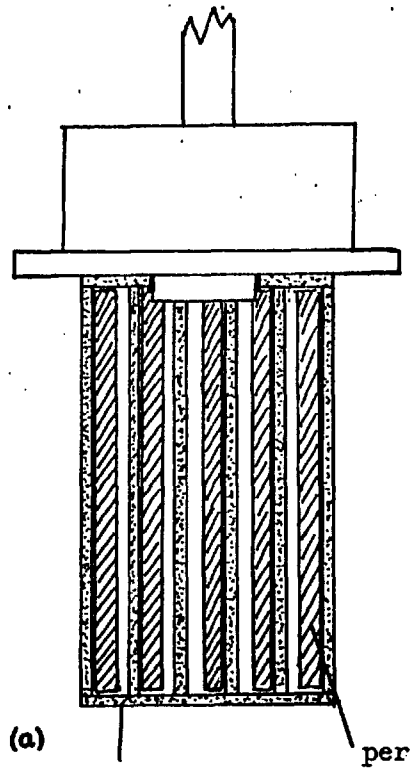

(a)

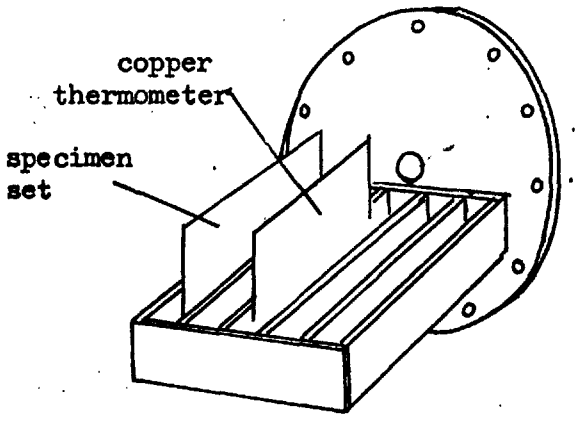

(b) Perspective view

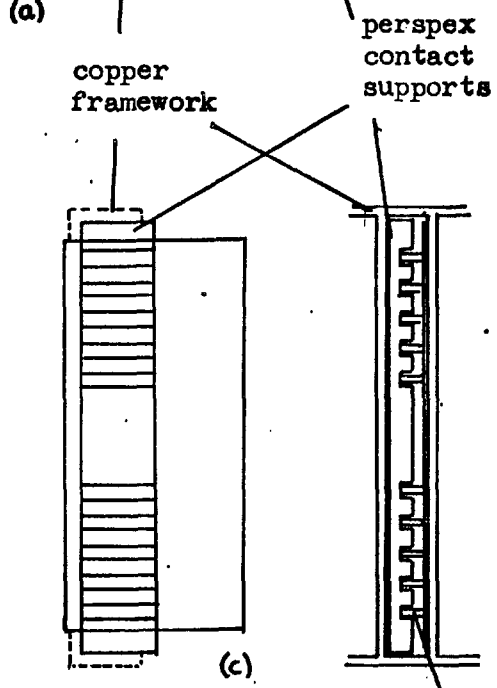

(c)

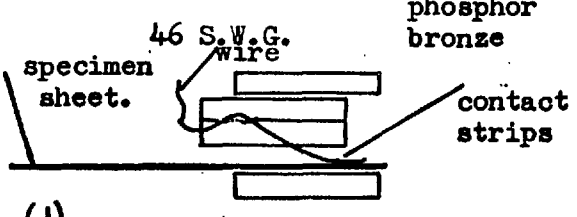

(d)

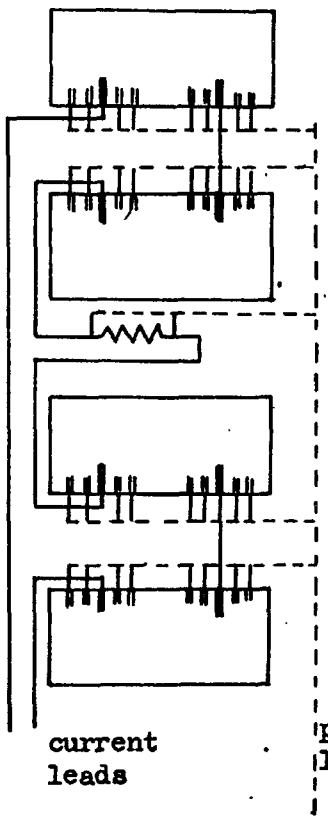

(e) Wiring inside the can.

Figure 6.9

these to the outside world are brought down the main pumping tube.

The details of the internal structure of the inner can are illustrated on page 98. Six copper strips, 1/16" x 3/8" section, are soldered to the top of the can. Between these are the film contact devices, consisting of pieces of perspex with grooves into which are fixed phosphor-bronze contact strips. These are shown in Figure 6.9(d). Each mica specimen sheet is placed between a copper strip and a set of phosphor-bronze contacts. The contacts press on the evaporated current and potential leads, and hold the specimen sheet against the copper strip. Enamelled 46 S.W.G. copper wires are soldered to the free ends of the phosphor-bronze contact strips.

To ensure good electrical contact a spot of colloidal silver is placed at each of the film to phosphor-bronze contacts. The important current contacts have, in addition, pieces of indium pressed between the perspex and the contact strip.

There are positions for four specimen sheets, each of which has four specimens (page 93). The electrical connections inside the can are sketched in Figure 6.9(e). The current leads are connected in series so that the same current flows through all specimens. All the wires are led to the top of the can and bunched together. The bundle passes in a spiral up the inner can support tube into the thermal anchor box, where it is wound several times round a sheet copper former which is soldered to the outer can lid. This thermal anchor is provided so that, when the cans are at low temperatures, heat coming down the wires from the room temperature end is taken up by the outer can and the helium bath, and does not reach the inner can.

The bundle of wires passes up the smaller pumping tube and out through an 'Araldite' seal at room temperature. In the junction box (Figure 6.7) the wires are joined to a corresponding set of much thicker wires which go to the resistance measuring circuit. Taking the wires by the route described avoids the need for a low temperature vacuum seal, which would be difficult to provide for so many wires.

Controlling the temperature of the inner can.

When the inner can is at a higher temperature than the outer can heat is lost from it by conduction and, at higher temperatures, radiation. If the temperature of the inner can is to remain constant the loss must be balanced by the heat supplied by the heater (Figure 6.8). The current through the heater is controlled by a feedback system which uses the copper resistance thermometer wound near the heater as a reference. The use of such a control system greatly facilitates the establishment of a controlled temperature, and reduces temperature drift caused by, for example, change of temperature of the outer can.

The control circuit.

A diagram of the control circuit is shown in Figure 6.10. A more detailed circuit diagram is given in Appendix II. The resistance thermometer forms one arm of a Wheatstone bridge, the output of which is amplified and used to control the current to the heater. The temperature of control is determined by the variable resistance (R). As the resistance of the thermometer changes from just below R to just above the heater current changes from its maximum value, to nearly zero, as shown in Figure 6.11. If the required amount of heat is provided by some current in this range the temperature of the can will be controlled, as large changes

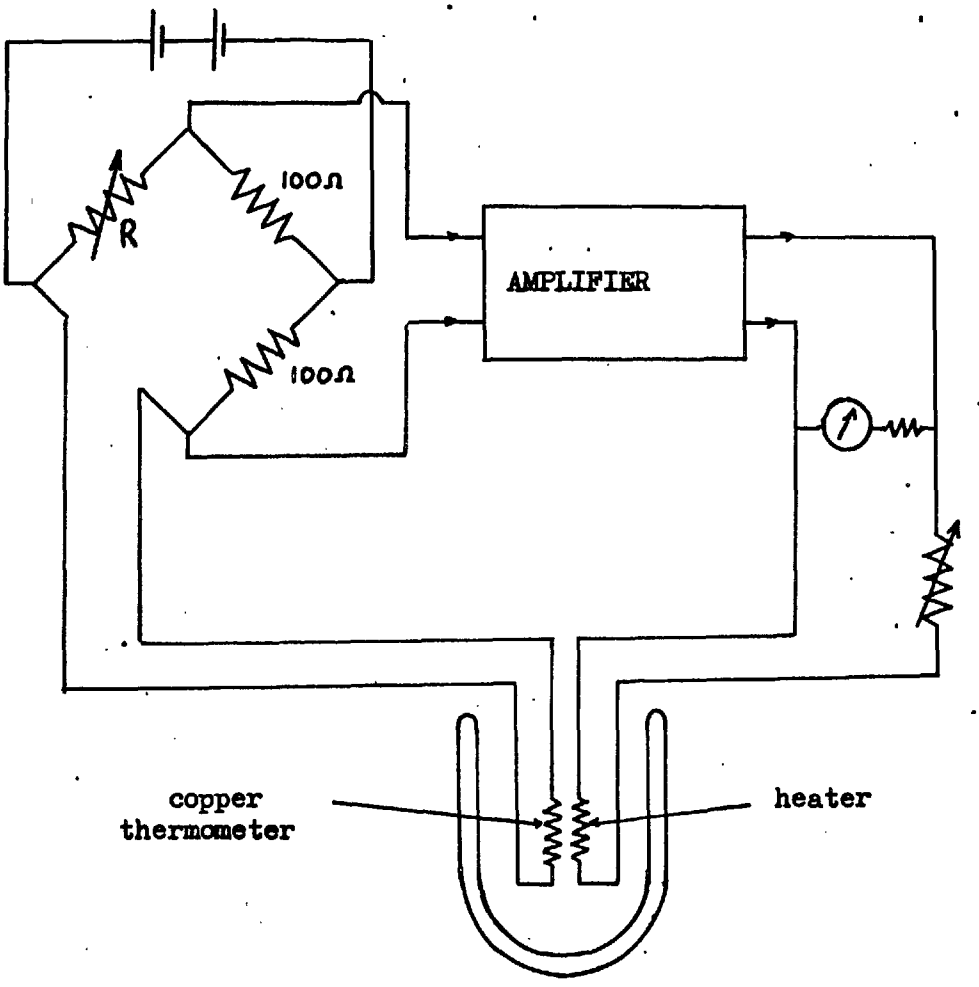

Figure 6.10 Temperature control.

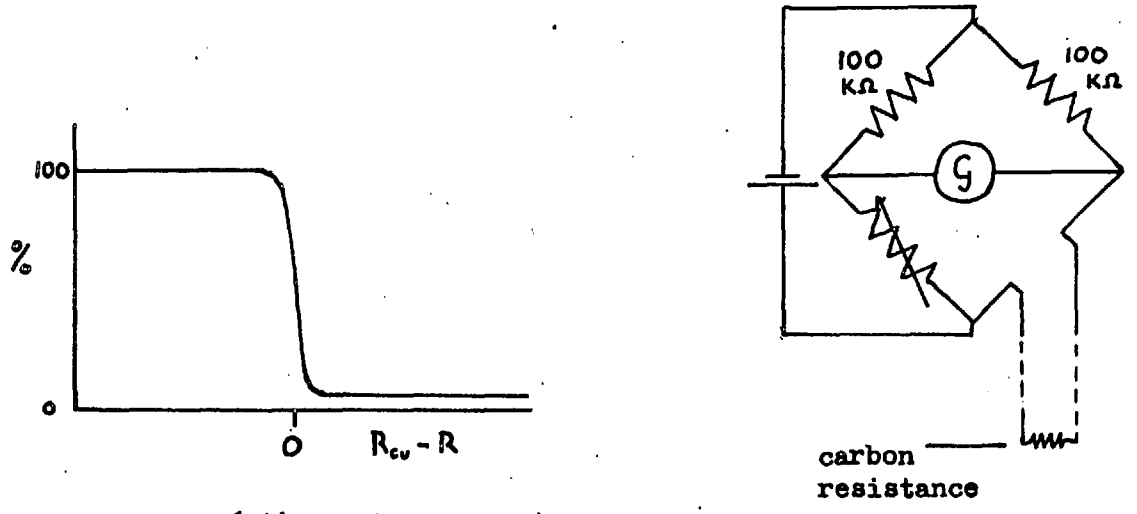

Figure 6.11 Heater current vs. thermometer resistance.

in the current are caused by small changes in temperature. The change in the thermometer resistance, required to produce a change in output of 50% at the balance point, represents a change of temperature of less than 1% over most of the temperature range.

The meter shows the fraction of full output being delivered, and thus indicates when the system is controlling. The variable resistance in the output circuit allows the scale of the output current to be altered to suit the various heat requirements over the temperature range. Extra current, not subject to the controller, can be passed through the heater to increase the heating rate at higher temperatures.

The effectiveness of control.

The control system is very effective in use, particularly at the higher temperatures, where changes during sets of measurements are usually less than 0.1°K. Good control at the higher temperatures is important in this work, as the film resistivities are compared with those for bulk at corresponding temperatures. Small differences between relatively large numbers are required, and uncertainty in the temperature would make the comparison unreliable.

As the controller depends on a copper resistance thermometer, it is not very effective below about 25°K. However, sufficiently constant temperatures can be obtained in this range by hand adjustment of the heater current. Accurate control is not required, as the resistivities of neither the films nor the bulk material change rapidly in this range.

The temperature of the specimens.

It is impracticable to measure the temperature of each specimen individually at the same time as its electrical resistance is measured.

The temperature measurement relies on the temperature of the inner can being constant over a period of time and being the same at all points in the can.

The constancy with time is ensured by the temperature controller described in the previous section. The inner can is constructed of copper and is filled with helium gas at a pressure of about 0.5 m.m. Hg during experimental runs. The specimens are thermally connected to the body of the can by the exchange gas and through the copper strips against which they are held.

The temperature measurement is made using a copper resistance thermometer mounted in the same environment as the specimens. This is shown in Figure 6.9(d). The thermometer consists of a sheet of mica round which a length of 38 S.W.G. commercial enamelled copper wire is loosely wound. It is held in place in the same way as the specimen sheets. In this position it can be expected to give a good estimate of the temperature of the specimens, and also a reliable indication of when they achieve thermal equilibrium.

Copper thermometers wound in a strain free manner have been found to be reliable and reproducible (White[48]). A general calibration can be used to obtain the temperature to better than 0.1°K if the residual resistivity ratio is less than 1/100. In the case of the thermometer used it is about 0.007. The function $(R(T) - R(4.2)) / (R(273) - R(4.2))$ is tabulated by White, so the residual resistivity and one fixed point are required to calibrate a particular thermometer. The fixed point used in this case was near the ice point and was determined by an accurate mercury thermometer.

The actual temperature is not required to great accuracy. What is required is the value of the resistivity of bulk material at the same temperature as the film. It is sufficient that the thermometer should be reproducible, as the resistivity of the bulk material is measured using the same thermometer.

The room temperature resistance of the copper thermometer is about 1 ohm, so the same measuring technique is used to obtain its resistance as is used for the film specimens.

A copper resistance thermometer is unsuitable for temperatures below about 20°K, so a carbon resistance thermometer is used to cover this range. A nominally 39 Ω $\frac{1}{4}$ watt resistor was attached to the top plate of the inner can (Figure 6.9(a)). Its resistance is measured using a simple Wheatstone bridge circuit (Figure 6.12). The high resistance arms were necessary to keep the current in the thermometer low, to prevent self heating. The accuracy required in this range is not high, so no elaborate calibration procedure is needed. The helium point and some points from the low end of the copper thermometer range are considered sufficient.

The measurement of resistance.

The thin film specimens have small resistances, much less than 1 ohm at low temperatures, and are necessarily remote from the resistance measuring circuits. In order to keep the heat leak from room temperature small, the connections to the specimens must be through thin wires which have resistances of over 10 ohms. A potentiometric method of resistance measurement is, therefore, an obvious choice.

The method is very simple. The specimens are provided with current and potential leads, and are connected in series by their current leads.

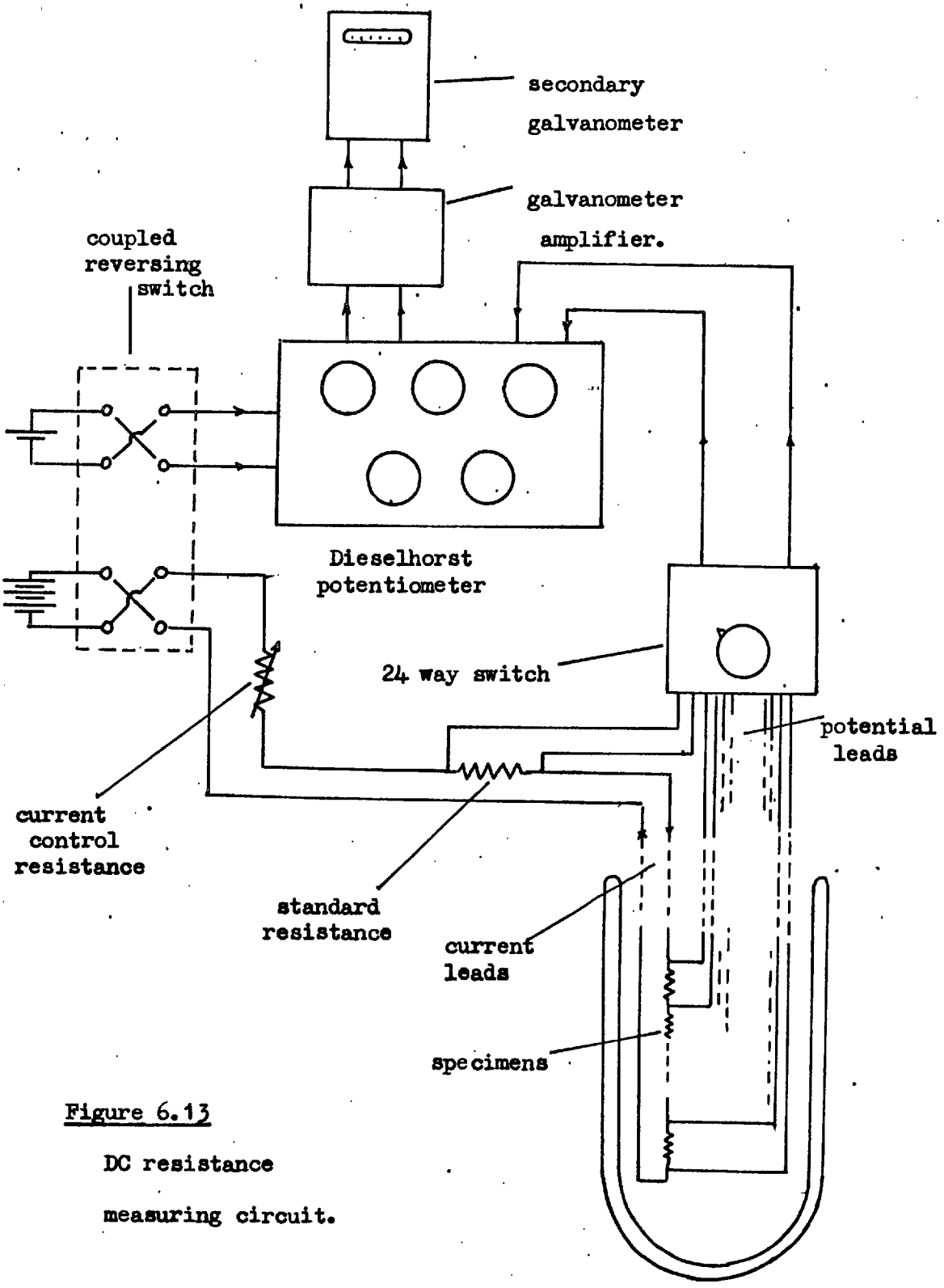

Figure 6.13

DC resistance

measuring circuit.

A current is passed through the specimens, the copper thermometer and a standard resistance (0.2 ohms), and the voltage developed across each resistance in the circuit is measured. The current is obtained from the voltage across the standard resistance, and the values of all the other resistances in the circuit can then be obtained from their respective voltages.

The voltages are measured using a Dieselhorst pattern potentiometer, which has five decade switches, giving up to 10,000 μV in steps of 0.1 μV. The out-of-balance voltage is amplified by a galvanometer amplifier, the output of which is displayed on a secondary galvanometer. A very sensitive indication of the balance point is thus obtained.

Thermals.

The temperature gradients in the voltage measuring circuits cause thermoelectric voltages of up to a few micro-volts to be set up. These are constant over a short period of time and are allowed for in the following way.

The potentiometer current and the specimen current are passed through a coupled pair of reversing switches. If there is no thermoelectric voltage, reversing the currents has no effect, and the true specimen voltage is obtained in each position. If a thermoelectric voltage is present, it is not reversed with the current, but it is added to the specimen voltage in one direction and subtracted in the other. The mean of the two voltages measured gives the true specimen voltage.

The circuit.

The D.C. resistance measuring circuit is shown in Figure 6.13. The potential leads from the specimens are taken into a 24 way, 2 pole, low

thermal switch. The output from this is available for voltage measurement by the potentiometer. The specimen current is supplied by a 6V accumulator and regulated by a variable resistance in series. The specimen current used is in the range 5 - 10 ma.

The procedure at a given temperature.

The resistance measurements are made only when the temperature of the inner can has stabilised at the required value. The specimen current is then also constant. The voltages across the copper resistance and the standard resistance need be measured only twice at a given temperature, as they are expected to be constant. Voltages are measured in the following order:

Copper resistance thermometer.

Standard resistance.

Specimen on the 1st switch position.

Specimen on the 2nd switch position.

— — — — —

— — — — —

Specimen on the 16th switch position.

Copper resistance thermometer.

Standard resistance.

The average values of the two temperature and specimen current measurements are taken as appropriate for all the specimens. Changes are usually small enough for this to be justified.

The procedure of a resistance measuring run.

The specimen sheets are placed in position and the inner can sealed with an indium 'O' ring. The vacuum tightness of the can is checked using

a helium mass-spectrometer leak detector. The outer can is sealed and similarly checked. Helium gas at a pressure of about 0.5 m.m. Hg is introduced to both the inner can and the inter-can space.

The apparatus is fitted into the cryostat and the outer dewar filled with liquid nitrogen. The cooling of the apparatus is hastened by running liquid nitrogen into the container at the top of the outer can. When the temperature is near 78°K, and no liquid nitrogen is left at the top of the outer can, the nitrogen gas is pumped out of the inner dewar and replaced by helium. If this were not done, solid nitrogen might condense on the walls of the dewar and prevent the liquid helium level being seen.

The apparatus is cooled to 4.2°K by transferring liquid helium from its transport vessel through a vacuum jacketed transfer syphon. The transfer is performed sufficiently slowly that the specific heat of the helium gas is fully used in the cooling process. Liquid helium has a very low latent heat of vaporization, and much more would be used if this alone had to cool the apparatus from 78°K to 4.2°K. The cryostat is filled with liquid helium to just above the top of the outer can.

The resistances at 4.2°K are measured and the exchange gas in the inter-can space is pumped out. The inner can is warmed up and brought to equilibrium at various temperatures, when the resistances are measured. Below about 25°K the temperatures are measured by the carbon resistance thermometer and the heater current is set by hand. Equilibrium is established quickly in this range as specific heats are small. Above about 25°K the temperature controller is used. At higher temperatures the liquid helium level falls below the bottom of the can, and is eventually lost, but

control is still effective as long as the temperature of the outer can is lower than that of the inner can.

Measurements are continued up to about room temperature, with an overnight break when the temperature is somewhere in the range 100°K - 200°K. The cans do not warm up to room temperature during this period as liquid nitrogen remains in the outer dewar long enough.

Above about 200°K the temperature of the outer can rises very slowly so heat is provided by a 500 ohm electrical heater wound on it. This is to avoid very large temperature differences occurring between the cans.

The resistances are usually measured at about 30 temperatures in the range 4.2°K to room temperature.

4) The Thickness of Thin Films.

Methods for estimating the thicknesses of thin metal films may be divided into three groups.

(a) Mass measurement methods[35,36]. The mass of material deposited in a given area is estimated, e.g. by weighing or by chemical analysis, and the average thickness calculated assuming that the film density is the same as the bulk density. In order to get sufficient mass for accurate measurement large substrates are required, so these methods are unsuitable for the films used in this work, as several small specimens of different thicknesses are produced at each evaporation.

(b) Multiple beam interferometric methods[49]. Fringes of equal chromatic order are usually used and the thickness at a single point at the edge of the film is obtained.

(c) Resistance methods[58]. The thickness is deduced from the shape of the specimen and its electrical resistance near room temperature, where

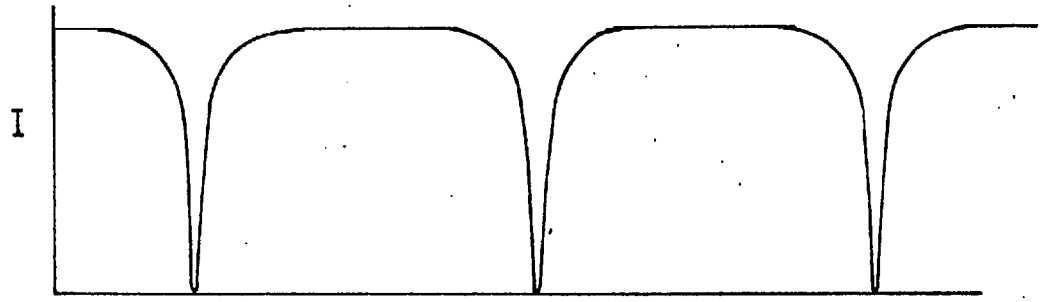

Figure 6.14

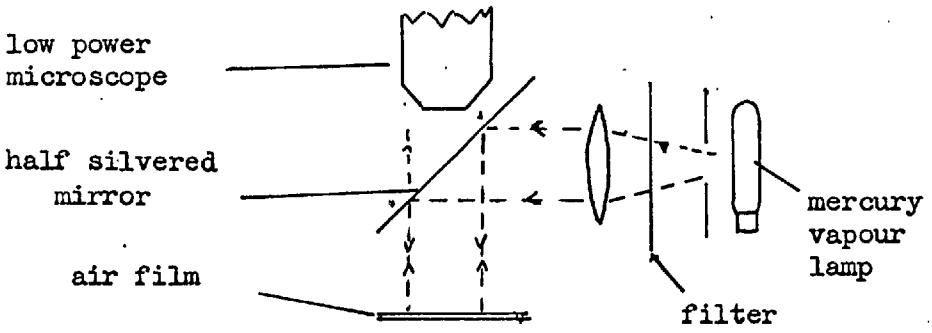

Figure 6.15

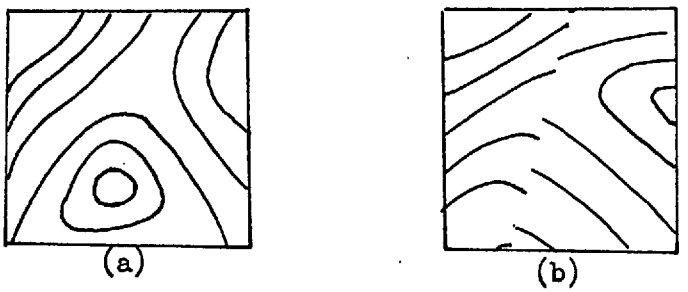

Figure 6.16

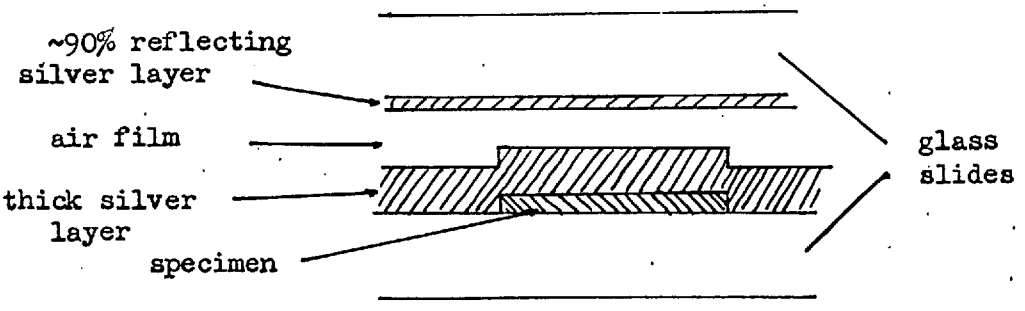

Figure 6.17

size effects are small.

A resistance method has been used to obtain the thickness of all the specimens discussed in the results chapters. The method is described in Chapter VII as it arises naturally from the analysis of the resistance results. The thickness of some specimens were measured by means of fringes of equal chromatic order, and the results compared, in Chapter VII, with the thicknesses obtained by the resistance method. A description of the fringe method will now be given.

Thickness measurement by multiple beam interferometry.

The use of multiple beam interferometry for the study of surface topology has been thoroughly investigated by Tolansky and described in his book[49], from which the methods employed here have been taken.

An air film bounded by surfaces which are good, but not total, reflectors has transmission and reflection properties which are critically dependent on the thickness of the air film. For the purpose of measuring metal film thicknesses, our interest is restricted to the reflection properties of an air film which has one surface totally reflecting and the other about 90% reflecting. Monochromatic light incident perpendicularly on the latter surface is totally reflected unless the thickness of the air film is close to $n\lambda/2$, where n is an integer and λ the wave length of the light. An indication of the form of the reflectivity thickness curve is given in Figure 6.14.

If the air film is not of uniform thickness, there are dark fringes where the thickness is $\frac{1}{2}n\lambda$. These contours of constant thickness are known as Fizeau fringes, and an arrangement for observing them is shown in Figure 6.15. The output of a mercury vapour lamp is filtered to leave only the

green line, and a half silvered mirror is used to allow perpendicular observation of the air film. A drawing of a typical fringe system is shown in Figure 6.16 (a).

The above method can be used to observe the thickness of an evaporated specimen film, provided it has sharp edges away from the edge of the substrate. A layer of silver is evaporated over the film and substrate sufficiently thick to give zero transmission. Tolansky has shown that the surface of this upper layer reproduces the features of the surface below to better than 20Å. A microscope slide, silvered to about 90% reflectivity, is pressed lightly in contact with the silvered specimen (Figure 6.17). The resulting air film changes thickness over its area in a gradual fashion, except at the edges of the specimen film. Such an air film, when observed with the arrangement of Figure 6.15, gives a fringe pattern like that shown in Figure 6.16(b). The fringe steps occur at the edge of the specimen film, and could, in principle, be used to obtain its thickness. In practice the fringes are used for preliminary observation only, and the thickness measurement is made by using fringes of equal chromatic order.

Fringes of Equal Chromatic Order.

The same interference film is used as for Fizeau fringes, but white light is used instead of monochromatic, and more information is obtained about a more restricted region. The method is best explained by considering the experimental arrangement used (Figure 6.18).

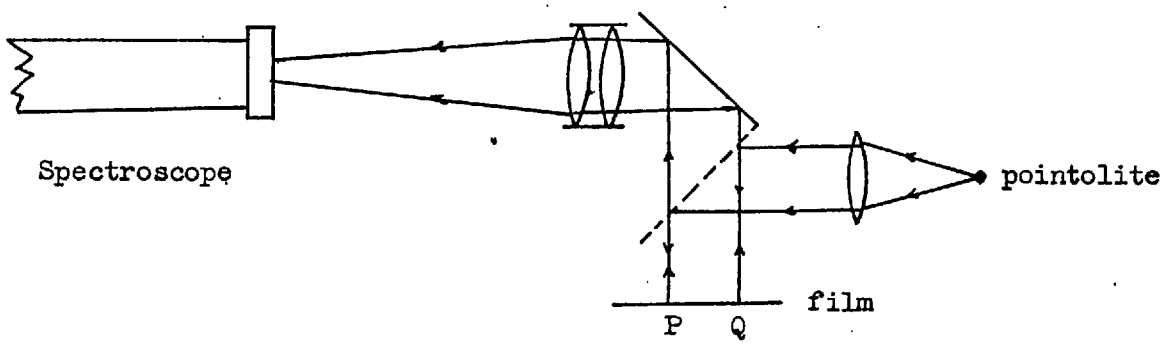

Figure 6.18 Apparatus for fringes of equal chromatic order.

White light from an Ediswan'Pointolite' is incident on the air film. The part of the reflected beam which passes through the half silvered mirror enters a good achromatic lens which projects an image of the surface of the air films on to the slit of a spectroscope. The slit receives light which has been reflected from a line (PQ) on the air film. A line along the spectrum produced is obtained from a single point on PQ, where the thickness of the air film is t(say). The interference condition is now realized for wavelengths λ_n, which satisfy the equation $n\lambda_n = 2t$, so a line along the spectrum has dark spots at these values of λ. The spectrum is built up from a set of lines from points on PQ with various values of t, so it is crossed by a set of dark lines, one for each value of n. The order of interference is constant for each fringe, hence the name.

Changes of thickness along PQ result in changing wavelength for the fringe across the spectrum. For a given n, λ is proportional to t, so changes of the thickness of the air film are directly related to the shape of the fringe. If the line PQ crosses the edge of a specimen film, the

abrupt change of thickness of the air film produces a step in each fringe, from which the thickness of the specimen film can be obtained. Plate 3 shows a photograph of a fringe system with steps.

Fringes of low order are most sensitive to change of film thickness, as $\delta\lambda = 2\delta t/n$, but the advantage is offset to some extent by the greater width of low order fringes. Fringes of order 10-30 are useful for measurement, and can be fairly easily obtained by varying the pressure on the microscope slide, while observing the Fizeau fringes.

A Hilger spectroscope with a reflection diffraction grating is used, and spectra are recorded on Ilford R40 plates. The mercury spectrum is superimposed on the fringe system to provide wavelength reference points. The fringe width is significantly greater than the resolution of the spectroscope, so the achievable accuracy is limited by the properties of the interference film.

Measurement of the fringe system.

To obtain the thickness of the specimen film from the step on a fringe, the order (n) and the wavelength change at the step ($\Delta\lambda$) are required. The wavelength of two fringes and the difference between their orders are required to establish the order of each fringe in the system. If the two fringes are well separated, the value of n obtained should be near enough to an integer to avoid ambiguity. Once the order is known for a given fringe, the thickness of the specimen film is given by $\frac{1}{2} n\Delta\lambda$.

A scale for measuring the fringe system was made by reducing a millimetre scale about 5 times on to a photographic plate. The spectrum and scale plate are projected together, and the fringe system measured in terms of the scale. The scale is calibrated by referring it to the mercury

spectrum superimposed on the fringe system. The fringes used to obtain the order of interference are chosen near spectral lines, one at each end of the spectrum. For step measurement the wavelength difference is taken as proportional to the difference between the scale readings. Measurement of a set of close fringes, which occur at wavelengths $2t/n$, showed that this procedure is justified. The step edges are usually a little rounded, so the wavelength difference is measured between the points X and Y (Figure 6.19) where the extrapolated main lines of the fringe meet the line through the step system, AB.

If systematic errors are discounted the accuracy of the thickness results obtained by the fringe method may be roughly estimated from the variations in the results for particular specimens. These were up to about 5%, a value also given for the accuracy of this method by Wolter[59].

Some thicknesses obtained by the fringe method are compared, in Chapter VII, with the thicknesses of the same films obtained from the resistance results. The agreement between the two methods is fairly good, but the fringe thicknesses are usually less than those from resistance measurements and lead to unreasonable results for the film resistivity. The cause of this discrepancy is probably the departure of the film edge from an ideal step shape, resulting from the spread of material under the edge of the mask. The section of a film edge is shown in Figure 6.20. It would not be possible to separate the effect of the 'tail' from the general shape of the fringe, and the thickness would be underestimated (Figure 6.21) This mechanism would lead to an error of constant percentage, and this is found roughly to be the case.

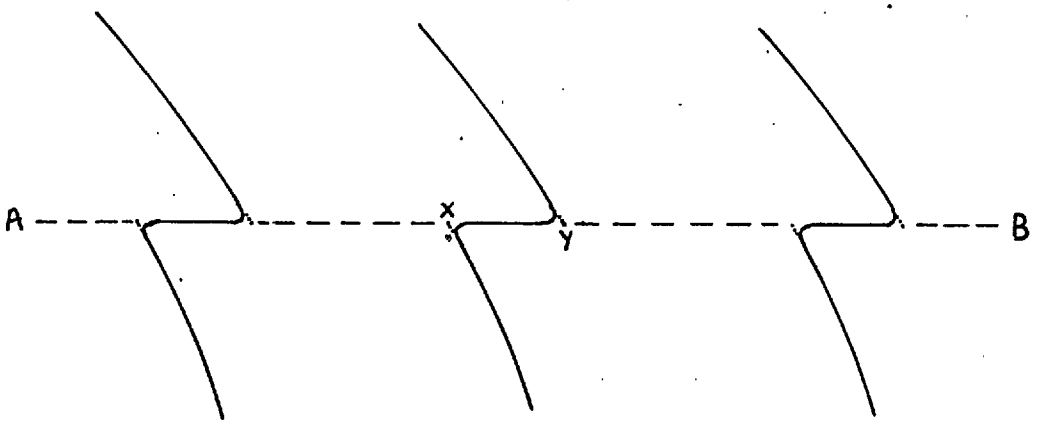

Figure 6.19

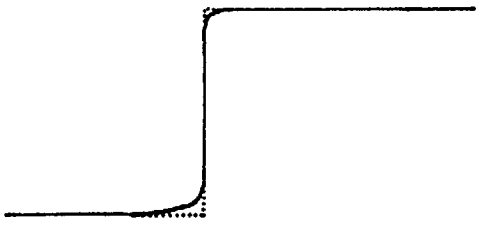

Figure 6.20

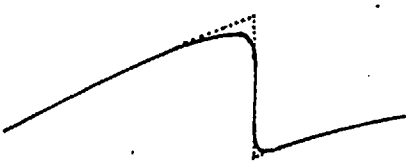

Figure 6.21

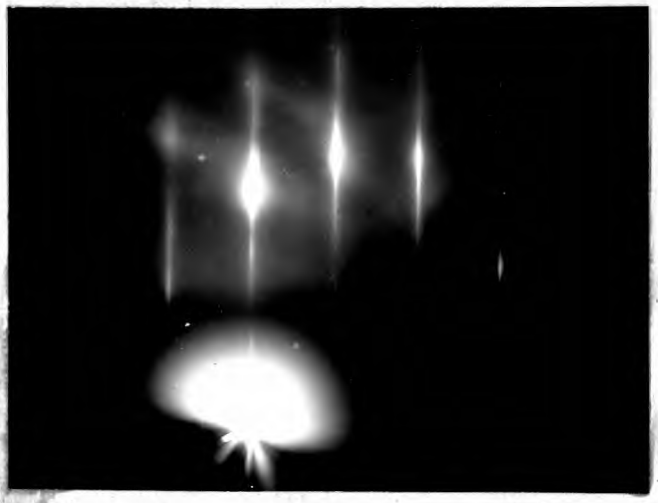

Plate 1

Electron diffraction pattern from an epitaxial silver film.

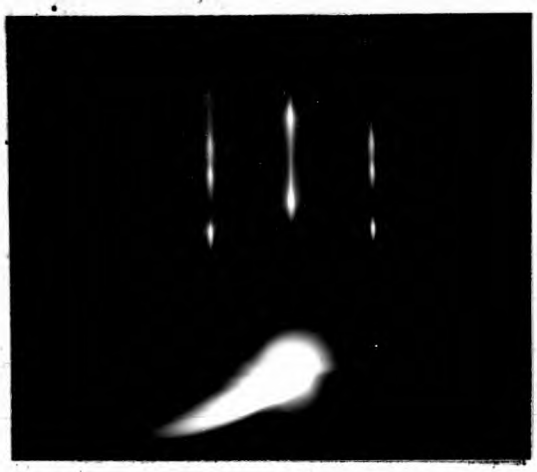

Plate 2

Electron diffraction pattern from a cold substrate silver film on mica.

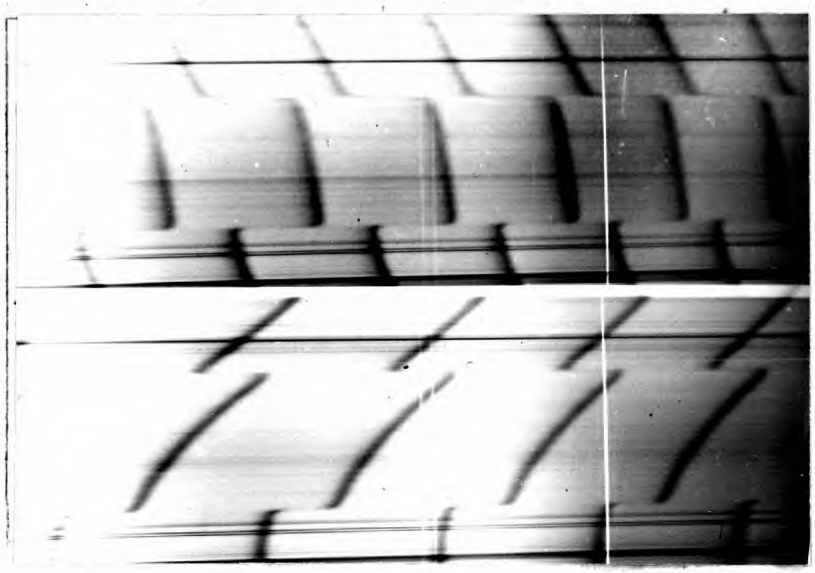

Plate 3 Fringes of equal chromatic order.

CHAPTER VII

ANALYSIS OF RESISTIVITY RESULTS

1) Resistance and Resistivity.

The experimental measurements of resistance give the resistance of each specimen at about 30 points in the temperature range $4.2^{\circ}K$ to about $300^{\circ}K$. The resistances are related to the more meaningful resistivities by a constant for each specimen, depending on its shape and thickness.

$$R_f(T) = C\,\rho_f(T), \qquad (7.1)$$

where $R_f(T)$ is the measured resistance at temperature T and $\rho_f(T)$ is the effective resistivity, i.e. the resistivity that would give the observed resistance if there were no size effects. Although the word 'effective' will not normally be used, it is always implied when films are being discussed. For a rectangular specimen of thickness t, length d and width ω

$$C = d/\omega t. \qquad (7.2)$$

The thin film specimens used in this work approximate to this simple form, and C can be obtained if d, ω and t can be measured.

The ratio d/ω

The specimens have the shape shown in Figure 6.4 (page 90), and their dimensions are measured as described on page 94. They are not quite of the ideal form required by equation 7.2 as the potential leads have finite width. The width of a specimen presents no problem, but the value which should be taken for its length is not immediately obvious.

The flow of current in a film of constant thickness is governed by the two dimensional Laplace equation $\nabla^2 V = 0$. A diagram of a single potential lead of a specimen is shown in Figure 7.1, drawn to scale, with a plausible set of current flow lines and equi-potential lines drawn in.

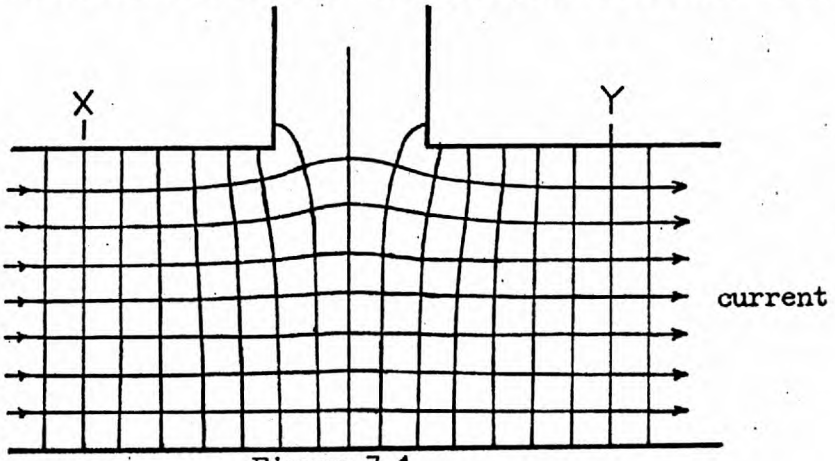

Figure 7.1

The voltage drop, for a given current, along a section of specimen containing a potential lead (XY) is less than along the same length of specimen without a potential lead. The effective length of a specimen (d*) is, therefore, less than the distance between the mid-points of the potential leads (d). The reduction cannot be greater than the width of a potential lead, which is 8% of d. In fact it must be very much less than this, as can be seen be considering the current pattern. If the potential drop in the region of the potential lead is to be reduced, the current flow must spread over a greater width. An increase of effective specimen width of as much as 30% is certainly an overestimate, as it is not possible to draw a consistent set of current and potential lines to fit this condition. An effective increase of 30% would result in a d* only 2% less than d.

An exact correction for d could be obtained by solving the Laplace equation, but the small increase in accuracy that would result does not justify the effort. The error is probably less than that involved in the measurement of d/ω, and certainly less than the error in the thickness as measured by fringes. The specimens are treated, therefore, as having potential leads of zero width separated by the distance d.

The thickness t.

The measurement of the thickness of films by the use of fringes of equal chromatic order is described in Chapter VI. The accuracy of these measurements is, at best, a few per cent.

The constant C.

The value of C obtained from d/ω and t has a probable error of about 5%, and this dominates the error in the resistivity, as the resistance is measured to well under 1%. The advantage of this direct method of estimating C is that no assumptions are made about the resistivity of the films. Its disadvantage is the low accuracy of C compared with the accuracy of the resistance measurements.

A method will now be described in which C is estimated from the specimen resistance at the high end of the temperature range, and the thickness obtained from C and d/ω .

2) Estimating C and t From the Film Resistance at the Higher Temperatures.

This method, which will be referred to as the 'fitting method', requires some assumptions about the resistivity of the films at the high end of the temperature range, i.e. above about 150°K.

These are:

(a) That the resistivity of a film is related to the resistivity of the bulk material from which it is made (ρ_b) by

$$\rho_f(T) = \rho_b(T) + \rho_m, \tag{7.3}$$

where ρ_m is a constant.

(b) That the bulk resistivity obeys Matthiessen's rule:

$$\rho_b(T) = \rho_l(T) + \rho_o, \tag{7.4}$$

where ρ_l is the ideal lattice resistivity and ρ_o is the residual resistivity.

The justification of (a) depends partly on an appeal to the theory of thin film resistance. All theoretical approaches agree that 7.3 is the appropriate form, provided that the ratio K (= t/l, where l is the bulk mean free path) is sufficiently large. Fuchs' theory is the most rigorous and shows that the deviations from the form 7.3 should be quite small down to K ~ 0.4 (page 58). The experimental results show that ρ_f is linear in ρ_l, but cannot show that the coefficient of ρ_b in 7.3 is accurately one.

The justification of assumption (b) depends on the structure of the material of the film being very similar to its structure in bulk. It was shown in Chapter IV that epitaxial films have the normal bulk lattice spacing, but have a high dislocation density. Matthiessen's rule is generally obeyed for dilute alloys, but even then cannot be taken for

granted. Alley and Serin[50] showed that departures from Matthiessen's rule occur in alloys of aluminium, tin and copper, but only at low temperatures and only to an extent of about 8% of the residual resistivity. The departures which occur when the residual resistivity is caused by dislocations are much more serious, and can be over 100% of the residual resistivity (Bazinski et al[40]). It appears, however, that Matthiessen's rule still holds closely enough in the temperature range used for the fitting method. A fuller discussion of the effect of dislocations on the resistivity of bulk silver is given in Chapter VIII (page 149).

Combining equations 7.1, 7.3 and 7.4 gives

$$R_f(T) = C(\rho_1(T) + \rho_c) \qquad (7.5)$$

Considering this equation graphically, if R(T) is plotted against $\rho_1(T)$ the slope of the line obtained would be C and the intercept on the R axis would be $C\rho_c$. Once C is known the resistivity at each temperature is given by R(T)/C, and the thickness of the film can be obtained using the measured value of d/ω:

$$t = d/\omega C. \qquad (7.6)$$

A graph plotting procedure is not in fact used. The resistance values are fitted to 7.5 numerically, using a computer.

3) Comparing the Methods for Estimating C.

The direct method uses t from fringes and d/ω to find C. The fitting

Thicknesses Å		Differences Å (1) - (2)	Differences %
(1) By fitting method	(2) By fringe method		
596	642	- 46	- 7.5
633	647	- 14	- 2.5
813	836	- 23	- 2.5
910	884	26	3.
916	875	41	5.
1072	1029	43	4.
1470	1302	168	12.
1866	1824	42	2.5
1884	1720	164	9
2370	2250	120	5
3005	2725	280	10
3120	2800	320	10
4170	3850	320	8

Table 7.1

Film thicknesses by fringe and fitting methods.

method finds C and uses d/ω to find t. If the same value of d/ω is used in both cases, comparing the two values of t obtained is an effective way of comparing the methods. The value of the resistivity obtained at a given temperature is proportional to the value of t, i.e. from 7.1:

$$\rho_f(T) = \frac{\omega t}{d} R(T). \qquad (7.7)$$

The thicknesses of a number of epitaxial silver specimens were measured by the fringe method, and the results are given in Table 7.1 with the results for the same specimens by the fitting method and the differences between them. Although the general agreement is fairly good, there are systematic differences between the two sets of values. The thicknesses of the thicker films from the fringe method are smaller than the corresponding thicknesses from the fitting method. The absolute differences increase with thickness, but the percentage differences show signs of being very roughly constant in this range. The thinner films do not conform to this pattern, but the differences involved are small in absolute terms, probably of about the same size as the errors involved in the measurement of the fringes.

At first sight it is not clear which method is to be preferred, and the direct approach might be chosen as it makes no assumptions about the resistivity of the film. It is shown below, however, that the use of the thicknesses obtained by the fringe method leads to unreasonable results for the film resistivities. It has been suggested earlier (page 115) that the discrepancy may be caused by the slight spreading of the silver

under the edges of the evaporation masks, as this would result in the thickness being underestimated by the fringe method.

Equation 7.7 shows that resistivity is proportional to t, so a lower value of t implies a lower film resistivity. The values of thickness given by the fringe method lead to low effective resistivities, in some cases lower than the ideal lattice resistivity of pure silver. This result seems improbable, as the bulk material of the films is expected to have a higher resistance than the ideal bulk, as it has a high dislocation content. In addition the size effect is expected to make a positive contribution.

The fitting method makes some reasonable assumptions which are supported by theoretical considerations and some experimental evidence. Above about 150°K R_f is found to be linear in ρ_1 to better than $\frac{1}{2}\%$, so errors larger than this can only arise if the film resistivity should be expressed in the form.

$$\rho_f(T) = (1 + c)\ \rho_1(T) + \rho_c, (T > 150^{\circ}K), \quad (7.8)$$

where c is a constant. A non-zero value of c could arise from failure of Matthiessen's rule for the bulk material of the film as a result of the high dislocation density, or from the failure of the high K limit of the thin film theory. It is shown in Chapter VIII that the errors in C and t arising from these causes are unlikely to be greater than 1% (pages 156 and 170). Thus it appears that both the film resistivity and the thickness can best be estimated by the fitting method, so this method has been used for all the specimens mentioned in this work.

4) The Fitting Program.

The values of the constants C and ρ_c for each specimen are obtained by fitting the high temperature resistance results to equation 7.5, using a computer. The program was written in Elliott autocode, and is run on an Elliott 803 computer. It was designed to accept data in a fairly raw form. Only a little preliminary calculation is required. The resistance of the copper thermometer is calculated at each point, and from this the values of the temperature and the ideal lattice resistivity are obtained using previously prepared graphs.

The remaining data are the 'as measured' voltages across the specimens and standard resistance. These are punched onto paper tape in the following arrangement:

Initial constants: Number of temperatures.

Number of specimens.

Number of points for fitting.

Standard resistance value.

Then for each temperature:

The Temperature.

Voltage across standard resistance

Voltage across specimen 1

to

Voltage across specimen 16

Then finally:

A list of $\rho_1(T)$, one for each temperature.

The program fits the high temperature values of $R_f(T)$ to 7.5, i.e. to

$$R_f(T) = C\,(\rho_f(T) + \rho_c), \qquad (7.9)$$

by a conventional least squares fitting,[51] which minimizes $\Sigma(R_f - R_c)^2$, where R_c is the value of the right hand side of 7.9.

An error in one or more of the voltages can easily arise as a misreading or copying mistake, and may then easily be very large. To prevent such errors distorting the fit obtained, the program was designed to ignore points which are inconsistent with the majority. The block diagram of the program (Figure 7.2) shows the procedure adopted for this, and also the general arrangement of the calculation. For each specimen a fit is produced, and the standard deviation of the experimental points from the fitted line is calculated. If any point is found to be more than $2\frac{1}{2}$ standard deviations away from the line, the fitting is repeated without the offending point. The rejection process may have to be repeated, as a very large deviation will swamp a merely large one. Points should excede $2\frac{1}{2}$ standard deviations with a frequency of less than 1 in 80 on the basis of normal fluctuations, so their rejection from groups of less than 20 points is not unreasonable.

The output tape of the fitting program is in a form which is acceptable as a data tape for other programs, so the results of past runs can be further analysed without having to repeat the fitting part. It gives all the information required; the fitting constants, resistivities and lists of the temperatures and lattice resistivities. It will be referred to as the intermediate data tape. Its first use is as the input

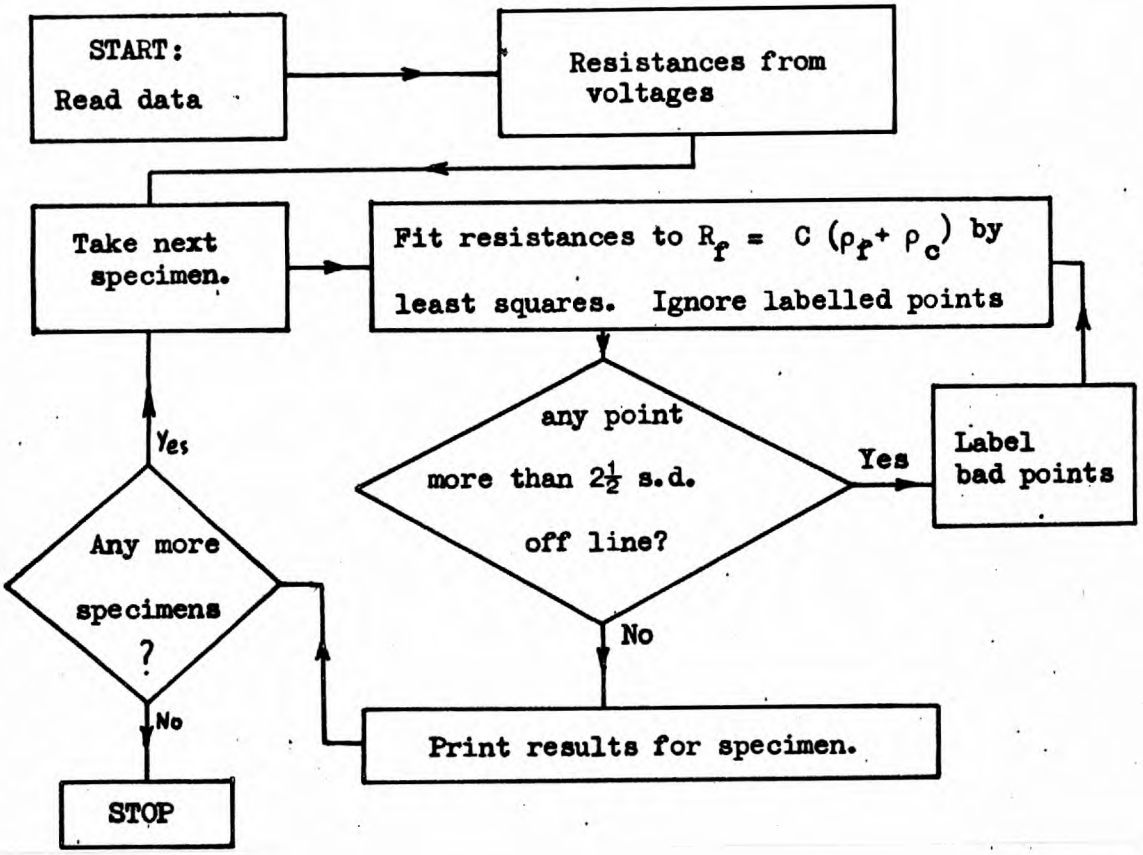

Figure 7.2 The fitting program.

to a short program which produces lists of results specimen by specimen. An example of the output for a single specimen is given on page 129. SIZE FACTOR is 1/C and RHO CONST is ρ_c. The first two columns give the temperature and resistivity and the third the difference between the film resistivity and the lattice resistance of the bulk silver at each temperature i.e. $(\rho_f(T) - \rho_l(T))$. The latter two are in $\mu\ \Omega$-cm. The last column shows the departures of the experimental points from the line fitted to the high temperature data, in units of .0001 $\mu\ \Omega$-cm. The thickness of the specimen is obtained by multiplying the value given for SIZE FACTOR by the measured value of d/ω.

SPECIMEN 7.

SIZE FACTOR : 14.3645

RHO CONST.: 0.0387

T	R	R-RO	R-R CAL
4.2	0.0221	0.0221	
11.0	0.0226	0.0224	
14.4	0.0234	0.0227	
17.1	0.0249	0.0233	
18.2	0.0262	0.0238	
21.0	0.0293	0.0247	
25.2	0.0361	0.0266	
29.7	0.0471	0.0284	
33.5	0.0596	0.0304	
38.3	0.0785	0.0315	
44.1	0.1062	0.0331	
50.2	0.1398	0.0339	
54.4	0.1631	0.0341	
58.0	0.1939	0.0424	
64.7	0.2275	0.0334	
70.1	0.2621	0.0341	
77.8	0.3137	0.0345	
78.5	0.3173	0.0351	
87.7	0.3765	0.0347	
99.8	0.4552	0.0355	
110.9	0.5264	0.0360	
122.9	0.6008	0.0363	
136.5	0.6874	0.0368	
150.2	0.7734	0.0374	- 13
164.3	0.8590	0.0379	- 7
178.8	0.9445	0.0381	- 5
192.2	10.2910	9.2999	GT 1.
206.5	1.1165	0.0385	- 1
220.8	1.2012	0.0382	- 4
235.5	1.2887	0.0387	0
249.9	1.3762	0.0402	15
250.0	1.3758	0.0388	1
264.5	1.4619	0.0399	12
278.4	1.5493	0.0393	6
293.1	1.6372	0.0392	5
308.0	1.7245	0.0375	- 11
322.6	1.8152	0.0372	- 14

CHAPTER VIII

THE RESISTIVITIES OF THE SILVER FILM SPECIMENS.

1) Introduction.

The results to be presented in this chapter are mainly for epitaxial silver films prepared by the method described in Chapter VI. Some of the epitaxial silver films have thin layers of aluminium or cold substrate silver on their free surfaces. The term 'cold substrate' is used for films or additional layers which are evaporated on to a substrate which is at room temperature. Some measurements were made on cold substrate silver films to see how they compared with the epitaxial films. The specimens cover a wide range of thicknesses.

The following list gives the types of specimen with the numbers of each type that were successfully measured. (Details are given in Appendix IV).

1.	Epitaxial silver.	72
2.	Epitaxial silver with a thin layer of cold substrate aluminium.	39
3.	Epitaxial silver with a thin layer of cold substrate silver.	15
4.	Cold substrate silver.	6

The resistivities of most of these specimens were measured throughout the temperature range. About 40 were measured only at 4.2°K and at sufficient points above 150°K to allow the fitting procedure to be used.

Orientation of thin films.

No attempt to control the orientation of the films with respect to the current direction was made. The symmetry of the epitaxial films about the

normal to the surface is essentially hexagonal, so no variation of the resistivity with direction in the plane of the film is expected.

The Results.

The results have been analysed by the fitting method described in the previous chapter. They will be discussed in terms of Fuchs' theoretical treatment, as this is the best starting point available, in spite of its simplifying assumptions. There are two questions of particular interest;

a) Can the experimental results be explained in terms of Fuchs' theory, and if so what values of the parameters l, the bulk mean free path, and p the surface specularity coefficient are appropriate?

b) If not, are there systematic deviations from the theory which might indicate in which respects it is inadequate?

There are several aspects of the resistivity of each specimen and of the specimens in groups. It will be convenient to consider the results under three main headings.

1) The resistivities at 4.2°K.

2) The ρ_c values from the high temperature fitting.

3) The variation of the film resistivities with temperature, particularly at low temperatures.

A section will also be devoted to a discussion of the bulk resistivity of silver, with particular reference to cold worked silver, as this appears to be especially relevant to the bulk resistivity of the material of the films.

2) The Film Resistivities at 4.2°K.

The epitaxial specimens,

The resistivities at 4.2°K of all the unmodified epitaxial films

measured are given on a log-log resistivity-thickness plot in Figure 8.1. The results are fairly scattered, particularly above about 1000 Å, and cannot be said to lie on a single line. They may be summarized by a line representing the general trend (AB in Figure 8.1), with two broken lines indicating the spread of the results about AB. The spread ranges from about ±12% at 600Å to nearly ±40% at 4000Å. The results for some very thick films are included in Figure 8.1, and will be discussed separately (page 138).

There are two aspects of the results that require explanation. The first is the form of the curve AB, which is a property of the films as a whole. The second is the spread of the results about AB, which involves differences between specimens of the same thickness.

The marked variation of resistivity over the thickness range is presumably due mainly to size effects. As a first step in comparing the results with the theory, the curves from Figure 8.1 are plotted in Figure 8.2 with curves from Fuchs' theory. If constant values of ρ_b (the bulk resistivity) and l are assumed for the whole range, the Fuchs' curves have the same shape on a log-log ρ_f-t plot as on a log-log ρ_f/ρ_b-t/l plot. A change of ρ_b or l results only in a change of the position of the set of Fuchs' curves on the ρ_f-t plot. The curves in Figure 8.2 assume that $\rho_b = 0.013$ and $l = 65000$Å. It is evident that the line AB does not fit a single Fuchs' curve, and could not be made to do so by any juggling with the values of ρ_b and l. The slope at about 1100Å is much greater than is found anywhere on the theoretical curves.

If these results are to be explained on the basis of Fuchs' theory,

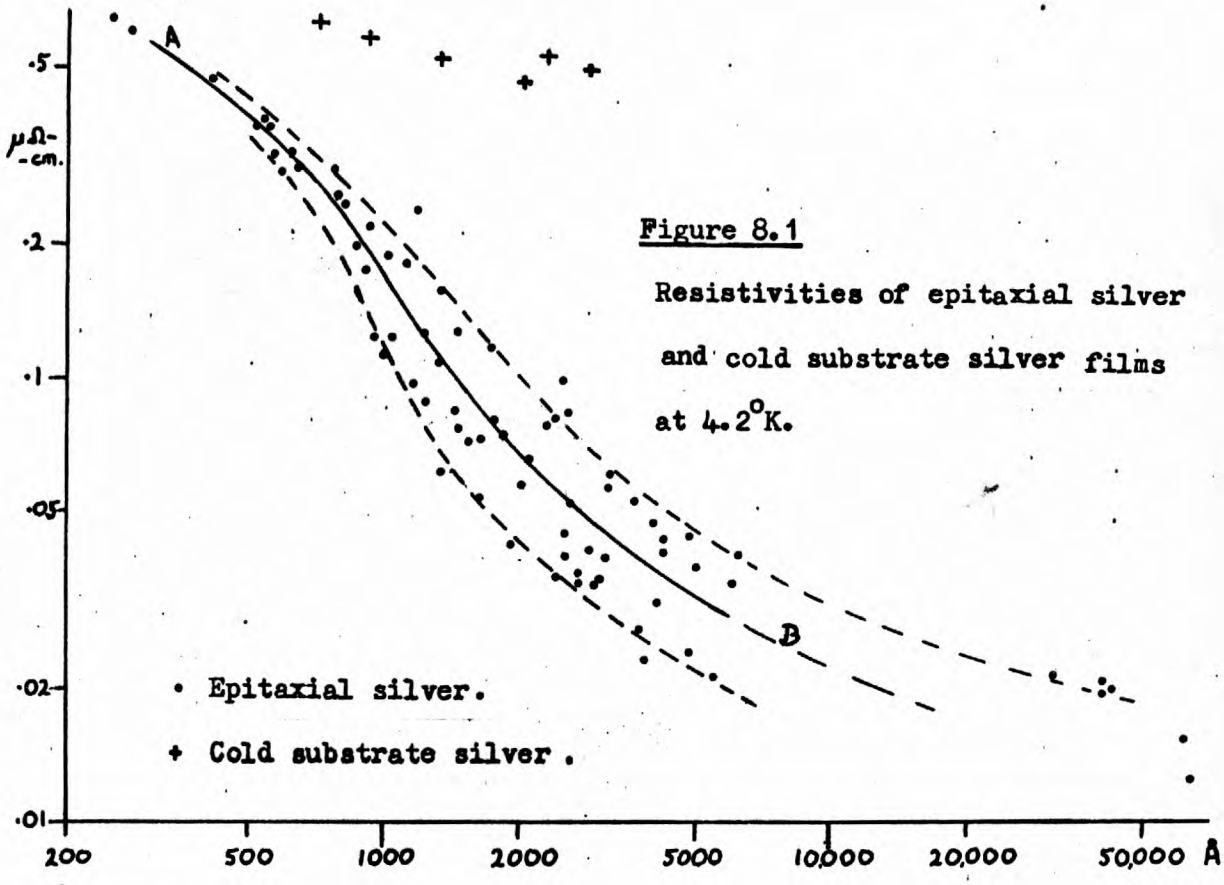

Figure 8.1

Resistivities of epitaxial silver and cold substrate silver films at 4.2°K.

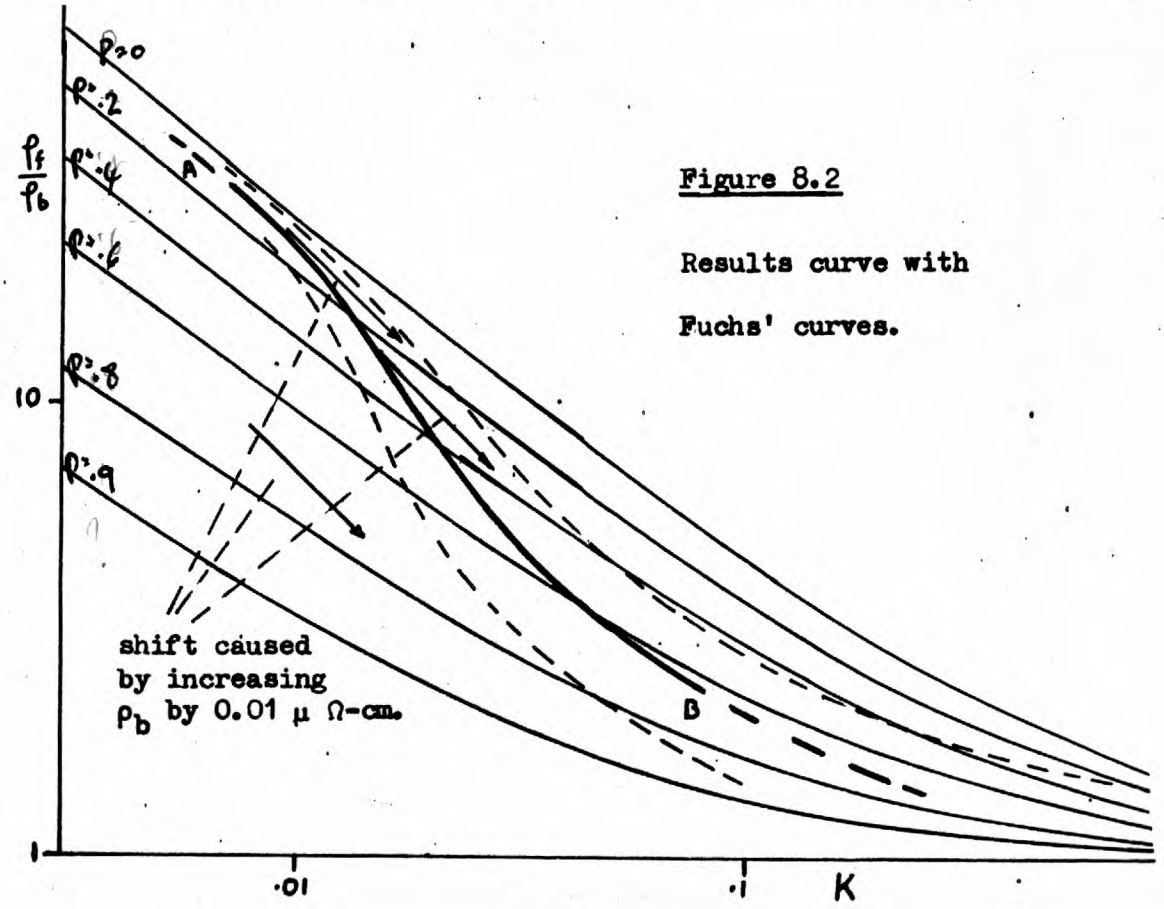

Figure 8.2

Results curve with Fuchs' curves.

there must be a general change of one or both of the parameters p and l with thickness, and also variations between specimens of a given thickness.

The specimens are in sets of four. Each set is on a single piece of mica and the four specimens are deposited during a single evaporation. Some of the 4.2°K results are given in Figure 8.3 with the sets distinguished, and it is seen that the points for a single set lie reasonably close to a smooth curve. The set curves are usually roughly parallel to AB, especially those which lie close to AB. This suggests, more clearly than Figure 8.1, that the line AB represents a general property of epitaxial films of silver prepared by the method described in Chapter VI.

Figure 8.3 shows that the large spread in the 4.2°K resistivities is a between set spread rather than a within set spread. The difference between sets must be attributed to some aspect of the preparation procedure which has been inadequately controlled. Although the cause of the differences is at present unknown, there is evidence of a relationship between the resistivities and fairly large scale surface features which are revealed by replica electron microscopy. A discussion of this subject will be given in Chapter IX (page 176).

Estimating ρ_b and l

It is impossible to determine the values of ρ_b and l for a single specimen. A number of specimens are required, all with the same values of ρ_b, l and p. If the thick film theory can be applied to the films under consideration, the resistivity can be expressed in the form

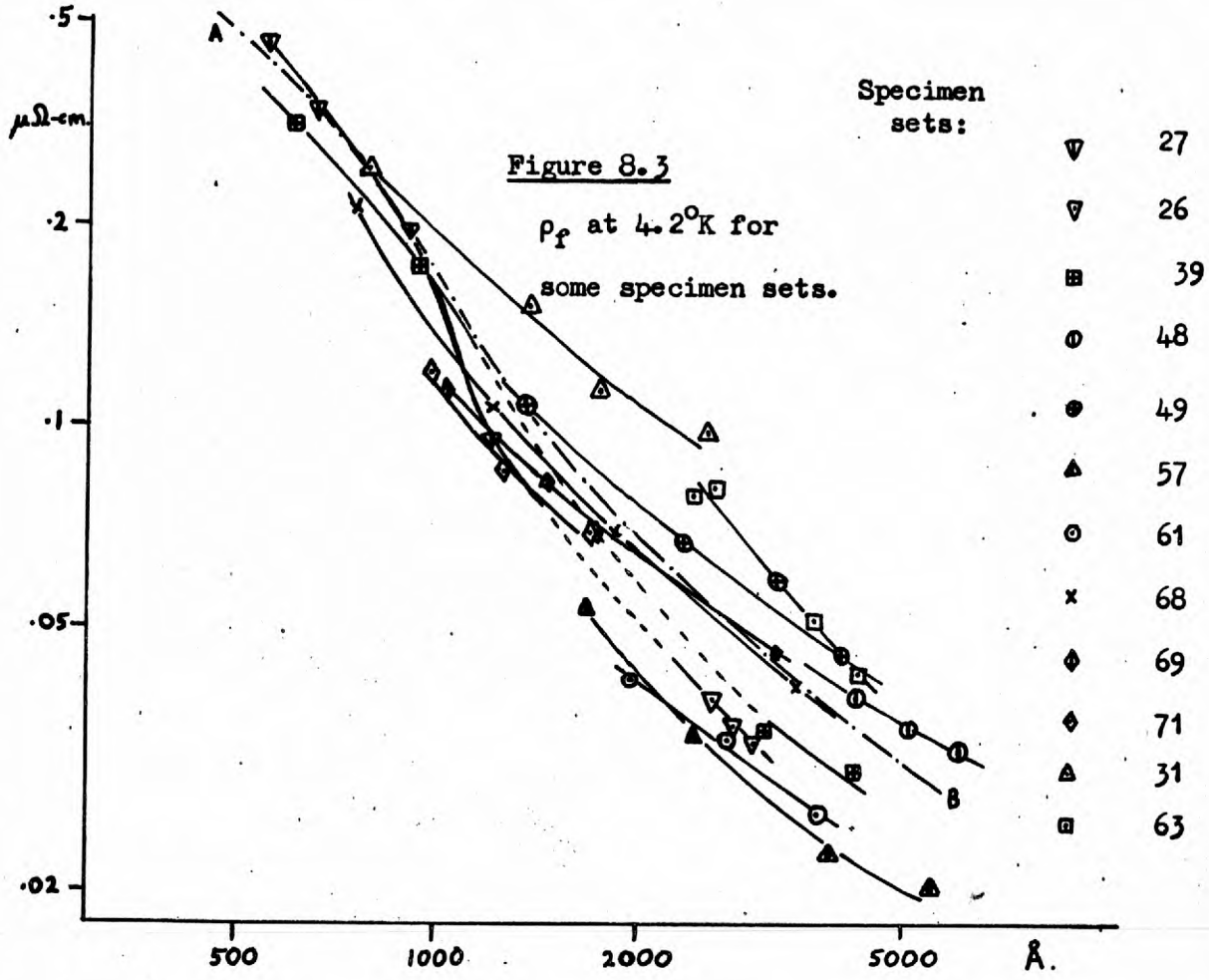

Figure 8.3

ρ_f at 4.2°K for some specimen sets.

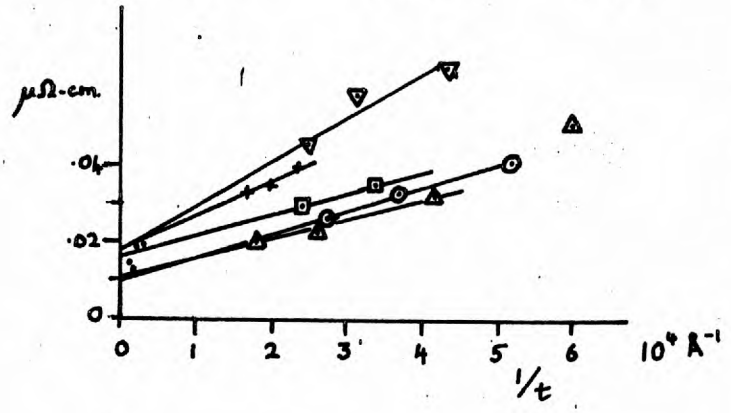

Figure 8.4

Extrapolation to infinite thickness.

Sets: ▽ 49 ▲ 57
+ 48 ⊙ 61
⊡ 39 • 52,54

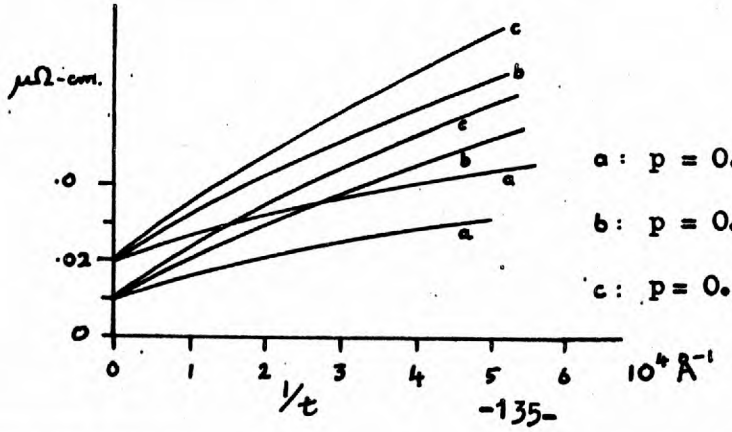

Figure 8.5

ρ_f vs. 1/t from Fuchs' theory.

$$\rho_f = \rho_b + B/t \ , \qquad (8.1)$$

where B is a constant. This form allows ρ_b to be obtained without involving l and p, by extrapolating a plot of ρ_f against 1/t to 1/t=0. The results for some of the thicker specimen sets are plotted in this way in Figure 8.4, and tentative extrapolations have been made for individual specimen sets. There appear to be variations in both the intercept and the slope of the lines. The intercepts give values for the bulk resistivity in the range 0.01 to 0.02 $\mu\,\Omega$-cm.

The constant in 8.1 is proportional to (1-p) (page 58), so variations of the slope indicate variations of p, low slope for high p.

It is pointless to pursue this approach much further, as it is improbable that equation 8.1 is valid for the films in Figure 8.4 at 4.2°K. The values of ρ_b and l are **not independent**, and in Fuchs' treatment the free electron model is used, so they are related by (page 31):

$$\rho_b = \frac{mv_F}{ne^2 l} \ . \qquad (8.2)$$

The free electron model is probably not too great a simplification in the case of silver. Shoenberg[5] has shown that the Fermi surface is confined to a single zone, and departs significantly from a sphere over only a small fraction of its surface. The radius of the main body of the Fermi surface is quite close to the free electron model (page 14). The electronic specific heat, which is proportional to the density of states at the Fermi surface, is only 2% above the free electron value[60].

Assuming, therefore, the free electron model the relationship between resistivity and mean free path in silver is

$$\rho_b = \frac{846}{l} \qquad (8.3)$$

where ρ_b is in $\mu\,\Omega$-cm and l is in Å.

Fuchs' theory shows that equation 8.1 is reasonably applicable provided K is greater than about 0.4. If the bulk resistivity is 0.02 $\mu\Omega$-cm the mean free path from the free electron model is 42000Å, so the specimens plotted in Figure 8.4 all have K values less than 0.4 and are outside the range where 8.1 can be applied.

To see to what extent the Figure 8.4 plot might be useful, the ρ_f-1/t curves calculated from Fuchs' theory are given in Figure 8.5 for two values of ρ_b and three values of p. Only in the region of 1/t below about 10^{-4} Å^{-1} is the approximation of equation 8.1 likely to be valid. The theoretical curves have a fairly straight region above 1/t = 10^{-4} Å^{-1}, and it is here that the points in Figure 8.4 lie. The curvature of this region of the curves is too small to be noticed in the experimental results, and extrapolation to zero 1/t always gives a value higher than ρ_b, so the values obtained from Figure 8.4 may be taken as upper bounds on the value of ρ_b. The true values are lower by between 0.002 and 0.006 $\mu\,\Omega$-cm.

The approximately linear region of the curves in Figure 8.5 above about 1/t = 10^{-4} Å^{-1} have slopes which depend on p, as do the slopes of the straight lines obtained in the simple high K case, but the slope for a given p is less. The variation of slope in Figure 8.4 may still, therefore, be taken as an indication of variation of p between specimen sets.

Very thick films.

Some very thick films were produced by evaporation on to heated mica. The method used was basically as described in Chapter VI, but a special filament in the form of a closely wound coil had to be used to hold sufficient silver. The filament coil was mounted horizontally about 6cm. above the substrate. The resistivities at 4.2°K are included in Figure 8.4. The electron diffraction patterns from these specimens have the usual epitaxial streaks and also a superimposed polycrystalline ring pattern. This is a normal result for very thick films, and is attributed to the presence of small departures from epitaxy which accumulate and become significant as the film grows thicker.

The thickness are 40000 to 60000Å so K is about 1 on the basis of the estimates of ρ_b obtained from Figure 8.4, so the size effect contribution must be quite small. For each of these films a lower bound on the bulk resistivity can be obtained from the high K theory, which should be applicable this time. If p is taken as zero the values of ρ_b obtained lie between 0.0075 and 0.015. It will be shown shortly that non-zero values of p are expected, so the estimated bulk resistivities of the thick films should be higher, e.g. if p=0.5 they lie between 0.01 and 0.017 $\mu\Omega$-cm. These values are similar to those obtained by extrapolation from thinner films. This agreement should perhaps be taken as an indication that the departures from epitaxy in the very thick films do not greatly influence the bulk resistivity, rather than as confirmation of the results from the thinner films. The polycrystalline rings may be caused by no greater number of dislocations per unit volume than are present in thinner films.

Estimating p

The rough estimates of ρ_b obtained may now be used to give corresponding values for p, as l can be obtained from the free electron relationship between l and ρ_b (equation 8.3). The ratios ρ_f/ρ_b and t/l define a point on the set of Fuchs' curves (page 56) which is associated with a particular value of p. As the estimates of ρ_b are fairly rough, the values of p have been obtained for the three values of ρ_b 0.01, 0.015 and 0.02 $\mu\,\Omega$-cm. The specimens are those used in Figure 8.4 and the results are listed in Table 8.1.

The values of p are quite high, showing that there is a substantial amount of specular scattering of the electrons at the film surfaces. The agreement within specimen sets, for a given value of ρ_b assumed, is fair. There are significant differences between specimen sets. These can be reduced if different values of ρ_b are assumed, but not eliminated without going outside the range estimated earlier for ρ_b. It appears, therefore, that variations in both p and ρ_b are involved in the variations found in the film resistivities.

Specimens less than 1500Å in thickness

So far the discussion has been mainly confined to those specimens with thicknesses greater than about 1500Å. The results for these are consistent with a bulk resistivity of about 0.01 —>0.02 $\mu\,\Omega$-cm and a surface specularity coefficient (p) 0.4-0.8. In Figure 8.2 the curve AB has been transferred to a Fuchs' plot assuming ρ_b to be 0.013 . $\mu\,\Omega$-cm and l to be the value obtained from the free electron relationship between ρ_b and l. The assumption of the free electron relationship constrains

Specimen No.	p (a)	(b)	(c)	Specimen No.	p (a)	(b)	(c)
39.3	.67	.75	.82	57.1	.77	.89	-
.4	.63	.74	.84	.2	.80	.89	.96
				.3	.72	.80	.86
49.1	.41	.52	.61	.4	.65	.71	.77
.2	.34	.42	.51				
.3	.40	.49	.56	61.1	.72	.78	.84
.4	.36	.42	.49	.2	.71	.79	.86
				.3	.73	.85	.92
48.1	.47	.60	.69				
.2	.49	.61	.71	(a) ρ_b = 0.01			
.3	.43	.60	.71	(b) ρ_b = 0.015			
.4	.31	.43	.58	(c) ρ_b = 0.02			

Table 8.1

The p values for epitaxial silver specimens.

(Note. Specimen sets are numbered in sequence of preparation. Specimens within a set are numbered .1 to .4)

the movement of AB on Figure 8.2, resulting from a change of ρ_b, and therefore 1, to a line of slope - 45°. Single points are constrained in the same way and Figure 8.2 shows the movements of a number of points on AB for changes of ρ_b of .01 $\mu\Omega$-cm.

It can be seen from Figure 8.2 that changing the value of ρ_b assumed for the specimens in order to reduce all points to a single curve would require very large changes of ρ_b. It would be similarly impossible to reduce the curve AB to a Fuchs' curve for a single value of p. This shows that variations in p are involved in the shape of AB, as well as in the scatter of points about AB.

It can also be seen from Figure 8.2 that the p values are quite low for films below 1000Å, ~0.1 —> 0.2. Figure 8.3 shows that for a given specimen set the change of resistivity with thickness usually follows a curve nearly parallel to AB, and it is assumed that the curve that is followed must relate to some condition of preparation which has been inadequately controlled. The change to low p at ~ 1000Å appears to be quite independent of conditions, a fact which is well illustrated by specimen set 57, which has members with very low resistivities at about 4000-5000Å and thinner members which are rapidly rising in resistivity as they approach 1000Å in thickness.

Specimens with a thin layer of aluminium.

The fraction (p) of electrons specularly reflected at the surface of a film is an important parameter in the theory of its resistivity. In the previous sections it was shown that p appears to have a general variation with the thickness of the film, and variations at given thicknesses between different specimen sets. It is probable that there are also

variations of ρ_b which complicate the interpretation of the results. If p could be varied independently of ρ_b, more definite results might be obtainable.

It seems unlikely that any method of increasing the value of p could be found, but decreasing it is quite feasible. To this end, thin layers of aluminium were evaporated on to the free surfaces of epitaxial silver films, after they had cooled to room temperature. Electron diffraction patterns from these surfaces showed a faint diffuse ring pattern, indicating a fine grained polycrystalline structure. The absence of any silver pattern showed that the surfaces were fully covered by the aluminium.

The resistivities at 4.2°K of all epitaxial silver specimens with aluminium layers are shown in Figure 8.6, with the curves from the untreated epitaxial films results (Figure 8.1) for comparison. The specimens with aluminium layers lie, in general, above the line AB, indicating lower values of p. The specimens with aluminium layers are not sharply separated from the untreated specimens, as the spread in the results for both is large. A line CD is drawn in Figure 8.6 which represents the general pattern of these results. It is given again in Figure 8.7, with AB and the Fuchs' curves based on $\rho_1 = 0.013$ and $l = 65{,}000$Å, as in Figure 8.2. The change in p brought about by the aluminium layer is seen to be typically about 0.1 at the thicker end of the range. At the thin end the specimens with aluminium layers move out of the range of the Fuchs' curves. This suggests, at first sight, that the constancy of ρ_b, implied in Figure 8.7, is not justified, and that ρ_b should be higher for the thinner films. It has already been shown, however, that large changes in ρ_b would be required to bring these points inside the range of the Fuchs' curves.

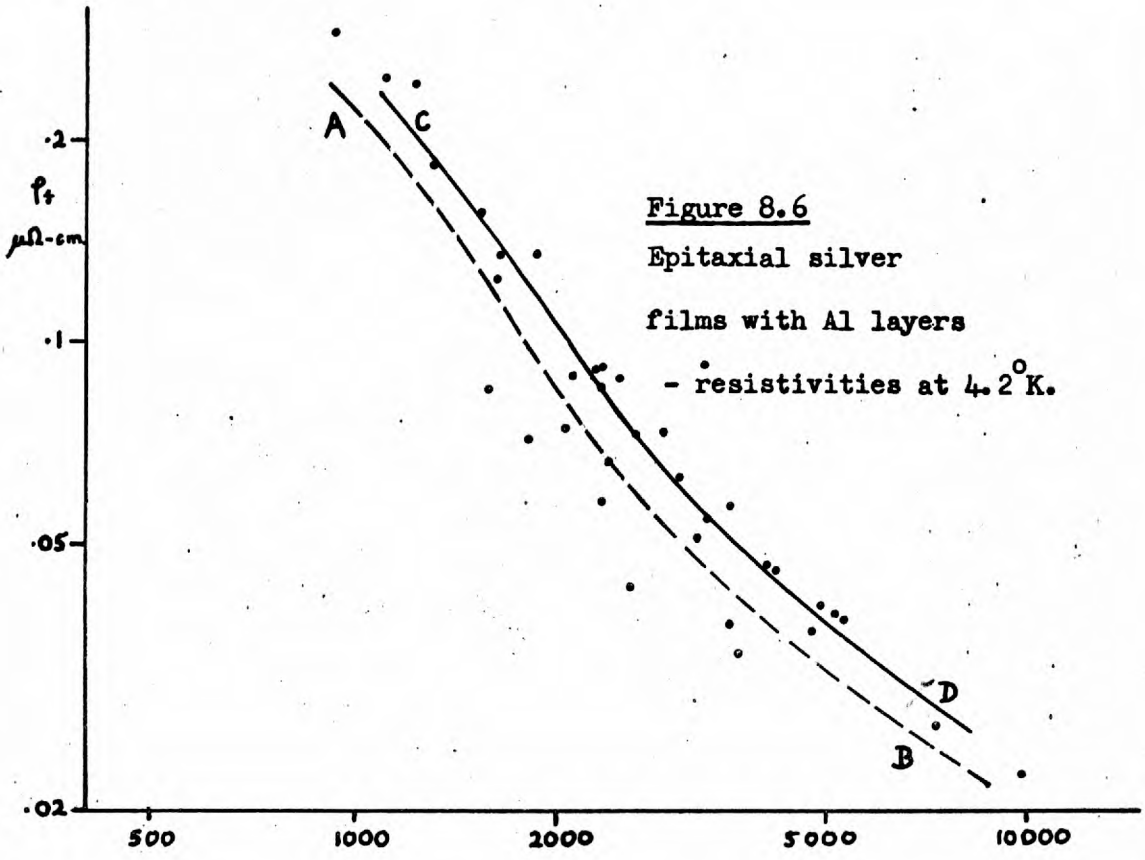

Figure 8.6

Epitaxial silver films with Al layers - resistivities at 4.2°K.

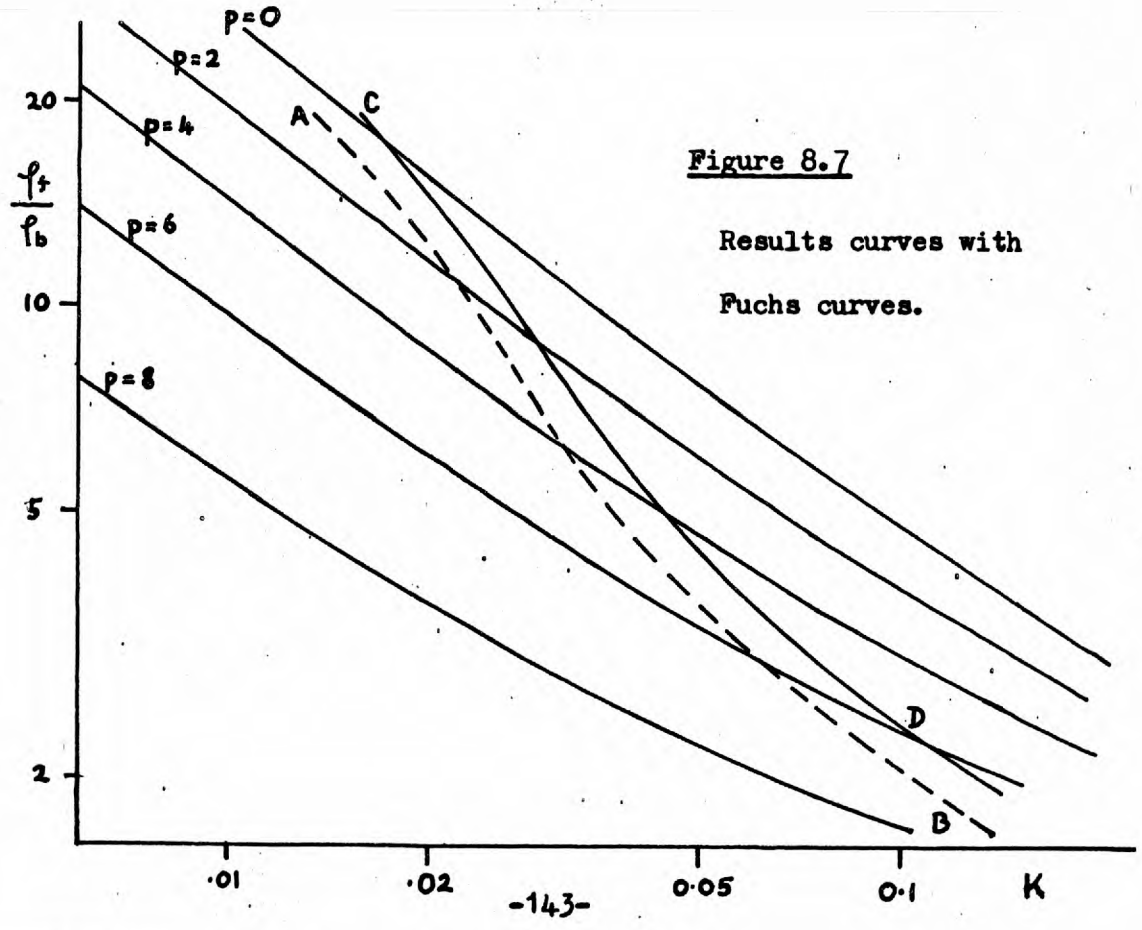

Figure 8.7

Results curves with Fuchs curves.

The spread of the resistivities at 4.2°K obscures the change of p produced by the aluminium layer, when all specimens are considered together. In an attempt to get more accurate information on the change produced by an aluminium layer, some specimen sets were prepared in the following way. Two sets of epitaxial specimens were evaporated together, with corresponding specimens as faras possible of the same thickness. They were allowed to cool to room temperature, and a thin (~60Å) layer of aluminium was evaporated over the surface of one of the sets. By this means it was hoped to produce specimens differing only in the presence or absence of an aluminium layer.

The resistivities at 4.2°K of 11 pairs of such specimens are shown in Figure 8.8. The aluminium layers result in increases in the resistivities by various amounts. If it is assumed that the bulk resistivities are the same for corresponding films, the changes in resistivity can be attributed

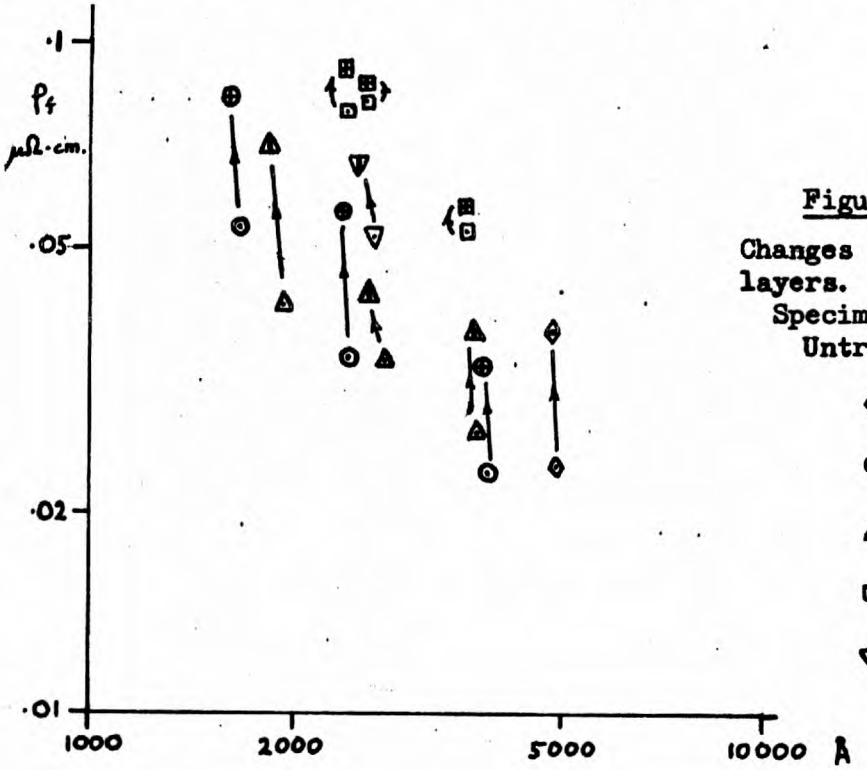

Figure 8.8

Changes caused by Aluminium layers.

Specimen sets: Untreated	+Al layer
◇ 59	◆ 58
○ 57	● 56
△ 61	▲ 60
□ 63	■ 62
▽ 67	▼ 66

to changes in p. This is not entirely justified as differences between sets evaporated at the same time can occur, as is shown by specimen sets 48 and 49 in Figure 8.3. The values of p estimated on the basis of the free electron model and a bulk resistivity of 0.015 $\mu\ \Omega$-cm are given for the specimen pairs in Table 8.2. The Δp column gives the difference between the p values for each pair. These show considerable variation, which may be partly due to the variation between the epitaxial specimen sets mentioned above. These results give specific instances of the trend illustrated by the general plot in Figure 8.7.

Specimen set pairs	p (a)	p (b)	Δp	Specimen set pairs	p (a)	p (b)	Δp
57/56	89	71	.18	63/62	.37	.26	.11
	80	59	.21		.31	.28	.03
	71	51	.20		.47	.40	.07
59/58	.86	.69	.17		.54	.50	.04
61/60	.78	.56	.22	67/66	.60	.46	.14
	.79	.70	.09		.50	.09	.41
	.85	.67	.18				

(a) Epitaxial silver film.

(b) Epitaxial silver film with Al layers.

Table 8.2 Changes in p caused by an aluminium layer.

Films with different values of p on the two surfaces.

Up to this point it has been tacitly assumed that p is the same at both surfaces of the films. Even if this is true of epitaxial films, it cannot possibly continue to be true when one of the surfaces is deliberately roughened. The theory of films with different surfaces has been discussed on page 59, and an expression appropriate for thick films obtained i.e.

$$\rho_f = \rho_b + \frac{3A}{8K}\left(1 - \frac{p_1 + p_2}{2}\right) \qquad (8.4)$$

where $A = \rho_b l$, a constant. The change from the usual thick film theory is that p is replaced by the average of p at the two surfaces. The extent to which the same substitution is justified at lower K has been discussed for an extreme case in which one surface is assumed to be specular (page 61). The errors arising from using the mean value of p in the one-p theory, in this case, were obtained. They are plotted against K for various values of $\bar{p}$ in Figure 3.11 (page 62). If these errors are typical of the whole range of p_1 and p_2, the error in ρ_f involved in assuming the one p form for the films with aluminium layers is less than 10%. The values of p obtained so far are, at best, the mean for the two surfaces. In cases where the surfaces are different, the value obtained underestimates the mean.

The effect of changing the p of just one surface will now be considered. This situation is just that which occurs when two specimen sets differ by only a thin layer of aluminium on one of them. The surfaces are characterised by (p,p_1) and (p,p_2) for the modified and unmodified films respectively. If the mean is obtained for both surfaces, the difference between the means $(\Delta\bar{p})$ is half the change of p at the free

surface.

$$\therefore \qquad p_1 - p_2 = 2\,\Delta\bar{p} \qquad (8.5)$$

The estimated mean for the modified film is expected to be a little low, making $\Delta\bar{p}$, and therefore $p_1 - p_2$, rather too large. The values estimated for $2\Delta\bar{p}$, for the films which have high values of p in the unmodified state, are typically 0.4. If there is a 10% error in ρ_f resulting from the use of $\bar{p}$ in the one-p theory this value would be reduced to about 0.3.

Films with 'cold-substrate' layers of silver

The results for untreated epitaxial silver films indicate a variation of p with film thickness. To see if the p values could be changed significantly by altering the state of the silver at the surface of the films, some specimens were prepared as follows. Epitaxial silver specimens sets were prepared in pairs and allowed to cool. A further thin layer of silver was evaporated on to the cold surface of one of the films. Electron diffraction observations of such films show that the surface layer is completely oriented on the epitaxial silver. The streaky effect is less marked, however, indicating a rougher surface.

A few specimen set pairs of this type were measured, but the results obtained were inconclusive. The p values calculated on the basis of the free electron model with $\rho_b = 0.015$ are given in Table 8.3. The changes of p produced by the silver layers are usually negative but are otherwise too variable to yield a clear picture.

Specimen set pairs	p (a)	p (b)	Δp	Specimen set pairs	p (a)	p (b)	Δp
39/38	.19	.00	.19	71/70	.59	.31	.28
	.30	.38	-.08		.61	.34	.27
	.75	.64	.11		.55	.31	.24
	.74	.59	.15		.49	.19	.30
69/68	.60	.64	-.04				
	.54	.56	-.02				
	.50	.48	.02				

(a) Epitaxial silver films

(b) Epitaxial silver films with 'cold-substrate' layers.

Table 8.3

Change in p case d by cold substrate layers of silver.

Silver films evaporated on to a cold substrate.

To get some quantitative idea of the improvement in the structure of films produced by epitaxial, rather than non-epitaxial, methods, some specimens were produced by evaporating silver on to a freshly cleaved mica at room temperature, and measured. Electron diffraction observations show that such specimens are well oriented, but the spots are less spread into streaks than those for films evaporated on to a hot substrate, indicating a rougher surface.

The resistivities at 4.2°K are shown in Figure. 8.1, where they are seen to lie well above the resistivities for plain epitaxial films.

If the free electron relationship $\rho_b = 846/l$ is assumed, the results are consistently explained in terms of a ρ_b of 0.3 - 0.35 $\mu\ \Omega$-cm, and a p in the range 0.1 to 0.4. The ρ_b is about 20 times larger than that found for most epitaxial films. As the bulk resistivity is proportional to the number of defects in the metal, this factor gives a measure of the structural improvement obtained by evaporating on to a heated substrate.

3) The Resistivity of Bulk Silver.

The sections following this will be concerned with the resistivities of silver films at temperatures between 4.2°K and about 300°K. The resistivity of the bulk material of the films is an important parameter in their effective resistivity, and it is desirable to know how it is related to the resistivity of bulk silver. This question has already arisen in connection with the fitting procedure in the previous chapter. It was assumed there that Matthiessen's rule applied to the bulk material of the films in the temperature range above 150°K i.e.

$$\rho_b = \rho_1 + \rho_{bc} \qquad (8.6)$$

It will be shown that this assumption is reasonably justified in the temperature range mentioned, but not at lower temperatures, especially below 100°K. In particular, the ρ_{bc} applicable to the high temperature region is not the same as the residual resistivity, and may differ from it by a factor of two.

The analysis of the thin film results is facilitated by having ρ_1 available in terms of the copper thermometer used in the resistance

measuring runs. The resistances of some bulk silver wires were measured in the same apparatus as is used for the films. They were drawn down from the same material as is used in the preparation of the films. The lattice resistivity was obtained from the measured resistances by subtracting the residual resistance, and multiplying by a size-shape factor which was obtained by assuming the room temperature results given by White and Woods[52].

The results obtained for a wire which had a residual resistivity of about 0.040 $\mu\ \Omega$-cm were found to deviate from the White and Woods results at lower temperatures (e.g. 2-3% at 80°K). It was realized that this might be caused by the failure of Matthiessen's rule, so further wire specimens were made, and annealed by heating electrically, in a vacuum, for about half an hour at near red heat. Specimens produced in this way had residual resistivity ratios ($R_{4.2}/R_{300}$) of about 1/500 (cf. 1/40 above), which is low enough to enable the value of ($\rho(T) - \rho\ (4.2)$) obtained to be confidently taken as the ideal lattice resistivity of silver at temperature T. The agreement with White and Woods is as good as their implied accuracy allows, and the residual resistivity ratio is lower than that of their specimen, (1/160).

The residual resistivity of unannealed, or partly annealed, wire is caused by lattice defects, and it will now be shown that their contribution is not temperature independent. Figure 8.10 shows the difference between the temperature dependent part of the resistivities of two specimen wires, one unannealed and one partly annealed, and the ideal lattice resistivity as obtained from a well annealed wire. The multiplying size-shape constant has been adjusted so that Matthiessen's rule is obeyed at high temperatures.

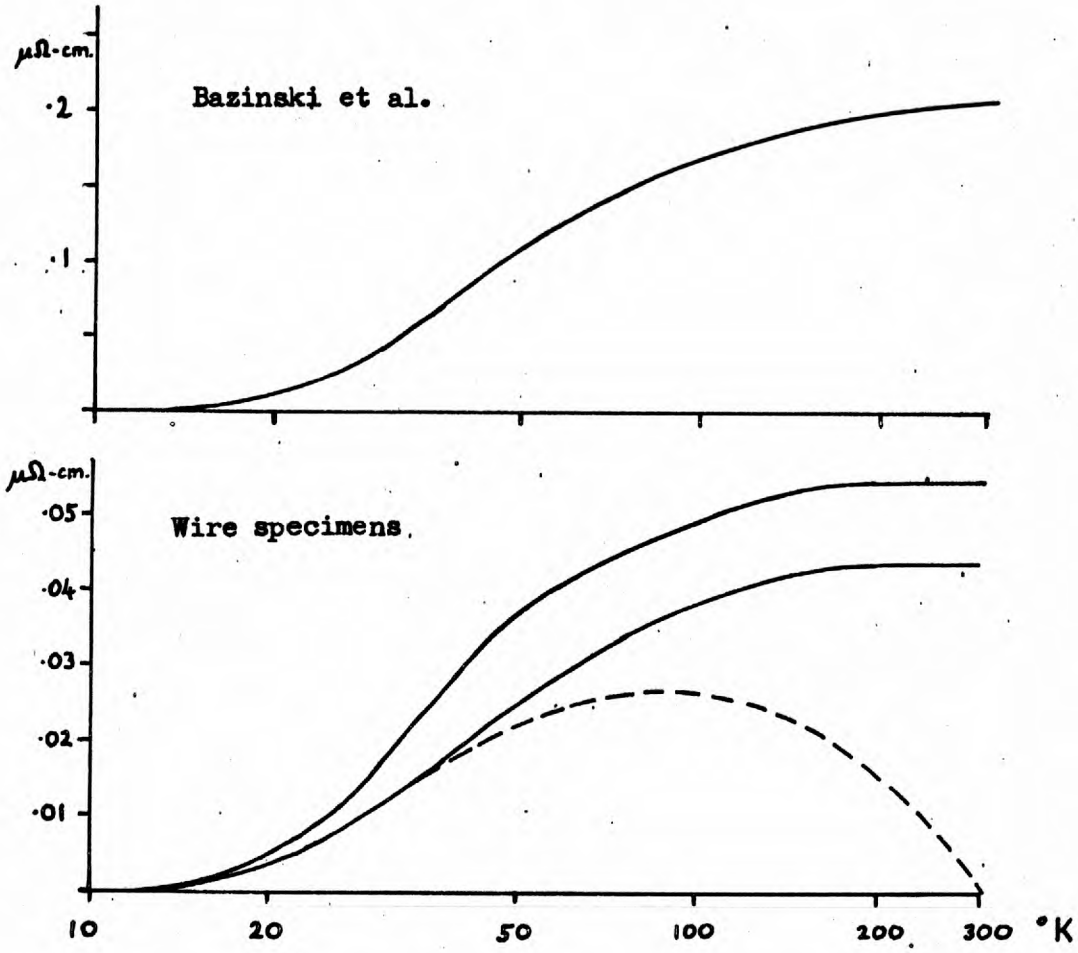

Figure 8.10 ($\rho_w - \rho_1 - \rho_o$) vs. temperature.

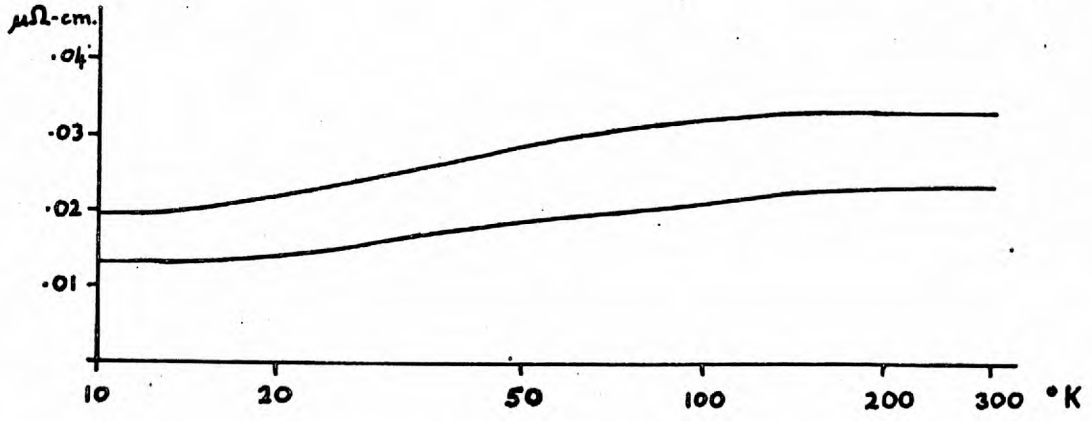

Figure 8.11 ($\rho_f - \rho_1$) for thick films.

The dotted line shows the curve obtained when one of the wires is normalized to the White and Woods value at 300°K. This requires a size-shape constant which is $\sim$ 3% lower.

The failure of Matthiessen's rule under these circumstances has been reported by Bazinski et al[40], who compared the resistivities of deformed and annealed specimens of accurately known shape factor. The results they obtained for silver are included in Figure 8.10, and have the same general shape as the result introduced above, but with a small linear temperature dependence at high temperatures.

These results lead to the conclusion that the resistivity of the bulk material of the films cannot be taken as $(\rho_1 + \text{constant})$ over the whole temperature range, if lattice defects play an important part in the residual resistivity. The work described in Chapter IV shows that epitaxial thin films have a high dislocation density, so the presence of dislocations is certainly important.

Bazinski et al. show that dislocations give rise to additional resistivity proportional to the dislocation density, and give constants for various metals. There have been no measurements of the dislocation density in epitaxial silver films on mica, but values have been obtained for epitaxial silver films on rocksalt (1.10^{11} to 3.10^{11} cm/cm^3 [29]) and epitaxial gold films on epitaxial silver on mica (10^{10} to 10^{11} cm/cm^3 [21]). It is not unreasonable to expect values similar to these for epitaxial silver films on mica. Using the constant for silver given by Bazinski et al, a dislocation density of 10^{11} cm/cm^3 would give an additional resistivity of 0.02 $\mu\,\Omega$-cm. This value is agreeably close to the bulk residual

resistivities obtained for the thicker films, but the uncertainty in the dislocation density makes it unreliable.

The temperature dependence of the bulk resistivity of the films may be approached more directly by considering the resistivity results for very thick films. These films have been mentioned before (page 138). Their thicknesses are 40,000 - 60,000Å and their residual resistivities 0.012 - 0.02 $\mu\ \Omega$-cm. The value of K is therefore ~1 if the free electron model is assumed. The resistivity results are plotted in Figure 8.11 in the form $(\rho(T) - \rho_1(T))$ against T, where $\rho(T)$ is the measured resistivity and ρ_o is the residual resistivity. It can be seen that the curves have the same general shape as the curves for the wire specimens. Fuchs' theory shows that size effects in thick specimens ($K > 0.4$) should contribute a nearly constant term, and the resistivity should, if anything, be less at high K (i.e. high temperature) (page 57).

In order to compare more effectively the curves in Figure 8.11, they are reduced by expressing them all as $\frac{\Delta\rho(T) - \rho_o}{\rho_m - \rho_o}$, where the terms are explained by Figure 8.12. The resulting curves are plotted in Figures 8.13 and 8.14. The former contains the wires and the latter the thick films. The results for both wires and films all lie close to a universal curve, which is shown in Figure 8.15, with dotted lines to indicate its uncertainty. The differences between wire and film-specimens are no greater than the differences between different film specimens. The close similarity between the reduced curves of cold worked wires and thick films confirms that dislocations play an important part

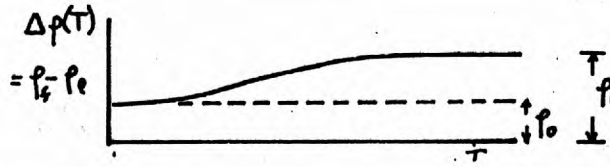

Figure 8.12
(N.B. ρ_m and ρ_o redefined here)

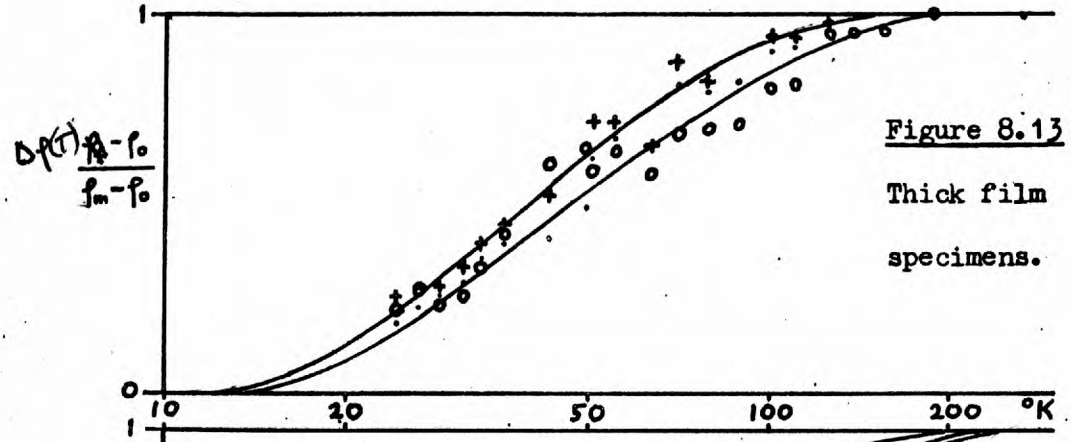

Figure 8.13
Thick film specimens.

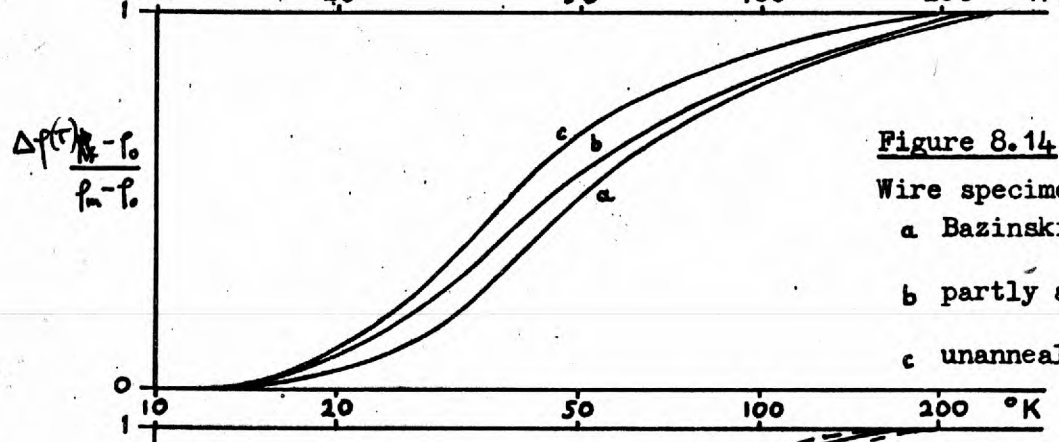

Figure 8.14
Wire specimens.
a Bazinski et al.
b partly annealed wire
c unannealed wire.

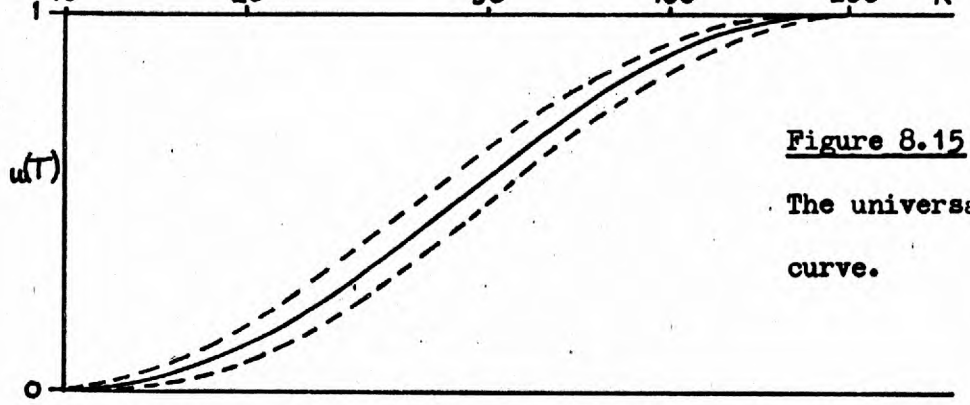

Figure 8.15
The universal curve.

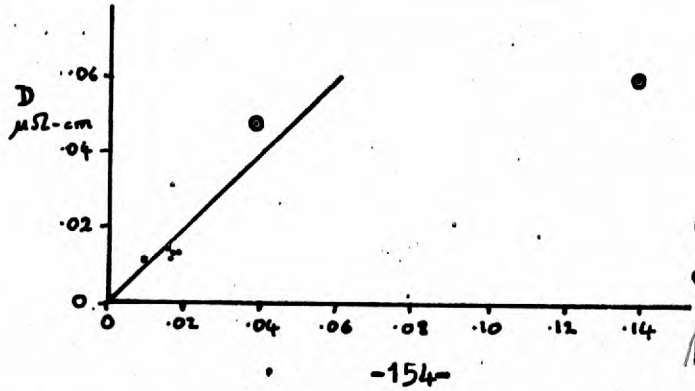

Figure 8.15 a
• Thick films.
● Wires.

in the residual resistivity of thin films.

An important outcome of the existence of a universal curve is the possibility of using it to predict the bulk resistivity of the material of the films at all temperatures. It will be expressed in the form:

$$\rho_b(T) = \rho_1(T) + \rho_o + \rho_A(T) \qquad (8.7)$$

The universal curve approach allows the additional term $\rho_A(T)$ to be replaced by $Du(T)$, where D is a constant and $u(T)$ lies between 0 and 1, and is the universal curve of Figure 8.15. The need to find a function has been replaced by the need to find a constant, a considerable simplification.

The value of D can be roughly related to ρ_o, as is shown in Figure 8.15 The actual 4.2°K resistivities have been given corrections to allow for the size effect, on the basis of $p = 0.5$. The nature of the line that should be drawn is not very clear, but the straight line which gives $D = \rho_o$ is not unreasonable. This line does not take account of the unannealed wire, but as a speculation it can be said that the partly annealed wire may be more like the films than the unannealed wire as the films are produced at a fairly high temperature, and may be effectively partly annealed.

The uncertainty in the non-ideal part of the bulk resistivity, $(\rho_o(4.2) + Du(T))$, is likely to be quite large as ρ_o is difficult to estimate accurately and the relationship between ρ_o and D is only roughly known.

The bulk resistivity and the high temperature fitting.

In the previous chapter it was shown how the resistivities of thin films specimens are obtained from the resistance by assuming that Matthiessen's rule holds in the high temperature region (> 150°K). This assumption has been made for all the specimens reported here, both wire and film. The results of Bazinski et al. for cold worked silver (Figure 8.10) show a small linear temperature dependence of $(\rho_{wire} - \rho_1)$ in the high temperature region, and it is of interest to see what error in the size-shape factor, and in ρ_c, might arise from ignoring this.

All film resistance measurements are fitted to the form

$$R_f(T) = C(\rho_1 (T) + \rho_c) , \qquad (8.8)$$

where C is the size-shape factor. If the temperature dependent part of the bulk resistivity should have the form $(1 + c)\ \rho_1(T)$, where c is a constant << 1, in the high temperature region, 8.8 becomes

$$R_f(T) = \frac{C}{1+c} \quad ((1+c)\ \rho_1(T) + (1+c)\ \rho_c) . \qquad (8.9)$$

Thus by assuming that the bulk temperature dependence is as for the ideal lattice, an error of 100 c % is obtained in both C and ρ_c.

How big is c in practice? The results of Bazinski et al. for highly strained wires give a c of 0.04. The additional resistivity caused by dislocations in films with a bulk residual resistivity of 0.02 $\mu\ \Omega$-cm is about ten times smaller, so c should be no more than 0.004 (0.4%). This justifies the assumption of Matthiesen's rule for the fitting method.

4) The Constant Term from the High Temperature Fitting.

In the section on the residual resistivity of the films, attempts to obtain values for 'p' were made difficult by the uncertainty about the constancy of ρ_b and p from specimen to specimen. Inferences could only be made by using several specimens of different thickness to vary K. Further difficulties were caused by the inapplicability of the high K limit to most of the films. In the temperature range above about 150°K, the bulk mean free path is short enough for the high K limit to be used, and variations in K occur as a result of change of temperature. It is possible in this range, therefore, to estimate p for a single specimen.

The applicability of the high K limit at high temperatures has already been exploited in the fitting method for finding the size-shape factor of specimens. The significance of the term ρ_c, obtained incidentally in the course of the analysis, will now be considered in terms of Fuchs' theory.

The fitting procedure yields ρ_c from

$$\rho_f = \rho_l + \rho_c . \tag{8.10}$$

If p is the same on both surfaces, Fuchs' high K limit gives

$$\rho_f = \rho_b + \frac{3\rho_b l}{8t} (1-p). \tag{8.11}$$

Matthiessen's rule is assumed for the bulk material of the films (page 149) so

$$\rho_c = \rho_{bc} + \tfrac{3}{8} \frac{\rho_b l}{t} (1-p). \tag{8.12}$$

On the basis of simple resistance theory $\rho_b l$ is a constant (A) so rearranging 8.12,

$$p = 1 - \frac{8t}{3A} (\rho_c - \rho_{bc}) \qquad (8.13)$$

The constant term ρ_{bc} has been shown, in the previous section (page 155), to be different from ρ_o, but roughly related to it by $\rho_{bc} = 2\rho_o$.

It is not easy to estimate ρ_{bc} with certainty so, as a basis for discussion, it is useful to evaluate p when ρ_{bc} is assumed zero. This gives a minimum value for p which will be referred to as p(min). Figure 8.16 shows values of p(min) plotted against thickness for epitaxial silver specimens. The values are fairly scattered, as is expected from the $4.2^{o}K$ result, and lie mainly in the range 0.2 to 0.5. The general trend is summarized by the line XY.

The effect of including ρ_{bc} in the estimation of p is independent of p(min), but proportional to ρ_{bc} and to t. The increase (Δp) resulting from a ρ_{bc} of 0.01 $\mu\Omega$-cm is plotted in Figure 8.16 . For films thinner than 1000Å Δp is small, so in this region p is quite well known, provided that ρ_o is not very much greater than the value estimated for thicker films (~0.01 - 0.02 $\mu\Omega$-cm). As the films get thicker ρ_{bc} become more important, but it is possible to be a little more confident about ρ_o (page 134). Eventually, certainly by 10,000Å, ρ_{bc} dominates the estimate, and uncertainties in ρ_o and in its relationship to ρ_{bc} loom too large for comfort.

The effect of reasonable values of ρ_o (0.01, 0.0125 and 0.015 $\mu\Omega$ cm)

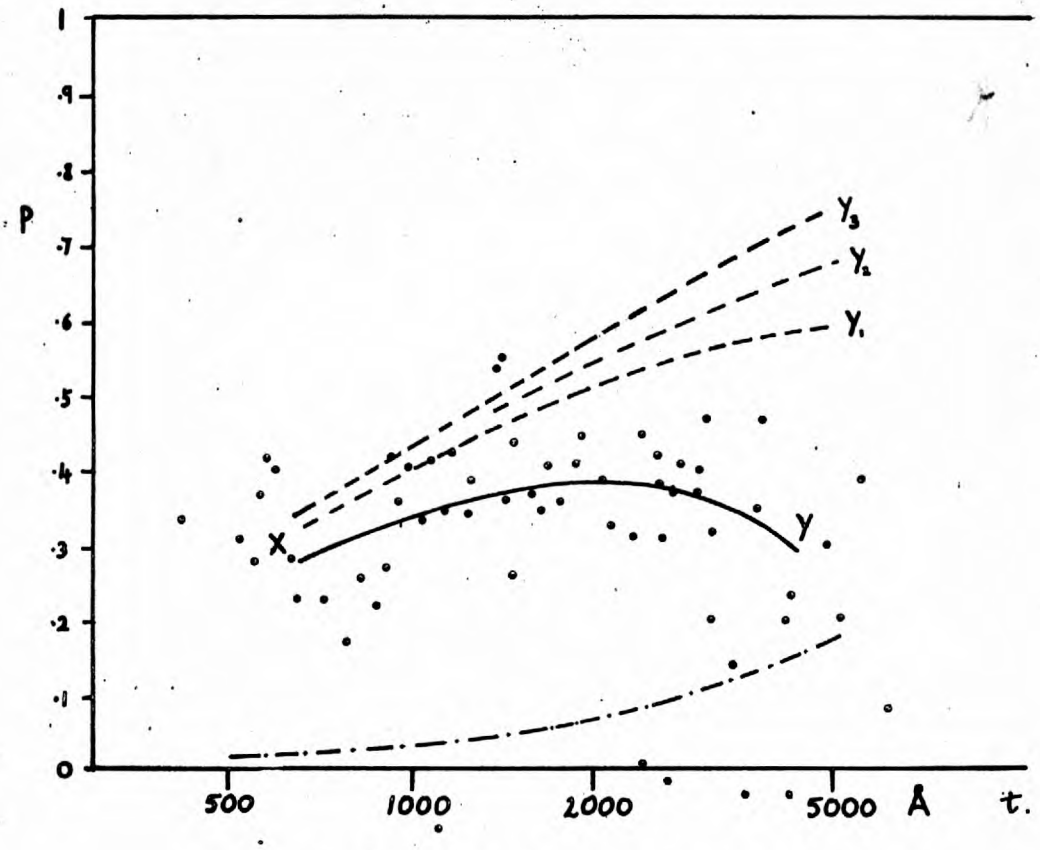

Figure 8.16 p(min) for epitaxial silver films

(—. —.—. Δρ for ρ_{bc} = 0.01)

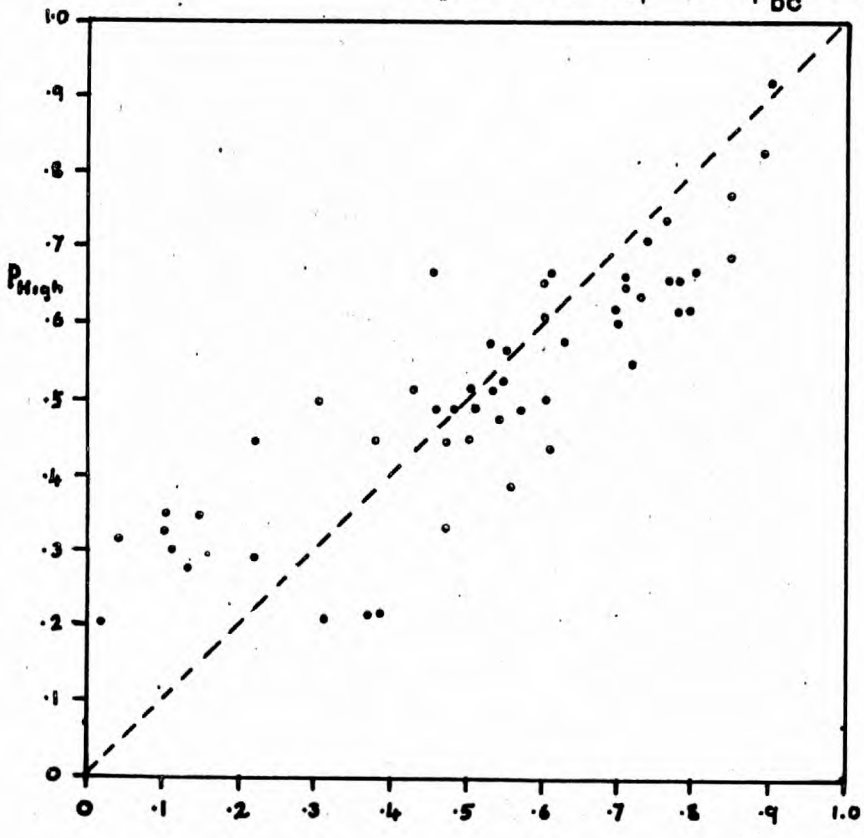

Figure 8.17

p(high temp.) vs p (low temp.) for epitaxial silver films.

on XY is shown in Figure 8.16a by XY_1 XY_2 and XY_3, on the assumption that $\rho_{bc} = 2\rho_o$. At the thick end of the range, about 2000Å —> 5000Å, the values of p for $\rho_o = 0.0125$ lie between 0.6 and 0.7, and agree well with the values obtained by superimposing the trend line AB of the 4.2°K results (Figure 8.1) on a set of Fuchs' curves with the same ρ_o. Changing the ρ_o assumed produces similar changes in the values of p estimated at both high and low temperatures. At the thin end of the range (below 1000 Å), there is a marked difference between the two approaches. The high temperature results point to values of p between 0.2 and 0.4, whereas the 4.2°K results give 0.1 or less.

A more detailed comparison of the high and low temperature values of p is given in Figure 8.17. Both estimates of p assume a ρ_o of 0.015 μΩcm The high temperature values are obtained from equation 8.13 and the low temperature values from the Fuchs' curves, as on page 139 . The agreement between the pairs of values is quite good, considering the large differences in K between the high and low temperature ends of the range. The p values above about 0.5 are mainly from the thicker films and here there is a tendency for the high temperature values to be lower than the low temperature values. The differences are usually less than 0.15 (~ 25%). The lower values of p are from the thinner specimens, and the tendency for the high temperature values of p, for these films, to be higher than the low temperature values is shown again in this plot.

It is not immediately necessary to go beyond the simple theory used so far in order to find possible causes for the discrepancies shown in Figure 8.17 for films at the thick end of the range. There may easily

be errors in both ρ_o, the bulk residual resistivity, and in the constant relating ρ_o to ρ_{bc}, the high temperature constant term. The error in ρ_o would change the two estimates by about the same amount, but the error in ρ_{bc} effects only the high temperature value. This could easily account for the discrepancies in the thicker films.

The value of ρ_{bc} is not so important for the p values estimated for the thinner films, and could not account for the discrepancies, especially as p(min) is larger than the low temperature value for these films. The p value estimated at low temperatures would be lower than that estimated at high temperatures if the two surfaceshad different values of p. This explanation would only be sufficient, however, if very large differences between the two surfaces could be assumed. Large scale features of the film structure, as revealed by replica electron microscopy, may be of importance, and will be discussed in the next chapter (page 176).

Epitaxial silver films with aluminium layers.

The p values estimated for films with thin aluminium layers do not behave noticeably differently from those for untreated films. The values for a number of the thicker specimen pairs, with and without aluminium layers, are listed in Table 8.3. The low temperature p values are higher than the high temperature values for both the treated and untreated films. The changes in p produced by the aluminium layers are, however, about the same at both high and low temperatures.

	Untreated			Treated			
Specimen	p (a)	p (b)	Specimen	p (a)	p (b)	Δp (a)	Δp (b)
57.2	.83	.84	56.3	.62	.71	.21	.13
.3	.66	.80	.2	.46	.59	.20	.21
.4	.58	.71	.1	.44	.51	.14	.20
59.3	.77	.86	58.2	.48	.69	.29	.17
61.1	.62	.78	60.4	.40	.53	.22	.25
2	.62	.79	.3	.58	.70	.04	.09
3	.72	.85	.2	.58	.67	.14	.18

Table 8.3

Films with Al layers.

The p values from high and low temperatures compared.

(a) High temperature values

(b) Low temperature values.

5) Variation of Film Resistivity with Temperature.

Below about 20°K.

The large increase in resistivity observed by Chopra[42] between 8°K and 12°K in fairly thick silver films has already been mentioned (page 85). He reported a twofold increase in resistivity in this range for epitaxial silver films 15,000 and 60,000Å thick, and a smaller increase for polycrystalline films on glass. It is shown below that no sign of this effect has been found in the present work.

The resistivities of several specimens were measured in some detail in the temperature range 4.2°K to 30°K. The results for some of these are plotted in Figure 8.18, and Chopra's results are given for comparison. The specimens cover a wide range of thickness, and two of them have thin aluminium layers on their free surfaces. The ones most closely resembling those used by Chopra are specimens 52.1 and 55.1, which have thicknesses of 40,000Å and 15,000Å respectively. The residual resistivity ratio (R(300)/R(4.2)) of the former specimen is 85, which is a little lower than the value quoted by Chopra for his specimens (110). Two specimens with higher resistivity ratios, and thicknesses of about 60,000Å were measured at the same time as 52.1 and 55.1, but with no points between 24.4°K and 4.2°K. The difference in resistivity between 24.4°K and 4.2°K is nearly the same for all four specimens, suggesting that 54.1 and .2 behave in the same way as 55.1 and 52.1

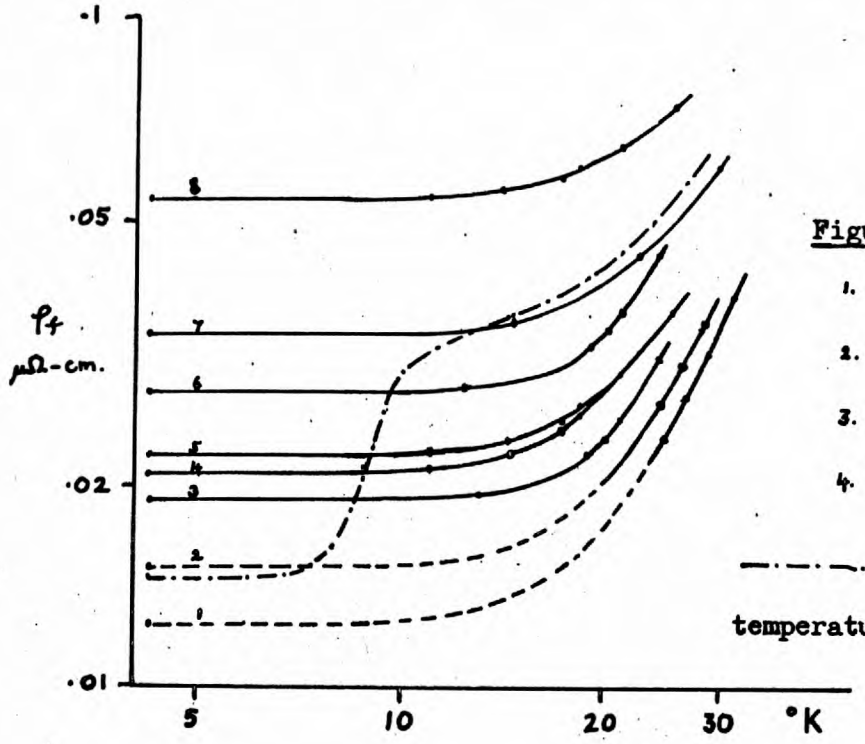

Figure 8.18

1. 54.2
2. 54.1
3. 52.1
4. 57.1
5. 58.4
6. 55.1
7. 48.3
8. 57.4

—·—·—·— Chopra's low temperature result.

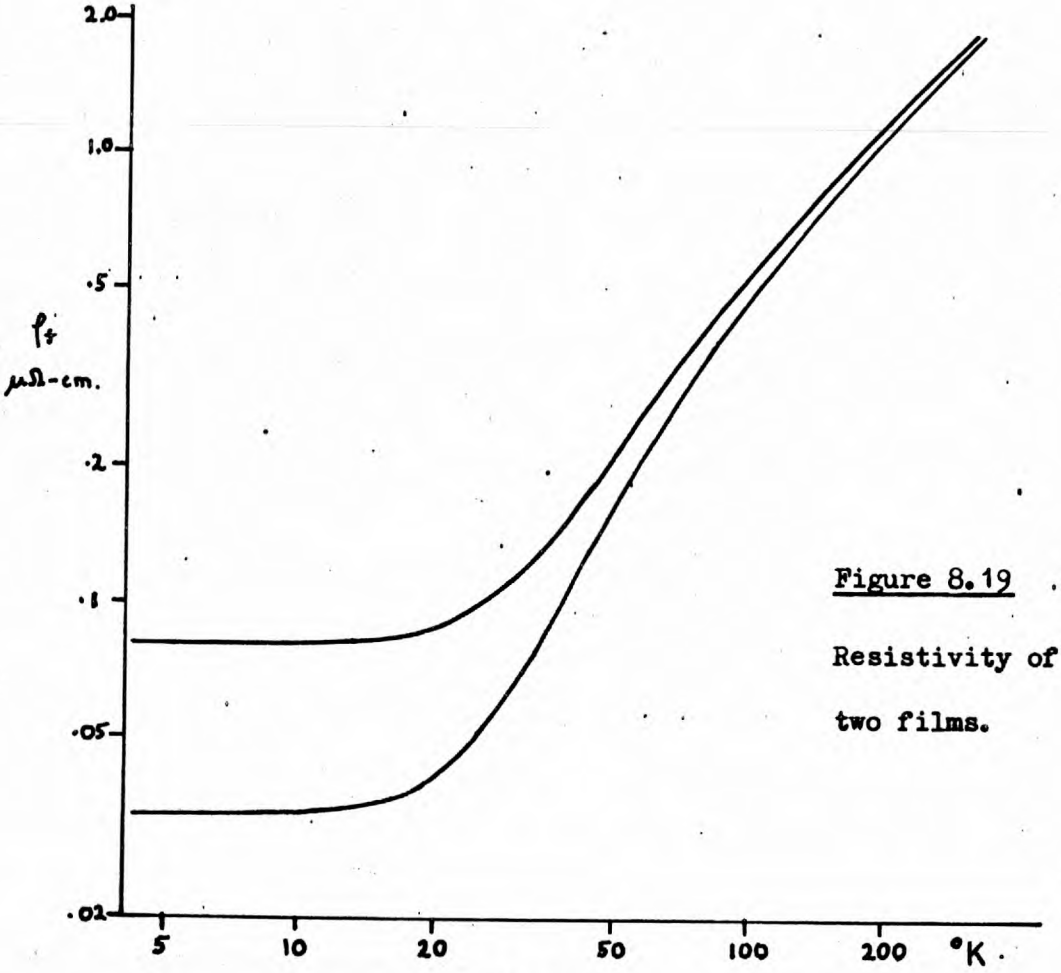

Figure 8.19

Resistivity of two films.

Specimen No.	$\rho(4.2^{\circ}K)$	$\rho(24.4^{\circ}K)$	difference
55.1	.0258	.0377	.0119
52.1	.0190	.0304	.0114
54.1	.0151	.0265	.0114
54.2	.0123	.0233	.0110

Table 8.4

The residual resistivity ratios of 54.1 and .2 are 106 and 130 respectively. The available points for these specimens are included in Figure 8.18.

The resistivities of some other specimens were measured at a few points below $20^{\circ}K$, and none shows any indication of behaviour significantly different from those mentioned above.

The full temperature range.

The resistivities of two film specimens are plotted against temperature in Figure 8.19, but this form of plot is of limited use, as changes brought about by the presence of the surfaces are obscured by the lattice term. A more useful plot is the difference between the film resistivity and the ideal lattice resistivity at each temperature. This is given for a number of films of various thicknesses in Figure 8.20.

The flat region at the high temperature end of the range is the result of the assumption of the fitting procedure, and a discussion of the information that can be obtained from this region has already been

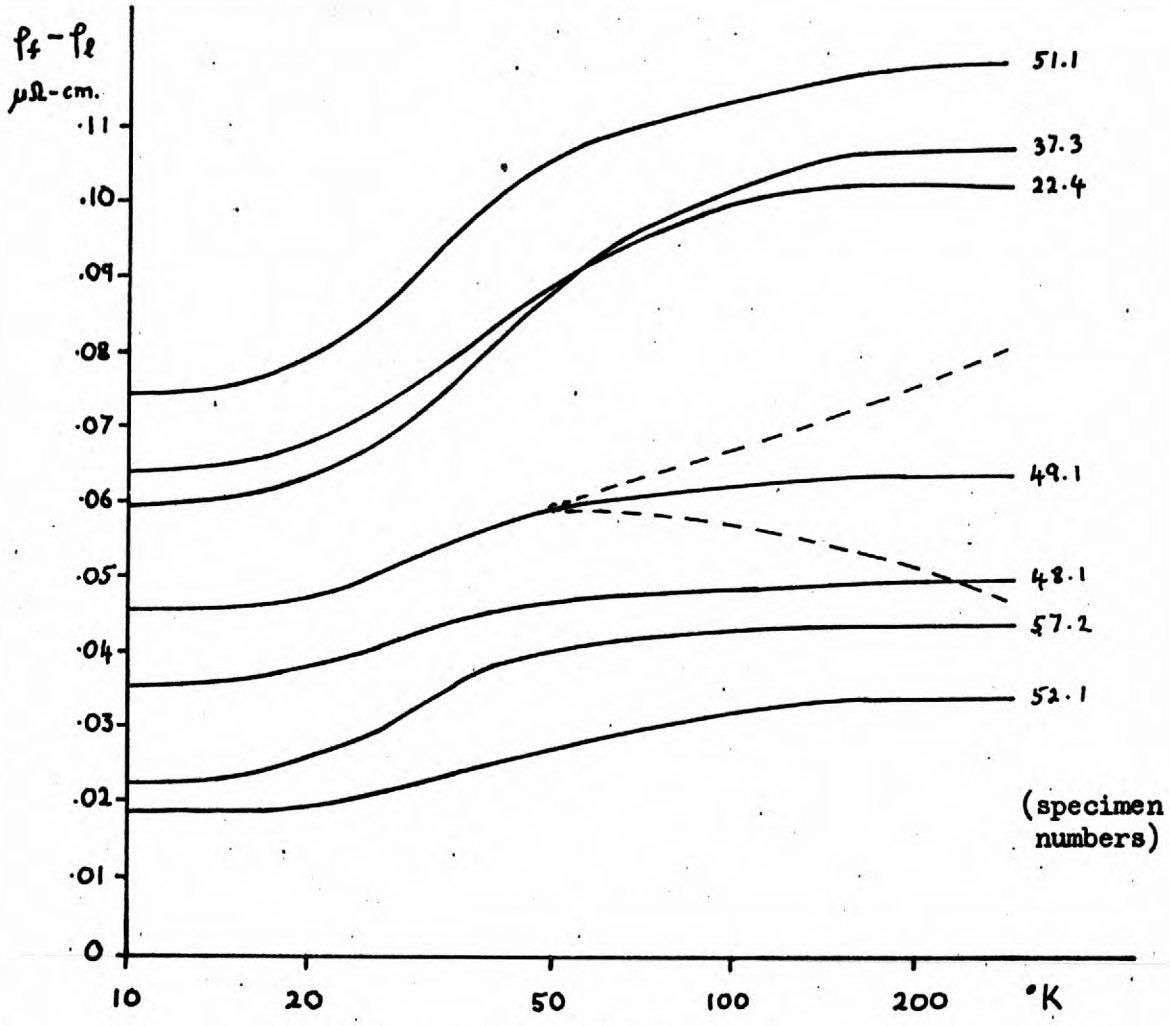

Figure 8.20

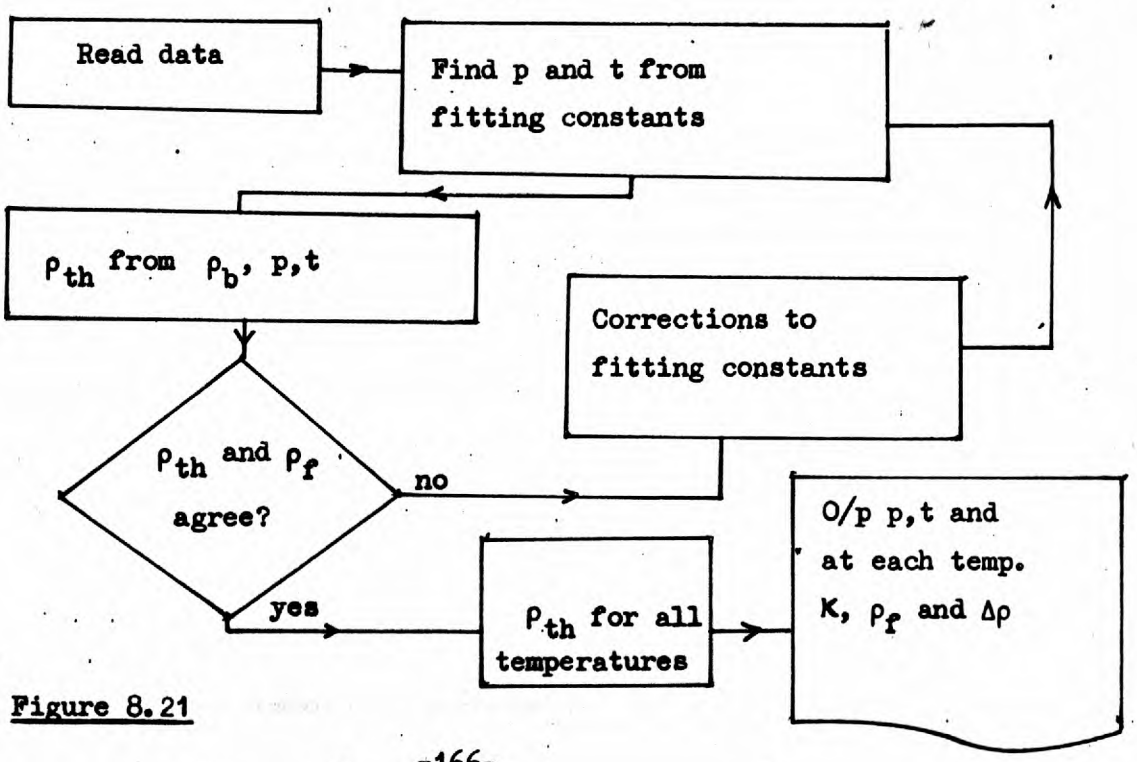

Figure 8.21

given. If this assumption is not justified, the effect on the low end of the temperature range would not be great. This is illustrated for one of the specimens in Figure 8.20. The broken lines show the effect of changing the size shape factor for the specimen by ±1%.

If Matthiessen's rule were obeyed by the films, $(\rho_f - \rho_1)$ would be independent of temperature. This is clearly not the case, as the curves in Figure 8.20 show a significant drop at low temperatures for all specimens. Fuchs' theory predicts a drop in $(\rho_f - \rho_1)$ at low K, and a drop is also expected as a result of the temperature dependent contribution made to the bulk resistivity by dislocations.

To what extent can the variation in the resistivity of the films with temperature be explained by Fuchs' theory? This question can only be answered by a detailed comparison of the film resistivities with those expected on the basis of Fuchs' theory. The way in which this comparison is made, and the computer program to put it into effect, will now be described.

Fuchs' theory has two parameters, K, the ratio of the film thickness to the electronic mean free path, and p, the surface specularity coefficient. As a single film is now being considered, it is reasonable to start by assuming that p is constant throughout the temperature range, and to ask whether the film resistivity can be explained in terms of the variation of the bulk resistivity with temperature. The assumption of Fuchs' theory, that electron scattering in the bulk is isotropic, is retained at all temperatures, so l, the mean free path of electrons, is obtained from ρ_b by $l = (846/\rho_b)$ Å, where ρ_b is in $\mu\ \Omega$ -cm.

Estimating the value of the bulk resistivity at a given temperature is complicated by the dislocation effect described on page 150. It was shown that the bulk resistivity may be treated as the sum of three terms.

(i) The ideal lattice resistivity, ρ_1.

(ii) The bulk residual resistivity, ρ_o.

(iii) The temperature dependent dislocation term, which is approximately expressed by a universal function, u(T), multiplied by a constant for a given specimen, D.

Both ρ_o and D can only be roughly estimated, and this limits the value of comparison with theory at low temperatures ($\simeq < 30^{\circ}K$), where these terms dominate.

The value of p used for a particular film is obtained from the high temperature resistivity of the film. This leaves only the two constants ρ_o and D to be fixed. They are treated as parameters for the comparison program.

The Comparison Program.

The program considers the experimental results for one specimen at a time, and has two objectives. The first is to make small corrections to the constants obtained by the high temperature fitting program (page 126) to take account of the slight departures from the large K form of the theory, which is assumed by the fitting program, when K is near to 1. The second is to take the value of p obtained from the high temperature results, and compare the resistivity expected on the basis of Fuchs' theory with the experimental results over the whole temperature range.

The program uses the intermediate data tape from the fitting program as input, and runs on the same computer. A supplementary data tape is also required to give the bulk residual resistivity, the length-width ratio (d/l) for each specimen, and the modification to the bulk resistivity required by the dislocation term. A block-diagram of the program is given in Figure 8.21.

The high temperature fitting expresses the measured resistance, R, in terms of the ideal lattice resistivity.

$$R = C(\rho_l + \rho_c)$$
$$\rho_f = \frac{R}{C} = \rho_l + \rho_c, \qquad (8.14)$$

where C and ρ_c are determined by a least squares fit. The film thickness is obtained from C, and the specularity coefficient, p, from ρ_c. The comparison program reconsiders the situation in the high temperature region, using the correct form of Fuchs' theory. The values of p and t obtained using the constants from the fitting program are used as preliminary estimates. The bulk mean free path at each temperature is obtained from the bulk resistivity, which includes all three terms, and, with t, gives a value for K(= t/l). The resistivity expected on the basis of Fuchs' theory can then be calculated (ρ_{th}). There is usually some disagreement between ρ_f and ρ_{th}, and the program analyses the differences and makes small corrections to and ρ_c, to improve the agreement. The new values of p, t and ρ_f are then obtained, and the process repeated until there is agreement between the measured resistivities and the calculated resistivities. Two

cycles are usually sufficient.

The fitting constants correction procedure is concerned with the high temperature results only. When final values of p and t have been obtained, the resistivity expected on the basis of Fuchs' theory is calculated for all temperature points. An output is produced giving p,t and, at each temperature, K, ρ_f and $(\rho_f - \rho_{th})$. The qualities $(\rho_f - \rho_{th})$ will be designated $\Delta\rho$, and curves obtained by plotting $\Delta\rho$ against T will be referred to as $\Delta\rho$ curves. Small values of $\Delta\rho$ at high temperatures confirm that the correction procedure has established agreement between the resistivities from the experimental results and those from theory. The $\Delta\rho$ curve shows to what extent this agreement persists at lower temperatures.

Some further details of the comparison program are given in Appendix III.

Results from the Comparison Program.

The results from the comparison program may first be used to provide an indication of the reliability of the fitting program based on the thick film approximation of the theory. The changes in the fitting constants are reflected in changes in p,t and ρ_f. The latter two involve C, the slope of the R vs. ρ_1 line, and the changes are small, usually much less than 1%. The value of p is obtained using ρ_c, which depends on the intercept, and the changes are more significant. A table (8.5) of p values obtained from both the fitting program and the comparison program, is given below. The fitting program always underestimates p, so the value it gives is still p(min). (page 158).

$\Delta\rho$ curves.

The main use of the comparison program is to produce $\Delta\rho$ curves.

Specimen No.	Thickness Å	Comp. Prog.	Fitting Prog.	Difference
57.1	5500	.76	.74	.02
39.4	4170	.63	.60	.03
49.1	4030	.48	.45	.03
57.2	3870	.72	.70	.02
56.3	3800	.54	.50	.04
26.1	2590	.59	.54	.05
57.3	2410	.62	.59	.03
56.2	2350	.46	.41	.05
49.3	2320	.49	.45	.04
57.4	1670	.55	.50	.05
56.1	1590	.46	.39	.07
39.1	596	.46	.43	.03

Table 8.5

Some values of p estimated by both the fitting program and the comparison program.

On the basis of these curves the specimens may be roughly separated into two groups. The first consists of specimens thinner than about 1000Å, and is characterised by a $\Delta\rho$ curve which rises rapidly with decreasing temperature below about 100°K. The second consists of thicker films, which give $\Delta\rho$ curves with little or no rise at low temperatures. Examples of the two types are given in Figure 8.22. It seems possible that the behaviour of the first group may be connected with the presence of holes in the films, and this possibility will be examined in the next chapter. Only the second group will be considered further in this chapter.

For a given specimen there are two parameters which can be only roughly estimated. These are the bulk resistivity at 4.2°K (ρ_o) and the scaling constant of the temperature dependent dislocation contribution. It was shown on page 155 that there appears to be a rough relationship between these parameters, i.e. $D = \rho_o$. This relationship has been assumed for most applications of the comparison program. If the assumed values of ρ_o alone are changed, only small changes in the $\Delta\rho$ curves result, and these are confined to low temperatures. The introduction of the temperature dependent dislocation term produces a larger effect, which reduces the values of $|\Delta\rho|$ at low temperatures in most cases. The uncertainties in ρ_o and D mean that the $\Delta\rho$ curves must be assumed to have uncertainties of the magnitudes and types indicated by the examples in Figure 8.22.

The $\Delta\rho$ curves for a variety of specimens were obtained from the comparison program with ρ_o and D both taken as 0.01 $\mu\Omega$-cm. Figure 8.23 shows the curves for three films all about 2400 Å thick, but with widely

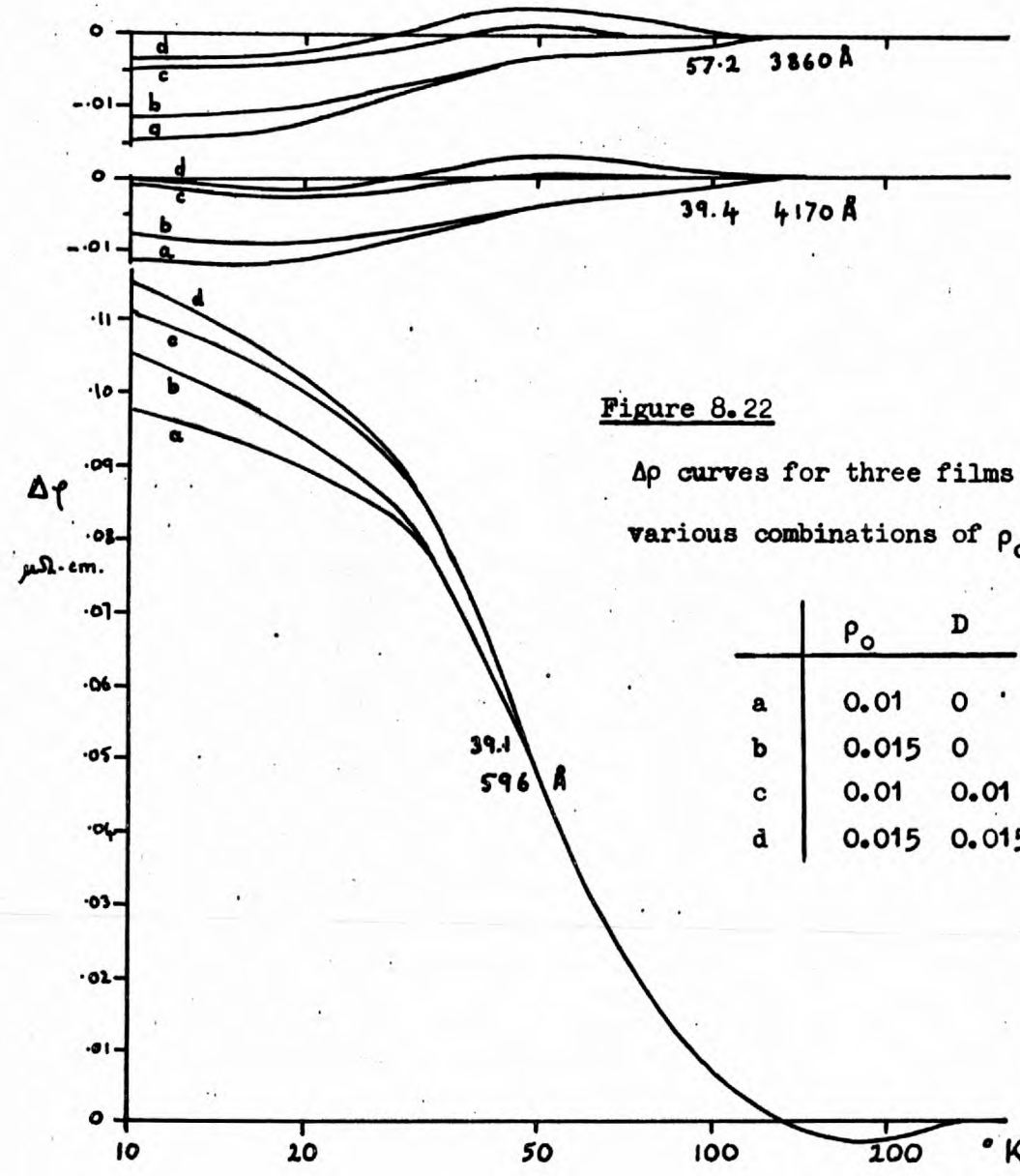

Figure 8.22

Δρ curves for three films with various combinations of ρ_o and D.

	ρ_o	D
a	0.01	0
b	0.015	0
c	0.01	0.01
d	0.015	0.015

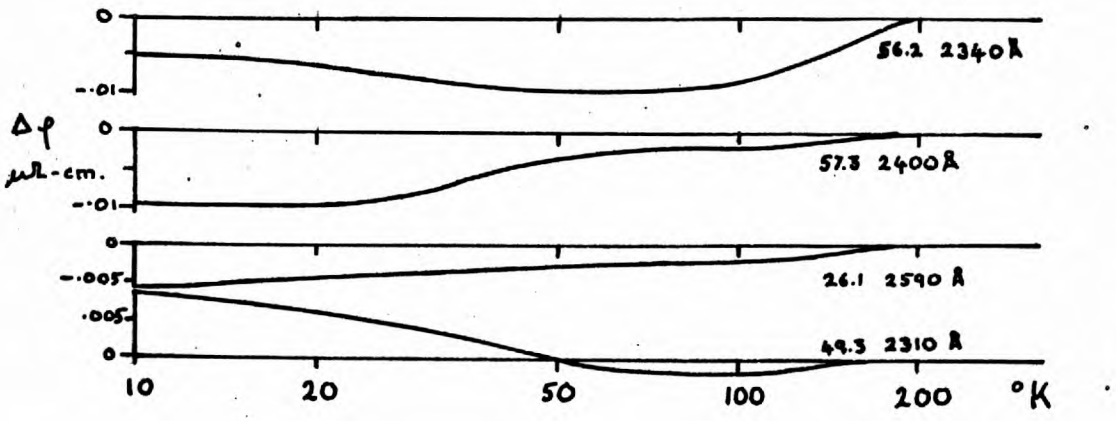

Figure 8.23 Δρ curves for film ~ 2400Å

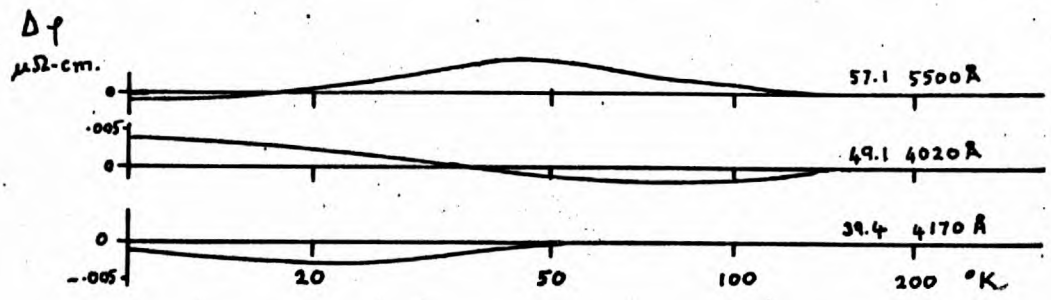

Figure 8.24 Δρ curves for thicker films.

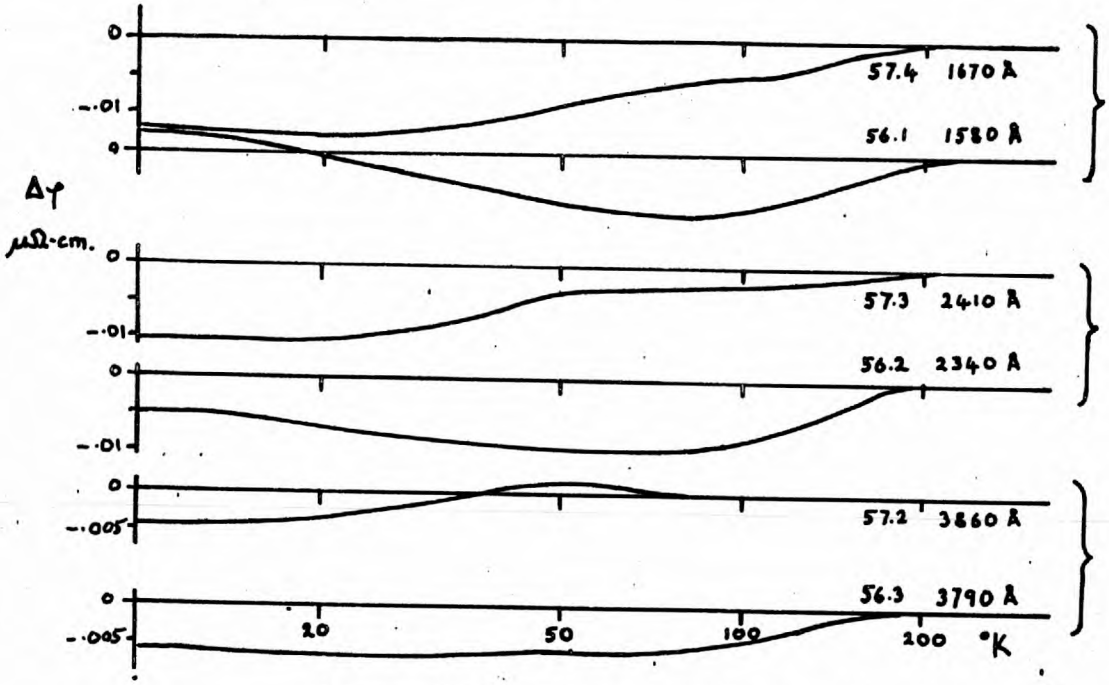

Figure 8.25 Pairs of specimen with and without aluminium layers

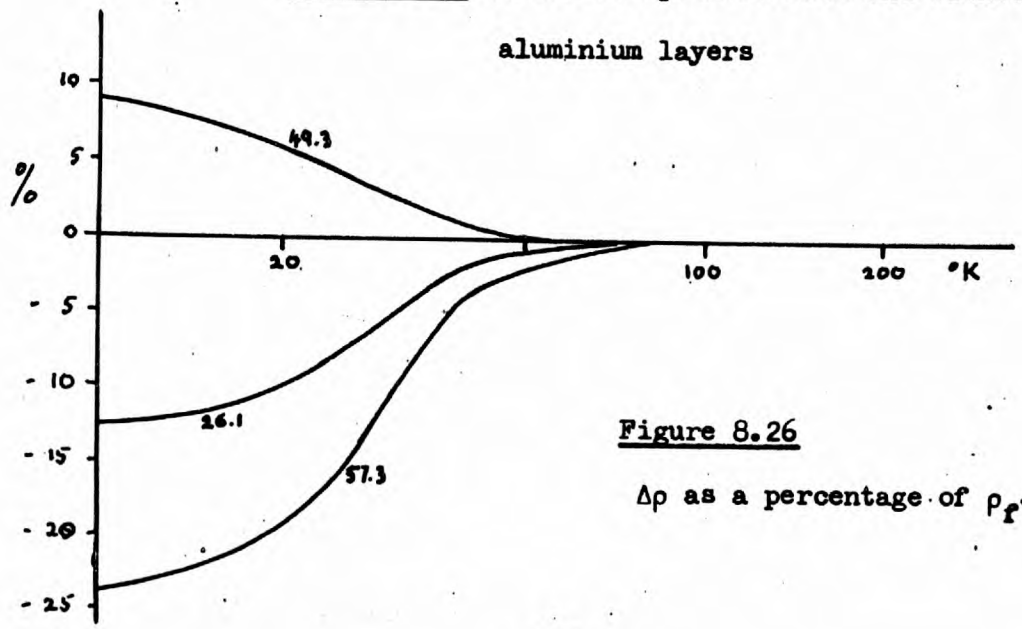

Figure 8.26

Δρ as a percentage of ρ_f.

different film residual resistivities. Figure 8.24 shows the curves for three thicker films, also with a range of film residual resistivities. In Figure 8.25 the results for a pair of specimen sets are given, one modified by a thin aluminium layer and the other unmodified. The agreement between theoretical and experimental values is good down to quite low temperatures. The error as a percentage of ρ_f is plotted for a few specimens in Figure 8.26. The large variations at low temperatures must be expected as a result of the uncertainties in the parameters ρ_o and D.

These results are interesting in their failure to show any features which can be attributed to the dominance of low angle scattering of electrons by phonons at low temperatures. Low angle scattering is expected to lead to higher film resistivities for a given bulk resistivity[45,53]. This subject is discussed in Chapter X, where an approximate theoretical treatment is given. The theory predicts significant positive departures from Fuchs' theory, especially for films of low p at about 30-40°K. The experimental results show mainly negative departures.

CHAPTER IX

FILMS IN THEORY AND FILMS IN PRACTICE

In this chapter and the next some aspects of the relationship between the films measured in practice and the films assumed in theory will be discussed. The first section of this chapter is concerned with the surface structure of the films as revealed by replica electron microscopy and the second with electronic structure. Chapter X is devoted to a discussion of an important consequence of low temperatures; the predominantly low angle nature of the electron scattering by phonons.

1) The Epitaxial Silver Film Surfaces

The electron microscopy work on replicas mentioned in earlier chapters will now be described. While examining replicas of epitaxial silver films C. Gonzales[32] of Imperial College found considerable variation between specimensprepared on different occasions, although the conditions of preparation were apparently the same. The films were prepared in the same evaporator and by the same method as the resistance specimens.

The replicas are prepared as follows. A thin layer of carbon is evaporated over the surface of the silver film to be examined. The carbon layer is then 'shadowed', to improve the contrast in the microscope, by evaporating a small amount of chromium from an angle of about 20° to the surface. The silver is dissolved away by leaving it in the vapour of nitric acid. The replica can then be floated on to a copper grid and examined in the electron microscope.

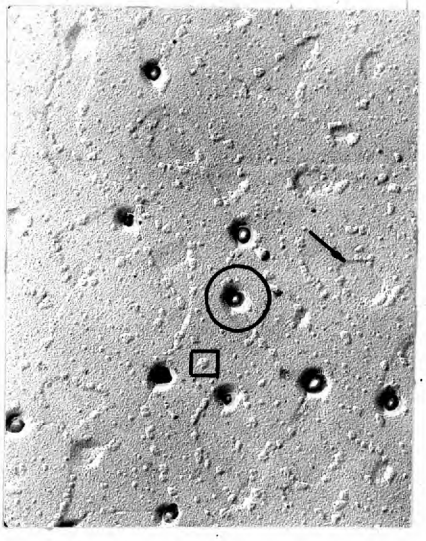

(a) Specimen 37.3

t = 1390 ρ_f = 0.060

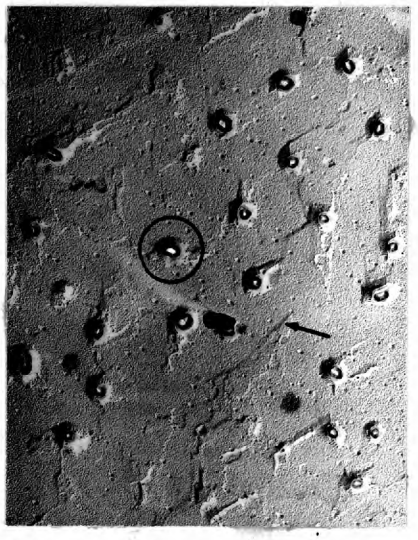

(b) Specimen 33.2

t = 1230 ρ_f = 0.122

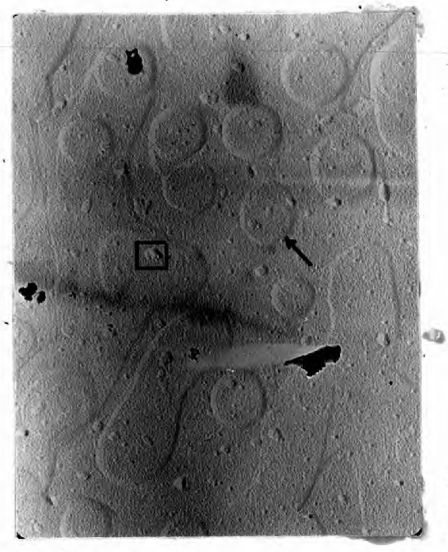

(c) Specimen 57.3

t = 2400 ρ_f = 0.030

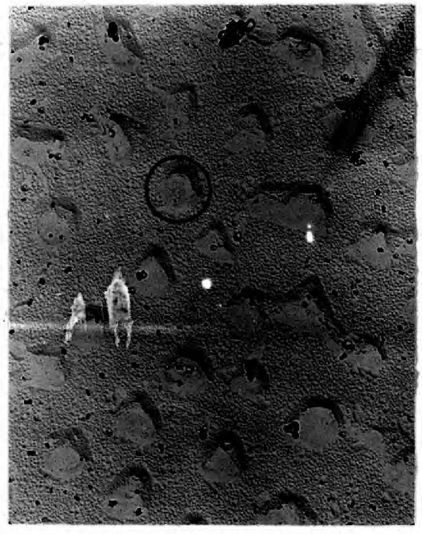

(d) Specimen 49.3

t = 2310 ρ_f = 0.067

PLATE 4 **Replicas of film surfaces**

t in Å. ρ_f at 4.2°K. Scale 5000Å/cm.

Replicas of six of the resistance specimens were prepared by Gonzales and micrographs of four of them are shown in Plate 4. These results illustrate the variable nature of the film surfaces. They are generally fairly flat with occasional features which are large on the atomic scale. The features shown in Plate 4 fall into three main groups, only two of which represent structures found on the surfaces of freshly prepared films. The large features, of the type shown by circles, are holes or depressions in the film surface. The lines, marked by arrows, are steps in the surface, probably ~100Å or less. The small bumps on the surface (as in the squares) are not seen on replicas from freshly made films and may be due to contamination acquired during storage.

The centres of the main features in (a) and (b) are white, showing that no chromium has been deposited there and suggesting that the features may represent holes rather than merely depressions. Confirmation of the presence of holes was obtained by observations with an oil immersion optical microscope. A part of specimen 33.2((b) in Plate 4) was observed and many faint spots of light were seen, distributed typically as in Figure 9.1 (a). The diameter of the spots was very roughly estimated, by comparison with a fine wire, to be ~ 2000 - 5000Å. Most of the spots were very faint, but a few were brighter, and around these a ring was seen.

These results are just as expected from holes with diameters small compared with the wavelength of light. They may be explained in terms of the Abbé theory of microscope image formation[61]. Parallel

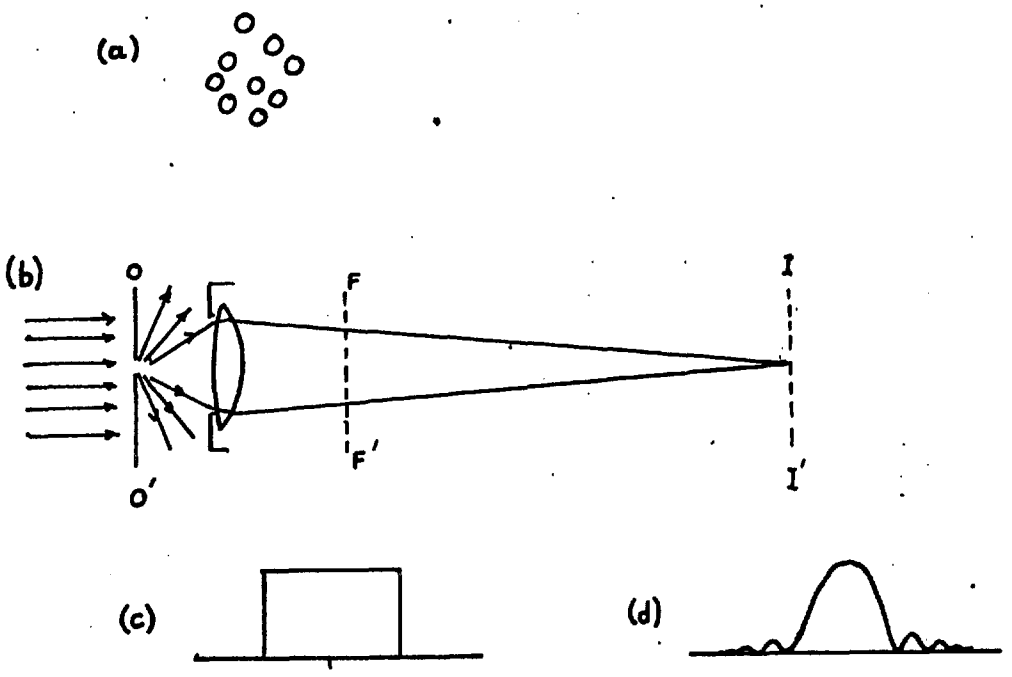

Figure 9.1

light is incident on the object plane. (Figure 9.1b). The Fraunhofer diffraction pattern of the object plane is formed at the focal plane FF, but with an angular cut-off determined by the aperture of the lens. The light leaving a very small hole is uniformly distributed over a wide angle, so the intensity distribution at FF' is as shown on 9.1 (c). The image formed at the image plane II' has the shape that would be required in the object plane to give the pattern (c) at FF' i.e. roughly as in 9.1 (d). The size of the image depends only on the microscope, while the brightness depends on the size of the hole in the film. Only the larger holes allow sufficient light through to allow the first ring to be visible.

Holes were seen optically in several films ~ 1200Å thick, but not in some thicker films. This is in agreement with the electron

micrographs, as only the depressions in the thinner films have white centres.

The six specimens examined point strongly to the conclusion that the variability of the residual resistivity of films of a given thickness is related to the density of surface features. This is illustrated in Plate 4 by the pairs (a),(b) and (c),(d). In each pair the films are of similar thickness, but have considerably different densities of surface features and the residual resistivities differ by about a factor of 2.

It is of interest to consider what effect the presence of holes in a film might be expected to have on its resistivity. At high temperatures the electronic mean free path is much smaller than the average distance between the holes. They then merely contribute to the overall shape of the specimen, and the size-shape factor will take account of them. At low temperatures, however, the mean free path is long compared with the separation of the holes and they contribute to the bulk resistivity. In a film with bulk resistivity 0.01μ Ω-cm the bulk mean free path is 80,000Å. If the holes in the film (b) are assumed to have their apparent surface diameter all the way through the film and to be the only scattering agent, the mean free path parallel to the surface is about 40,000Å , indicating a contribution to the resistivity of about 0.02 μ Ω-cm. This rough estimate is about one third the difference in resistivity between film (a) and (b) (Plate 4).

The presence of holes in the thinner films offers a possible explanation of the results for the thinner films described in

Chapter VIII, page 172. The measured resistivities at low temperatures are higher than expected from the high temperature results on the basis of Fuchs' theory. The density of holes required to explain the results for films below 1000Å would, however, have to be at least four times greater than in specimen (b), Plate 4.

2) The Electronic Structure in Thin Films.

Restriction on k_z.

The free electron structure in thin films is usually assumed to be independent of thickness. This is not exactly true, as the surfaces impose boundary conditions on the electronic wave functions which restrict the values of the z components of the wave vector (k_z) to $\pi n/t$, where n is an integer and t the thickness of the film[54]. The electron states are thus confined to planes in k-spaces parallel to the film surfaces (Figure 9.2). There are ~ 2t/c such planes in the first Brillouin zone, where c is the lattice spacing perpendicular to the film surface. Silver films about 1000 Å thick would have about 200 planes crossing the Fermi sphere.

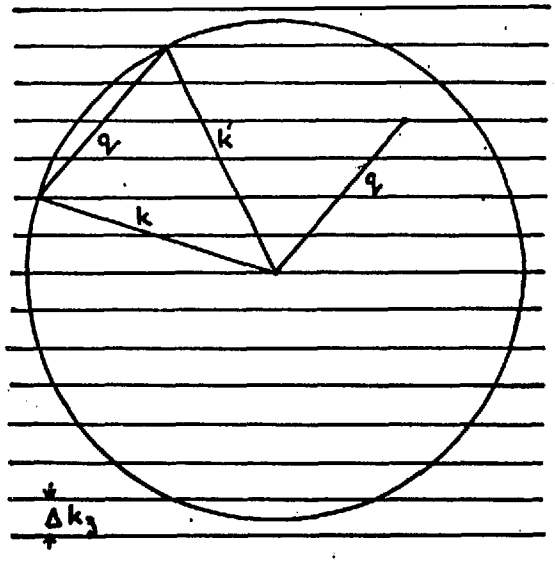

Figure 9.2

Crittenden and Hoffman[55] have suggested that the restrictions

on the values of k_z may reduce the resistivity, but it seems likely that this will not happen unless the films are very thin. If the intrinsic scattering probability is isotropic (impurity scattering) the rate of scattering depends only on the number of final states available at the Fermi surface. There are as many states per unit volume in the film as in the bulk and the fact that they are confined to particular planes does not reduce their effectiveness as final states. When the electron scattering is by phonons the availability of phonons of the right wave number must be considered. The distribution of states in phonon wave-number space (q-space) is identical to the distribution of electron states in k-space. The phonons required to excite transitions between electron states must have values of q_z which are integral multiples of Δk_z, and the phonons all have just this property (Figure 9.1), so scattering probabilities are unaffected by k_z quantization. It must be emphasized that this argument is only applicable if $q >> \Delta k_z$ for most of the phonons, i.e. it would break down in very thin films at very low temperatures. The experimental films, however, are thick enough for the condition given above to be satisfied at temperatures where phonon scattering is important.

Non-Spherical Fermi Surface.

The Fermi surface in silver is nearly a sphere over much of its area (Chapter I), and this gives credibility to the assumption of the free electron model. However, silver is not a free electron metal; it has a zone structure. The Fermi surface has necks to the [111] zone

boundaries and electron scatterings may be of the Umklapp type. The possibility of Umklapp processes makes it more reasonable to assume

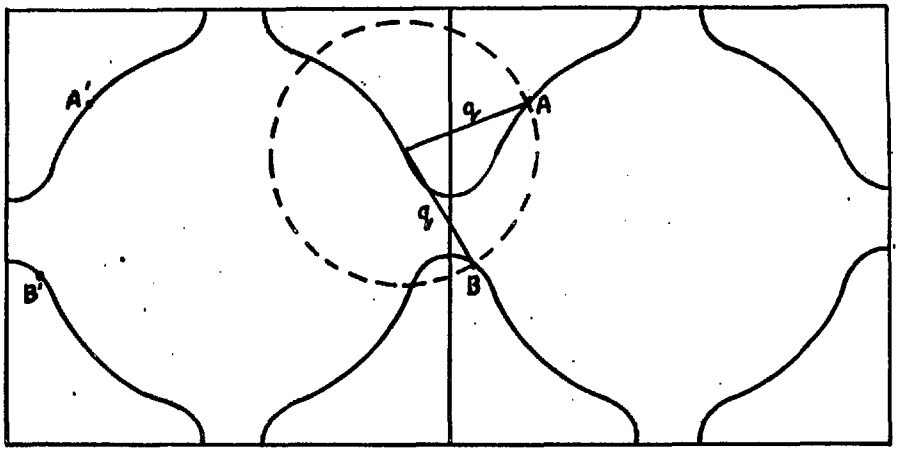

Figure 9.3 Umklapp scattering.

that phonon scattering is isotropic, especially at high temperatures. The Debye phonon model for a free electron metal includes a frequency cut off which limits the scattering of electrons to about 79° by normal processes, so even at high temperatures the scattering would not be isotropic. When Umklapp processes are included scattering is not so limited. In Figure 9.3 the small q scatterings to A and B are equivalent to scatterings to A′ and B′ in the original zone. The assumption of isotropic scattering is, therefore, probably quite reasonable, especially above the Debye temperature (200°K for silver) when large areas of the Fermi surface in adjacent zones are accessible to phonon induced transitions.

CHAPTER X

THE PHONON-SURFACE EFFECT

1. Introduction

In the resistance size effect theories of Fuchs and Dingle isotropic scattering of electrons is assumed. While this is probably a reasonable assumption at the Debye temperature and above, it cannot, with confidence, be maintained at low temperatures when low angle phonon scattering predominates. It was suggested by Olsen[45] that the low angle scattering may be of greater importance in thin specimens than in bulk specimens. The argument is put as follows [56]. The current in a thin film or wire is carried mainly by electronstravelling parallel to the surface. If one of these electrons is scattered through a small angle, it will soon reach the surface where it will be scattered through a large angle. The original low angle scattering is, therefore, finally equivalent to a large angle scattering. For a given bulk resistivity, the film resistance is expected to be higher when the scattering is mainly low angle than when it is mainly isotropic.

Although the phonon-surface effect is certainly expected to exist, the above argument is oversimplified. It would apply directly to a beam of particles which could only lose particles and not gain them. The situation in a metal is rather more complicated than this, and must be approached from the Boltzmann equation point of view.

The Boltzmann equation in the absence of a magnetic field was obtained in Chapter II. From equation 2.19, page 23:

$$\frac{e}{\hbar} E \cdot \nabla_k f_o(\underline{k}) + \underline{v}(\underline{k}) \cdot \nabla_r g(\underline{k},\underline{r}) = \dot{g}(\underline{k},\underline{r}) \Big|_s \qquad (10.1)$$

where $g(\underline{k},\underline{r})$ is the equilibrium change in the distribution function caused by the electric field. The scattering term has the form

$$\dot{g}(\underline{k},\underline{r})\Big|_s = \int (g(\underline{k},\underline{r}) - g(\underline{k};\underline{r}))\ Q(\underline{k},\underline{k}')\ d\underline{k}' \qquad (10.2)$$

and it is here that differences in the type of scattering make themselves felt. The simplifying assumptions 1,2 and 3(a) made in Chapter II page 25 will be retained i.e.:

1) Energy surfaces are spherical in k-space

2) Electrons are scattered on constant energy surfaces.

3(a) The intrinsic scattering probability depends only on the angle through which the electron is scattered.

Phonon scattering involves change of the electron energy, so these assumptions really exclude phonon scattering. However, it may not be unreasonable to ignore the energy changes, as the calculation of the current involves an average across the Fermi surface. An electron scattered to a point on the Fermi surface contributes the same amount to $\int g dk$, and hence to the current, whether it changes its energy on scattering, or not. The above objection also applies to Fuchs' theory, and has been ignored in applying that theory to the high temperature film results, so it is consistent to continue to ignore it at lower temperatures. The

aspect of phonon scattering expected to be of importance is its angular dependence, and this is incorporated in the theory by allowing Q to depend on Ψ, instead of keeping it constant as in Fuchs' theory.

With the above assumptions the scattering term becomes, introducing polar coordinates in k-space,

$$\dot{g}\Big]_s = \int (g(\theta,\phi,k,\underline{r}) - g(\theta',\phi'; k,\underline{r},)) \, Q(\Psi) \, k^2 \sin\theta d\theta d\phi \tag{10.3}$$

When the bulk case was being considered (page 30) the scattering term was reduced to the simple relaxation time form $g(\theta,\phi,k)/\tau$ where

$$\tau = \frac{1}{2\pi} \int (1 - \cos\Psi) \, Q(\Psi) \sin\Psi \, d\Psi \tag{10.4}$$

The bulk conductivity is then $ne^2\tau/m$. This simple form for $\dot{g}\Big]_s$ is no longer obtained in the more general case of thin specimens. Figure 10.1 (a) shows a $g(\theta)$ curve for a film with isotropic scattering (Fuchs' theory) and 10.1 (b) shows the $g(\theta)$ curve for the corresponding bulk case. If the scattering is mainly low angle, e.g. with $Q(\Psi)$ as in 10.1 (c), the rate of scattering from $\theta = 90^\circ$ will clearly be much greater in the film than in the bulk. The values of $(g(\theta) - g(\theta'))$ are much larger, in the range defined by $Q(\Psi)$, in the film than in the bulk. To allow comparison with the bulk case, the scattering integral

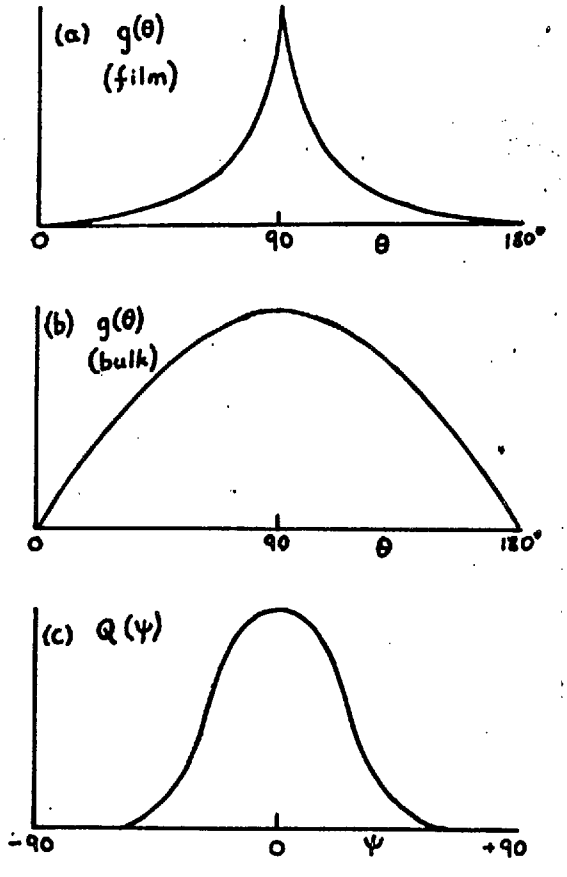

Figure 10.1

at θ divided by the value of g at θ (i.e. $\dot{g}(\theta)\big]_s$ / g(θ)) is considered. This goes down as θ moves away from 90°. The form of g(θ) shown for the film assumes a constant value of $\dot{g}(\theta)\big]_s$ / g(θ) (Fuchs' theory, τ = const, $\dot{g}\big]_s \propto g$), so it cannot be the solution when scattering is mainly low angle. As scattering from the peak shown in 10.1 (a) is high for low angle scattering, the change in g required can be expected to involve a smoothing out of the peak.

2) Previous Calculations of the Phonon-Surface Effect.

Three calculations of the phonon surface effect will be mentioned. Two of these are concerned with wires, and although they are not of immediate concern in the present work the methods used are considered.

Blatt and Satz[56] start with the assumption that the mean free path in wires (l_w) can be split up as follows:

$$\frac{1}{l_w} = \frac{1}{l_{ph}} + \frac{1}{l_i} + \frac{1}{l_s} + \frac{1}{l_{ps}} \qquad (10.5)$$

The component mean free paths are:

l_{ph} - normal phonon scattering.

l_i - impurity scattering.

l_s - surface scattering.

l_{ps} - phonon-surface scattering.

The phonon surface term is obtained by considering an electron initially travelling parallel to the surface of the wire. The electron is scattered repeatedly through angles $\sim T/T_D$, where T is small compared with T_D (the Debye temperature), and eventually reaches the surface. The average distance required for this is taken as l_{ps}. The phonon-surface contribution calculated for electrons parallel to the surface is assumed to apply for all directions, and the resistivity of the wire is taken as proportional to $1/l_w$.

The lack of rigour of this method, which is admitted by the authors, makes it difficult to assess whether it can be expected to give even approximate estimates for the phonon surface-effect. The method is restricted to very thin wires (diameter $<< l_w$), and it is asserted that the bulk of the current is carried by electrons moving parallel to the surface of the wire. This is not true for thin wires, though it is for thin films (page 65). The electrons moving parallel to the surface are of decreasing significance as the wire becomes thinner, so the phonon-surface effect should decrease similarly. The method described above predicts an increased phonon-surface effect with decreasing wire diameter.

Lüthi and Wyder [57] used a Monte Carlo method to estimate the phonon-surface effect in wires. A computer program simulated electron paths in the wire, allowing a constant probability of scattering by phonons and impurities in each small increment of length. The angle of scatter was made T/T_D for each phonon scattering and selected randomly from the isotropic sphere for impurity scattering. When a path reached the surface an isotropic scattering back into the wire was generated.

The mean free path was taken as the total distance travelled by the electron divided by the total number of effective scatterings. An effective scattering was defined as one which randomized the electron direction. Each impurity and surface scattering is counted as one effective scattering, but not each phonon scattering. The number of scatterings through a small angle θ required to randomized direction is $\sim 1/\theta^2$, so each phonon scattering was assumed to contribute only $(T/T_D)^2$ to the total number of effective scatterings.

This simple Monte Carlo method is open to several objections, of which the two most important are the following. The resistance is assumed to be proportional to the mean free path of the electrons. This assumption is based on the relationship obtained from the Boltzmann equation in the bulk case, when scattering is isotropic and the angular dependence of g is cos θ (page 30). It is by no means obvious that this result can be extended to the more general case where g has a different angular dependence. It was shown in the previous section that the angular dependence of the scattering influences the resistivity by changing the scattering term. No provision for this is made by Lüthi

and Wyder, so it is not easy to see how their method would be expected to estimate the phonon-surface effect.

Azbel and Gurzhi[53] obtained a formula for thin film resistivity which includes the phonon surface effect. The effect of low angle scattering is introduced by allowing the relaxation time τ to depend on θ. The thin film limit only is treated, i.e. $K \ll 1$ and the function g for the isotropic case has a very narrow peak at $\theta = 90^{\circ}$ (Figure 10.2). The width of the peak is $\sim$ K radians.

In this region each low angle scattering is taken to be as effective as a large angle scattering, so the relaxation time is decreased by a factor which is the reciprocal of the number of low angle scatterings required to be equivalent to one high angle scattering. The phonon surface effect is assumed to be unimportant away from the peak in $g(\theta)$, so an ad hoc function is used for the phonon contribution to the relaxation time which is $\sim\tau_b(T/T_D)^2$ at $\theta = 90^{\circ}$ and $\sim\tau_b$ near $\theta = 0$ and 180°. The crossover occurs at $\sin\theta = \sim T/T_D$. The function is:

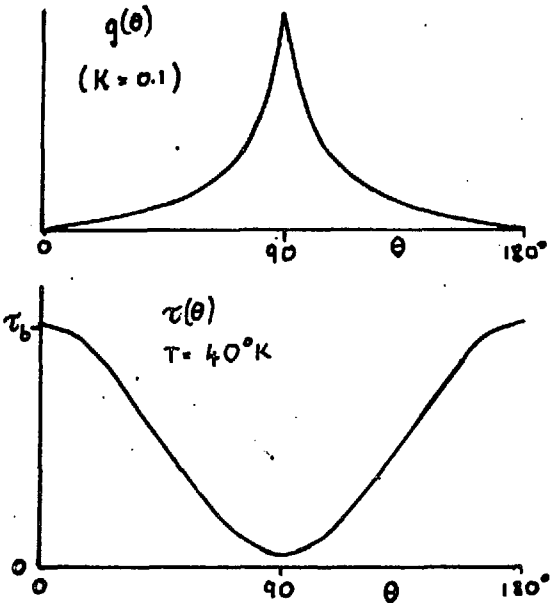

Figure 10.2
$g(\theta)$ from Fuchs theory and $\tau(\theta)$ from 10.6.

$$\tau(\theta) = \tau_b \left(\left(\frac{T}{T_D} \right)^2 + \sin^2 \theta \right) \qquad (10.6)$$

The transport equation was solved with this $\tau(\theta)$ and a formula obtained for ρ_f/ρ_b. Contributions are included from both phonon and impurity scattering.

$$\frac{\rho_f}{\rho_b} = \frac{1}{K \log \left(1 + \frac{1}{x}\right)} \qquad (10.7)$$

where

$$x = \frac{d}{l} + \frac{d/l_{ph}}{(T/T_D)^2 + (d/l_i)^2 + (d/l_{ph})^{2/3}}$$

and l_{ph} = effective m.f.p of phonons in bulk.

l_i = impurity mean free path in bulk.

l = total effective bulk mean free paths.

This result predicts that the resistivity of a film should rise more rapidly with temperature than expected from Fuchs' theory at low temperature. The shape of the curve depends on the values of t, l_i and l_p. Two examples are given in Figure 10.3. The films have the same value of K(0.01) at T=0, but different values of bulk residual resistivity. The first has a very low bulk residual resistivity, and the film resistivity rises sharply at about $T = 0.03\ T_D$. The second has a residual resistivity

comparable with the films described in the experimental part, and the film resistivity rises more slowly with temperature.

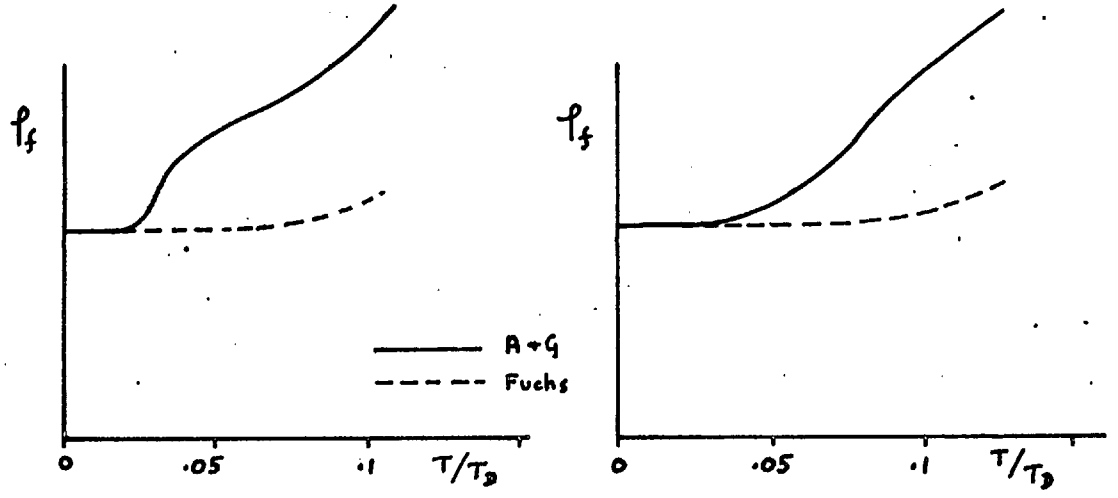

Figure 10.3 Examples of Azbel and Gurzhi's results

Azbel and Gurzhi's calculations do not allow for any dependence of $\tau(\theta)$ on $g(\theta)$, and are confined to very thin films. In the next section a numerical method for estimating the phonon-surface effect will be described which has neither of these limitations.

3) Numerical Calculations of the Phonon-Surface Effect.

The discussion of the phonon-surface effect given so far shows that Fuchs' theory cannot be expected to apply to films when the scattering is largely low angle. In order to calculate the magnitude of the effect to be expected for the films measured in the experimental part, a numerical method was developed which is based on the Boltzmann equation approach. The methods used by Blatt and Satz and Lüthi and Wyder were felt to be too loosely related to the Boltzmann theory

to allow them to be used with confidence. The method described below is, in effect, a development of the method used by Azbel and Garzhi to allow for the relationship between the relaxation time $\tau(\theta)$ and the function $g(\theta)$.

The form of the Boltzmann equation to be solved for films of a free electron metal is obtained from equation 10.1 and 10.3 with the assumptions on page 185 . The electron velocity v is the Fermi velocity

$$v \cos\theta \frac{\partial g}{\partial z}(\theta;\phi,k,z) + \frac{e}{\hbar} E \frac{df_o(k)}{\partial k} \sin\theta \cos\phi$$

$$= \int (g(\theta,\phi,k,z) - g(\theta',\phi',k,z)) k_F^2 Q(\Psi) \sin\theta' d\theta' d\phi \qquad (10.8)$$

In both bulk material and films with isotropic scattering g depends on ϕ only through a factor $\cos\phi$. It will now be shown that this is also true in the present case by assuming that g can be expressed in a form proportional to $\cos\phi$, and putting it in equation 10.8 i.e. assuming

$$g(\theta,\phi,k,z) = \frac{e}{\hbar} E \frac{df_o(k)}{dk} \cos\phi \; u(\theta,z) \qquad (10.9)$$

Equation 10.8 then becomes

$$v \cos\theta \cos\phi \frac{\partial u(\theta,z)}{\partial z} + \sin\theta \cos\phi$$

$$= \int (u(\theta,z) \cos\phi - u(\theta',z) \cos\phi') Q(\Psi) k^2 \sin\phi' d\theta' d\phi'$$

(10.10)

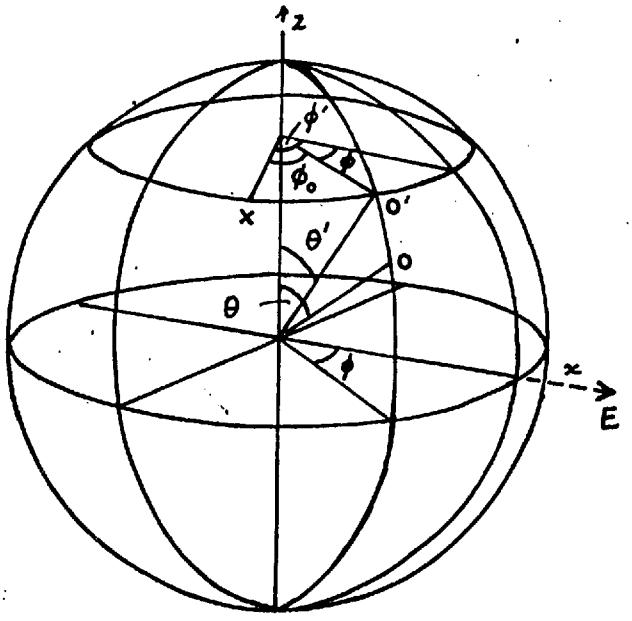

Figure 10.4

If the right hand side can be shown to be proportional to cos ϕ, with no other ϕ dependence, all ϕ terms can be eliminated from the equation, confirming that g has the form given in 10.9. In figure 10.4 O is (θ,ϕ) and X is (θ',ϕ'). θ and θ' are kept constant and X moves on a line of constant θ'. Q may be written as $Q(\theta,\theta',\phi_o)$ where $\phi_o = \phi' - \phi$. Q is an even function of ϕ_o.

The integral may now be written in two parts with ϕ' replaced by $\phi_o + \phi$, i.e.

$$\text{(a)} \quad u(\theta,z)\cos\phi \int_0^{\pi} d\theta' \sin\theta' \int_0^{2\pi} k^2 Q(\theta,\theta',\phi_o)\, d\phi_o \qquad (10.11)$$

$$\text{(b)} \quad \int_0^{\pi} d\theta'\, u(\theta' z) \sin\theta' \int_0^{2\pi} d\phi_o\, k^2 \cos(\phi_o' + \phi)\, Q(\theta,\theta'\, \phi_o)$$

The ϕ_o integral in (a) is independent of ϕ. The ϕ_o integral in (b) may be expanded to

$$\int_0^{2\pi} Q(\theta,\theta';\phi_o)\,(\cos\phi_o \cos\phi - \sin\phi_o \sin\phi)\, d\phi_o \qquad (10.12)$$

The second part is zero, as Q is an even function of ϕ_o and sin ϕ_o and an odd function. (b) is finally

$$\cos \phi \int k^2 \cos \phi_o \; Q\,(\theta,\theta',\phi_o)\; d\,\phi_o . \qquad (10.13)$$

Now cos ϕ cancels through 10.10, leaving an equation for $u(\theta,z)$

$$\Psi \cos\theta \; \frac{\partial\, u(\theta,z)}{\partial z} + \sin\theta$$

$$= R_1\, u(\theta,z) - \int R(\theta\ \theta')\; U(\theta';z)\; \sin\theta' d\,\theta' \qquad (10.14)$$

where $R_1 = \int Q(\Psi)\; k^2 \sin\Psi d\Psi$, a constant for a given function $Q(\Psi)$ and $R(\theta,\theta') = \int k^2 \cos\phi_o\; Q(\theta,\theta',\phi_o)\; d\,\phi$.

If the right hand side is of the form $\frac{u(\theta,z)}{\tau(\theta,z)}$, and the boundary conditions are as used by Fuchs' (page 46), the equation 10.14 has an analytic solution. Although $\tau(\theta,z)$ is not independent of $u(\theta,z)$ the simplified equation, i.e. with the right hand side of 10.14 replaced by $u(\theta,z)/\tau$, forms the basis of an iterative method for obtaining a solution. A solution u_1 is first obtained with a constant τ,τ_1. This solution is put in the scattering integral to give a new relaxation time function, $\tau_2(\theta,z)$, which is used to calculate a new solution u_2. The iteration is repeated until an unchanging solution is obtained. If this process were to be successfully implemented the solution obtained would be the solution of 10.14 under the boundary condition assumed, and could be used to obtain ρ_f/ρ_b for films with low angle

scattering. Although there is no difficulty in principle with the method given above, a simplified version has been used which is expected to give a reasonable approximation to the results that would be obtained from the complete method, and requires a less complicated computer program.

The function u depends on z, so τ must also depend on z. The most important variation of τ, however, is with θ, as it is the high rate of scattering out of the peak in $g(\theta)$ that is expected to be most significant. The peak becomes less symmetric away from $z = t/2$, but the width remains about the same (Figure 3.6 page 49), so it is not too unreasonable to take τ as independent of z. This is done in the simplified calculation and $\tau(\theta)$ is obtained at each iteration by the use of the scattering integral with $u(\theta', z)$ replaced by its average over z, i.e. $\bar{u}(\theta)$.

At each iteration the solution of the following equation is required.

$$v \cos\theta \frac{\partial u(\theta,z)}{\partial z} + \sin\theta = \frac{u(\theta,z)}{\tau(\theta)} \qquad (10.15)$$

An equation of this type was solved in Chapter III (page 47), giving

$$u(\theta,z) = \tau(\theta) \sin\theta (1 - C(\theta) e^{-z/\tau(\theta) v \cos\theta}) \qquad (10.16)$$

The Fuchs' partially specular boundary condition gives

$$C(\theta) = \frac{1 - p}{1 - p e^{-t/\tau(\theta) v \cos\theta}} \qquad (10.17)$$

The average of $u(\theta,z)$ over z is

$$\bar{u}(\theta) = \frac{1}{t}\int_0^t u(\theta,z)\,dz = \tau(\theta)\sin\theta\left(1 - \frac{(1-p)(1-e^{-w})}{w(1-pe^{-w})}\right) \tag{10.18}$$

where $w = t/\tau(\theta)\, v\cos\theta$. Thus, given $\tau(\theta)$, $\bar{u}(\theta)$ is obtained directly from the formula.

The other main stage in each iteration is the calculation of $\tau(\theta)$ from $\bar{u}(\theta)$. From 10.14:

$$\frac{1}{\tau(\theta)} = R_1 - \frac{1}{\bar{u}(\theta)}\int R(\theta,\theta')\,\bar{u}(\theta)\sin\theta' d\theta' \tag{10.19}$$

R_1 and $R(\theta,\theta')$ are independent of $\bar{u}(\theta)$ and can be calculated for a given $Q(\Psi)$ before stating the iteration process.

<u>The scattering function, $Q(\Psi)$.</u>

The shape of the scattering function is obtained from the Debye model of lattice vibration. The mean number of phonons in a particular element of q-space at temperature T is n(q) where

$$n(q) \propto \frac{q\,dq}{e^{\frac{\hbar}{}\, q/ckT} - 1}\,. \tag{10.20}$$

Phonons in element dq scatter electrons into an equal sized element in k-space (Figure 10.5). It is assumed that the probability of an electron being scattered by a phonon in element dq at q is proportional

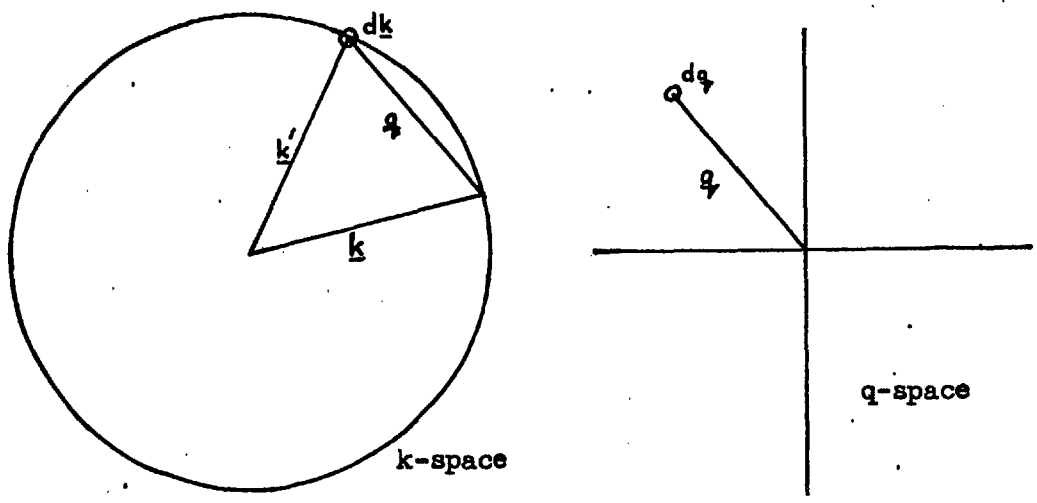

Figure 10.5

to the number of phonons in the element, i.e. to n(q). As q is related to the scattering angle Ψ by $q = 2k_F \sin \Psi/2$, the number of phonons per unit q-space may be expressed in terms of Ψ.

$$n(\Psi) \propto \frac{\sin \Psi/2}{e^x - 1} \qquad (10.21)$$

where $x = \frac{2T_D}{T} \sin \Psi/2$.

This gives the shape of the scattering function and it is necessary to find a scaling constant to give $Q(\Psi)$. The constant is established by the requirement that the $Q(\Psi)$ should give the observed bulk lattice resistivity of silver at the temperature concerned. From page 30:

$$\sigma_{ph} = \frac{ne^2\tau}{m} = \frac{2\pi ne^2}{m} P \int (1-\cos \Psi)\, n(\Psi) \sin \Psi d\Psi \qquad (10.22)$$

where P is the constant.

The residual scattering is assumed to be entirely isotropic and contributes a term to the scattering integral which is independent of $\bar{u}(\theta)$ and can be included in R_1.

The resistivity ratio, ρ_f/ρ_b.

When the iteration process has yielded a solution, i.e. when two consecutive solutions are close enough, the ratio of the film conductivity to the bulk conductivity is calculated.

$$\frac{\sigma_f}{\sigma_b} = \frac{\frac{1}{t} \int g_f(\underline{k}, z)\, d\underline{k}\, dz}{\int g_b(\underline{k})\, d\underline{k}} \qquad (10.23)$$

The factors common to g_f and g_b cancel (cf. page 50) leaving

$$\frac{\sigma_f}{\sigma_b} = \frac{\int \sin^2\theta\ \bar{u}_f(\theta)\, d\theta}{\int \sin^2\theta\ u_b(\theta)\, d\theta} \qquad (10.24)$$

The bulk u, $u_b(\theta)$ is $\tau_b \sin\theta$,

$$\therefore \quad \frac{\rho_f}{\rho_b} = 2\tau_b/3 \int \sin^2\theta\ \bar{u}(\theta)\, d\theta\,. \qquad (10.25)$$

Some program details.

In very thin films $\bar{u}(\theta)$ changes very rapidly at angles close to $\theta = 90^\circ$ and slowly elsewhere. The θ range is, therefore, divided in two. The point of division and the number of intervals in each part of the range are program parameters. The set of θ values are fixed throughout

a calculation, so computing time is saved by obtaining cos θ, sin θ and $R(\theta,\theta')$ once only at the beginning instead of each time they are required. $R(\theta,\theta')$ is calculated for the standard values of θ and for a number of values of θ' on either side of θ. The integrals at all parts of the calculation are by Simpson's rule.

The program steps are summarized below.

1) Parameters read in: T, ρ_o, p, $\rho_{ph}(T)$, θ division point and numbers of intervals for θ ranges.
2) $n(\Psi)$ calculated from formula 10.21.
3) Constant to give $Q(\Psi)$ calculated from $n(\Psi)$ using 10.22 with $\sigma_{ph} = 1/\rho_{ph}(T)$.
4) Cos θ and sin θ for all values of θ.
5) $R(\theta,\theta')$ for each θ value. θ': equally spaced values on either side of θ, the range being determined by the angular spread of $Q(\Psi)$
6) $\bar{u}(\theta)$ from $\tau(\theta)$ by formula 10.18. The change in $\bar{u}(\theta)$ permitted is limited to prevent oscillation.
7) New $\tau(\theta)$ from $\bar{u}(\theta)$ by numerical integration of 10.19.
8) Is the change in $\bar{u}(\theta)$ since previous iteration small?

   No. return to (6)

   Yes. ρ_f/ρ_b from 10.25.

The program was written in Fortran IV and run on the IBM 7090 computer at Imperial College. About 25 secs. were required for each value of ρ_f/ρ_b.

Stability of the iteration process.

The simple version of the iteration process described at first is extremely unstable, giving wildly oscillating values of $\bar{u}(\theta)$ and $\tau(\theta)$. When $\bar{u}(\theta)$ is far removed from a solution the changes in $\tau(\theta)$ obtained are in the right direction but much too large. The oscillations can be controlled by limiting the change in $\bar{u}(\theta)$ allowed at each iteration to some fraction (~ 10%) of its value at the previous iteration. The function $\bar{u}(\theta)$ then changes in a steady manner and a reasonable solution is obtained within 10 - 30 iterations. The solution is judged to be reasonable when the values of $\bar{u}(\theta)$ generated by one iteration are all within 1% of those obtained from the previous iteration. In most cases the difference is much less than 1%. The error in the value of ρ_f/ρ_b is quite small (<0.1%) as many of the errors in $\bar{u}(\theta)$ are cancelled by the integration.

The results.

The change in $\bar{u}(\theta)$ brought about by the change from isotropic to low angle scattering is, as expected, a smoothing out of the peak at $\theta = 90^\circ$ (Figure 10.6). The reciprocal of the relaxation time is also shown. This is proportional to the rate of scattering out of an element in $\underline{k}$-space, so the negative regions imply a net gain by scattering. These regions receive the electrons scattered out of the peak and they lose electrons only by surface scattering.

The program was run for various values of K, T and p. The results are given in Table 10.1 with the Fuchs' values for

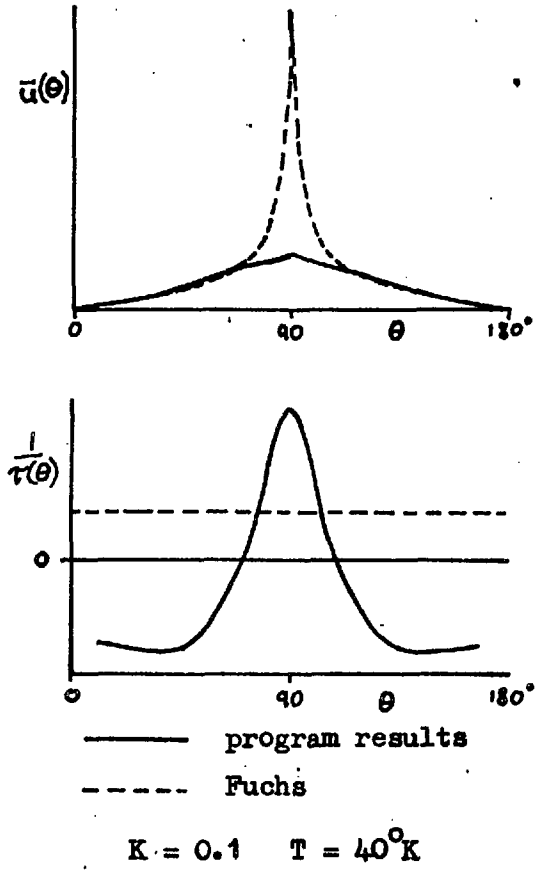

comparison. The residual resistivity in all cases is 0.01 μ Ω-cm, i.e. roughly the value found for the experimental films.

Figure 10.6

The results for each value of K may be plotted as the change in ρ_f/ρ_b brought about by the change from isotropic scattering to low angle scattering, i.e. the difference between the program results and Fuchs' results. The result for K = 0.1 are plotted in Figure 10.7. The results up to about 60°K seem quite reasonable. At very low temperatures the residual isotropic scattering is most important and Fuchs' results hold. As the temperature and number of phonons increases the phonon-surface effect

p	$T^{\circ}K$	K(=t/l)				
		0.01	0.03	0.1	0.3	1.0
0	(Fuchs)	26.1	11.24	4.781	2.466	1.462
	100	33.22	14.46	5.996	2.884	1.549
	60	33.90	14.73	6.062	2.896	1.549
	40	36.48	15.61	6.287	2.941	1.559
	25	37.77	15.80	6.207	2.886	1.536
	20	36.42	15.15	5.950	2.893	1.517
	15	30.4	13.7	5.454	2.630	1.465
0.4	(Fuchs)	13.98	6.412	3.030	1.791	1.253
	100	17.9	8.02	3.538	1.932	1.280
	60	18.3	8.12	8.553	1.932	1.278
	40	19.4	8.43	3.613	1.940	1.280
	25	19.6	8.38	3.550	1.906	1.260
	20	18.9	8.03	3.433	1.886	1.261
	15	16.9	7.33	3.235	1.822	1.235
0.8	(Fuchs)	5.46	2.855	1.673	1.250	
	100	6.78	8.29	1.772	1.275	
	60	6.84	3.30	1.770	1.2717	
	40	7.08	3.34	1.774	1.2647	
	25	6.97	3.31	1.748	1.244	
	20	6.78	3.19	1.702	1.245	
	15	6.09	2.97	1.658	1.222	

Table 10.1.

Phonon-surface effect.

Program results - ρ_f/ρ_b

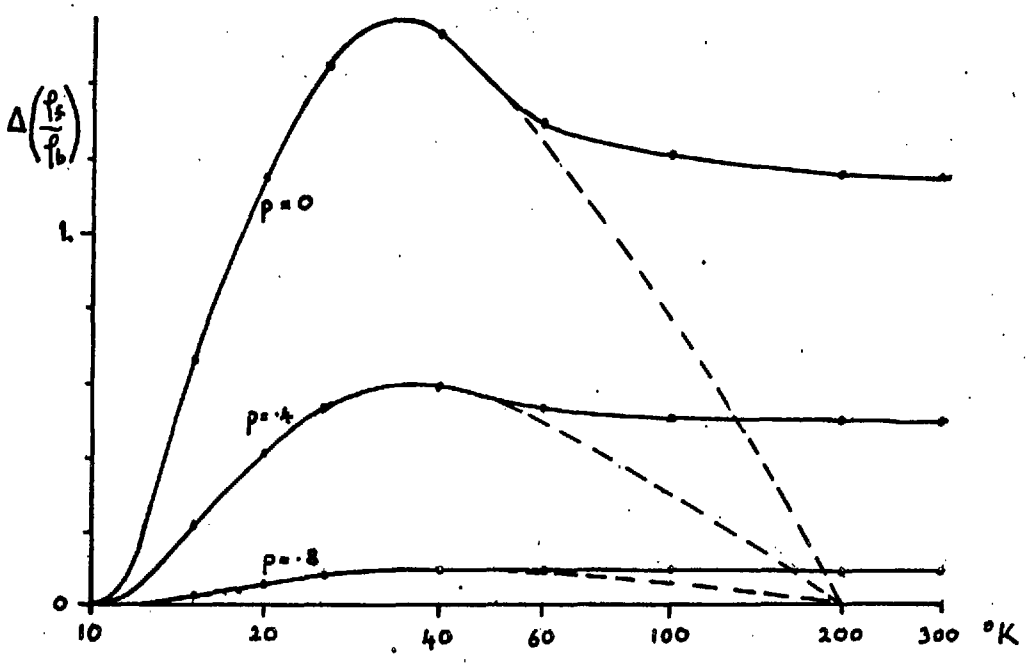

Figure 10.7 $\Delta\left(\frac{\rho_f}{\rho_b}\right)$ vs. temperature when K=0.1

becomes more important. At higher temperatures, when the scattering angles increase, the effect begins to decrease, but it does not fall to zero at high temperatures. This is a consequence of the Debye phonon model, which limits the maximum angle of scatter to about 79°. As the scattering is expected to be isotropic at high temperatures (page 183), it is more realistic to assume that $\Delta(\rho_f/\rho_b)$ is zero above about 200°K (the Debye temperature for silver) and that the curves have the forms indicated roughly by the broken lines.

Comparison with Azbel and Gurzhi.

A few of the results from the program are compared in Table 10.2 with results from the formula obtained by Azbel and Gurzhi. The agreement is quite good, especially at 40°K. This is perhaps because the principle result of both methods is to smooth out the peak in

	ρ_f/ρ_b				
K	Fuchs	T = 20°K		T = 40°K	
		A and G	V	A and G	V
0.01	26.1	42.0	36.4	38.5	36.5
0.03	11.24	18.1	15.1	15.7	15.6
0.1	4.78	7.49	5.95	6.49	6.27

Table 10.2

$g(\theta)$ and leave the rest of the Fermi sphere relatively unchanged.

Comparison with the experimental results.

To be useful for comparison with the experimental result the phonon-surface effect results needs to be expressed as the change in resistivity vs. temperature for films of various thickness. In this form they will then be directly comparable with the $\Delta\rho$ curves obtained near the end of Chapter VIII, i.e. the differences between the measured resistivities and the resistivities expected on the basis of Fuchs' theory.

Films of thicknesses 1000, 2000 and 5000Å are taken as examples. The program results above 60°K are modified as in Figure 10.7 to be in agreement with the assumption of isotropic scattering a high temperatures. $\Delta(\rho_f/\rho_b)$ is plotted against K for each temperature. The values of K

for the three films at each temperature are calculated from $\rho_b(T)$ and the thicknesses, and the appropriate values of $\Delta(\rho_i/\rho_b)$ obtained from the curves. The increase in resistivity for the film is then $\rho_b \Delta(\rho_f/\rho_b)$.

The final results are plotted in Figure 10.8 as $\Delta\rho$ vs. T for the three films and for three values of p: 0, 0.4 and 0.8. When p=0 the phonon surface effect is very large but falls rapidly as p is increased (Figure 10.9).

There are several specimens among the experimental films which have thicknesses about 2000Å and with p about 0.4 - 0.6. The maximum at about 40°K, predicted by the calculation, for such films should be clearly seen in the experimental results. There is no convincing indication of the effect in the results, in fact the deviation from Fuchs' theory is usually negative (Figure 8.25).

Chopra[42] obtained silver film resistance results which he attributed to the phonon surface effect (page 164). The films concerned were very thick, 60,000Å, and had residual resistivity ratios which indicate a bulk residual resistivity ~ 0.01 μ Ω-cm. The results obtained from the program do not support the conclusion that the rapid rise in resistance at about 10°K can be explained by the phonon surface effects. The phonon-surface effect is small in films 5000Å thick, and would be very small in much thicker films.

Conclusion.

The theoretical calculation of the phonon surface effect shows that it should be large enough to be observed in the films measured in the

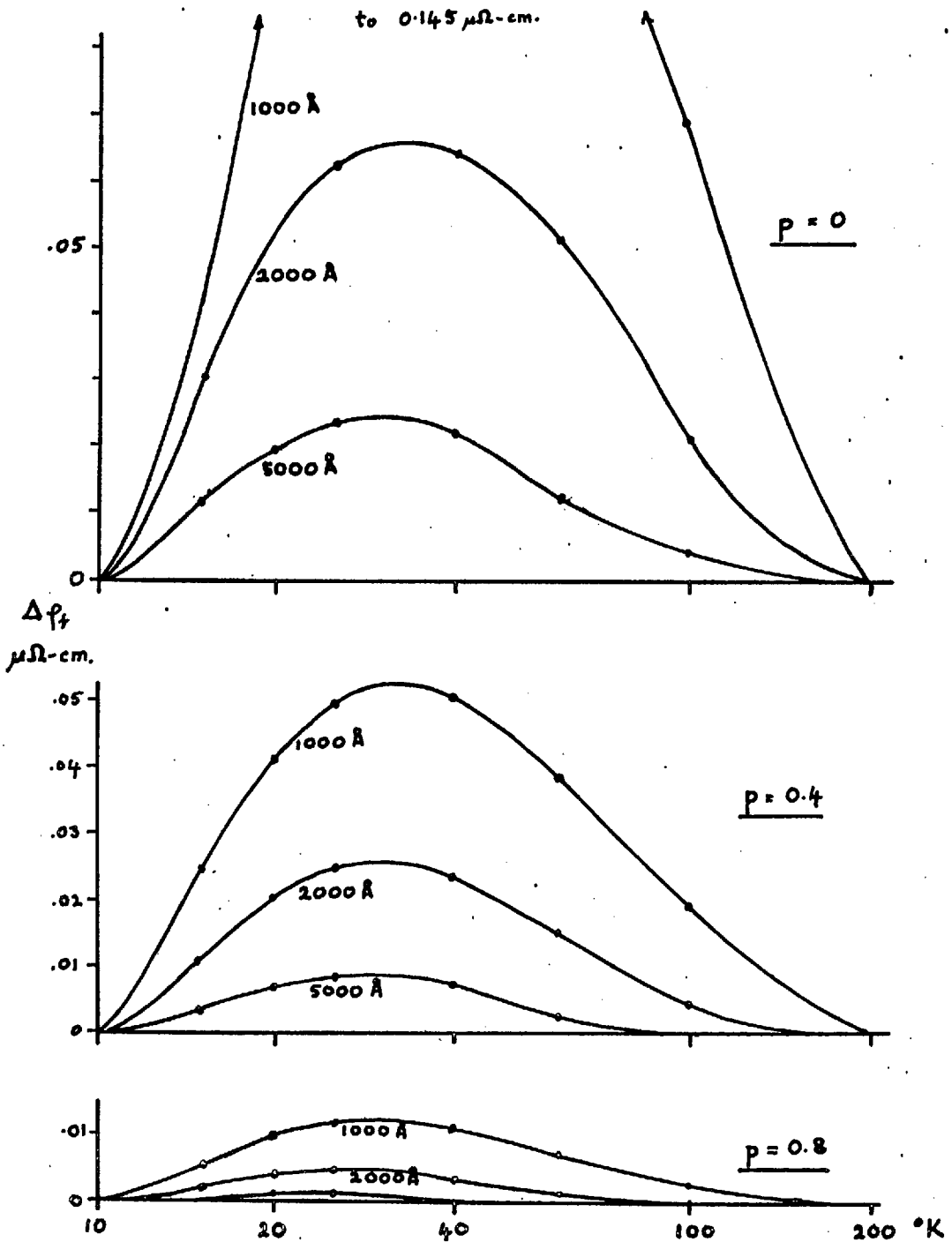

Figure 10.8. Calculated $\Delta\rho_f$ vs. T curves.

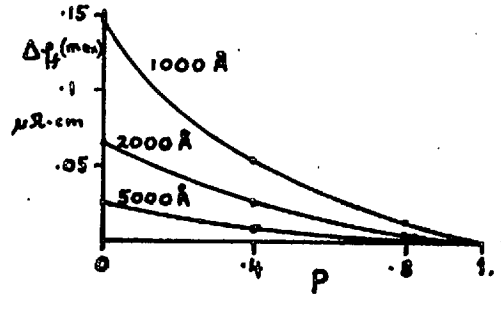

Figure 10.9

$\Delta\rho_f$ (max.) vs. p

experimental part. The effect was not observed.

The solution of the Boltzmann equation was obtained by an approximate method that assumed τ to depend on θ but not on z. However, it seems unlikely that this approximation would cause large errors in the results. The program could be developed to include variations of τ with z, but it would not be worthwhile without more positive experimental indication of the phonon surface effect.

A more serious error might have been the omission of Umklapp processes, which allow phonons of small q to induce effectively large angle scatterings. The inclusion of Umklapp processes would be a necessary first step in any refinement of the theory of the phonon surface effect.

CONCLUDING REMARKS

The work reported in this thesis has provided a picture of the electrical resistivity properties of epitaxial films of silver. From this a direction for future work could be decided.

The results have been interpreted mainly in terms of Fuchs' theory, and two principle difficulties have arisen:

1) The variable film structure. This was shown by the variation in resistivity between films of the same thickness, and confirmed by the electron microscope work of C. Gonzales. This type of variation was partially overcome by the use of sets of four specimens evaporated together. In addition to the variation between specimens of the same thickness, there appears to be a tendency for the thinner films to have holes in them.

2) Dislocation resistivity. The temperature dependent resistivity of the dislocations in the films complicates the comparison of results with theory at intermediate temperatures. This effect was reduced to a single parameter by comparison with partially annealed wire, and very thick films, which yielded a 'universal curve'. However, it is impossible to be sure that the universal curve used is completely appropriate for the dislocation configuration in the films.

In spite of these difficulties the comparison of the results, for individual films, with Fuchs' theory resulted in agreement, within a few per cent, down to ~ 50^{o}K, i.e. covering a range of K(=t/l) from ~5 to ~1/5. There was no definite evidence of large deviations from Fuchs' theory. In particular there was no sign of the phonon surface

effect, either as described by Chopra, or as calculated in Chapter X. The calculations ignore Umklapp processes and the phonon surface effect would be less if these were important, so the absence of the effect may indicate that Umklapp processes make an important contribution to the resistivity at quite low temperatures.

Further work in this field would have to be initially directed at the preparation of films with reproducible properties. An ultra high vacuum system would be required, not necessarily because a high vacuum is needed, but in order to be able to control the composition of the residual gas. A method of cleaving the substrate in a controlled atmosphere would probably also be necessary. The object would be to find the factors causing variable film structure by the use of both resistance measurements and electron microscope observations.

If films of different thicknesses could be prepared with constant structure, the bulk residual resistivity could be accurately estimated, and the dislocation contribution might be more directly obtainable. It may well, however, be rather difficult to achieve a structure independent of thickness, as each new layer has the previous layer as a substrate, so any changes are cumulative.

APPENDIX I

A Solution of the Boltzman equation for the bulk case when Q is a function of Ψ and k only.

It will be shown that the solution has the same form as in the simpler bulk case considered in Chapter I, page 28. The solution is assumed to be of the form $G(k)\cos\theta$. This leads to a scattering term proportional to $G(k)\cos\theta$ and an expression for the relaxation time $\tau(k)$.

$$\dot{g}\Big]_s = \int (G(k)\cos\theta - G(k')\cos\theta')\, Q(\Psi,k)\,\delta(k-k')$$

$$k'^2 \sin\theta'\, d\theta'\, d\phi'$$

$$= G(k)\, k'^2 \int (\cos\theta - \cos\theta') \qquad (A1.1)$$

$$Q(\Psi,k)\sin\theta'\, d\theta'\, d\phi'$$

The integral is over the whole of the Fermi surface, so the same result is obtained if the polar axis is changed to OA (Figure A1.1) and the integration taken over Ψ and φ. i.e.:

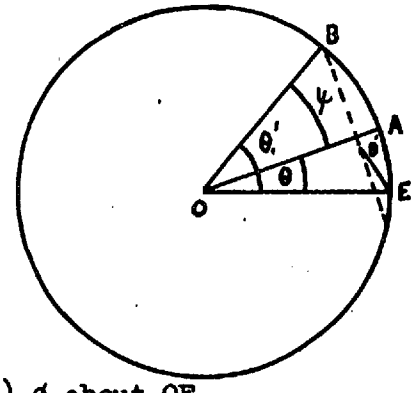

(a) φ about OE

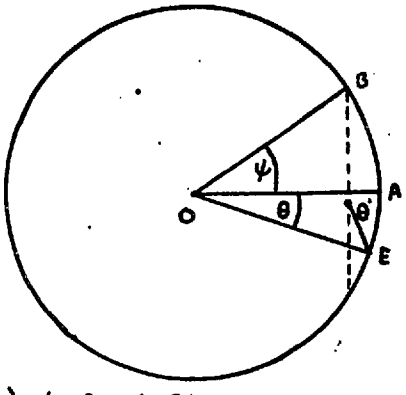

(b) φ about OA

Figure A1.1

$$\dot{g}\Big]_s = G(k)\, k^2 \int (\cos\theta - \cos\theta')\, Q(\Psi,k) \sin\Psi \; d\Psi \, d\phi \qquad (A1.2)$$

θ' must be expressed in terms of Ψ and θ,

$$\cos\theta' = \cos\theta \cos\Psi - \cos\phi \sin\theta \sin\Psi, \qquad (A1.3)$$

(by use of spherical trigonometry formulae). The integral now becomes:

$$\int (\cos\theta - \cos\phi \sin\Psi \sin\theta - \cos\Psi \cos\theta)\, Q(\Psi) \sin\Psi \, d\Psi \, d\phi$$

$$= \cos\theta \int (1-\cos\Psi)\, Q(\Psi) \sin\Psi \, d\Psi \, d\phi - \int d\Psi \sin^2\Psi \sin\theta \int d\phi \cos\phi \qquad (A1.4)$$

$\int_0^{2\pi} \cos\phi \, d\phi = 0$ so the second term is zero.

The scattering term is now:

$$\dot{g}\Big]_s = 2\pi k\, G(k) \cos\theta_o \int (1 - \cos\Psi)\, Q(\Psi) \sin\Psi \, d\Psi$$

$$= G(k) \cos\theta / \tau(k) \qquad (A1.5)$$

where $\tau(k) = 1/2\pi k^2 \int (1-\cos\Psi)\, Q(\Psi) \sin\Psi \, d\Psi \qquad (A1.6)$

With the scattering term reduced to the form in A1.5 the Boltzman equation solution is (from equation 2.29 page 28)

$$G(k) \cos\theta = \frac{Ee}{h} \tau(k) \frac{df_o(k)}{dk} \cos\theta, \qquad (A1.7)$$

confirming that the solution is of the form assumed.

APPENDIX II

The Temperature Controller.

The temperature controller is based on a silicon control rectifier (SCR). The SCR is a diode which will not conduct in the forward direction until a pulse has been applied to a gate electrode. When there is an alternating voltage across the SCR a pulse must be applied to the gate during each forward half cycle. (Figure A2.1) The average current through the SCR depends on the phase relationship between the gating pulses and the supply voltage, so the small gating pulses control the large currents which the SCR can carry.

The control circuit (Figure A2.2) varies the phase of the gating pulse in response to the output of the Wheatstone bridge circuit. The DC output from the bridge in first amplified by a long tailed pair amplifier (low drift) then by a conventional 2 stage DC amplifier. The DC level at X (Figure A2.2) depends, therefore, on the bridge output. It is made the zero point for an AC input to a Schmidt trigger. This AC is mains frequency but 90° out of phase with the main supply to the SCR. The Schmidt trigger fires (transistor A turned off, B turned on) when the input voltage at Y becomes sufficiently positive. The time at which this happens depends on the DC level at X (Figure A2.3). The gate pulse for the SCR is derived from the collector of B by the CR circuit following.

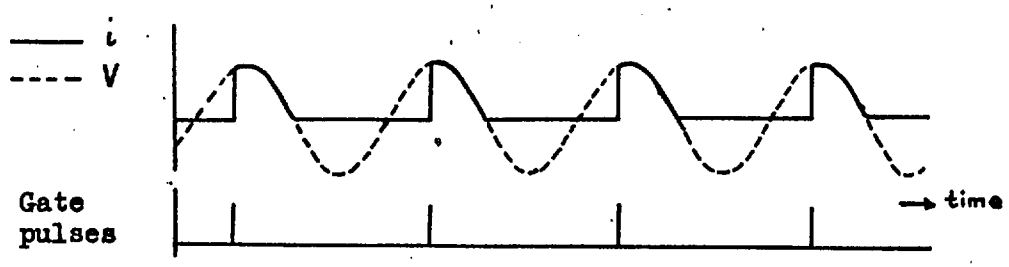

Figure A2.1 Current through SCR.

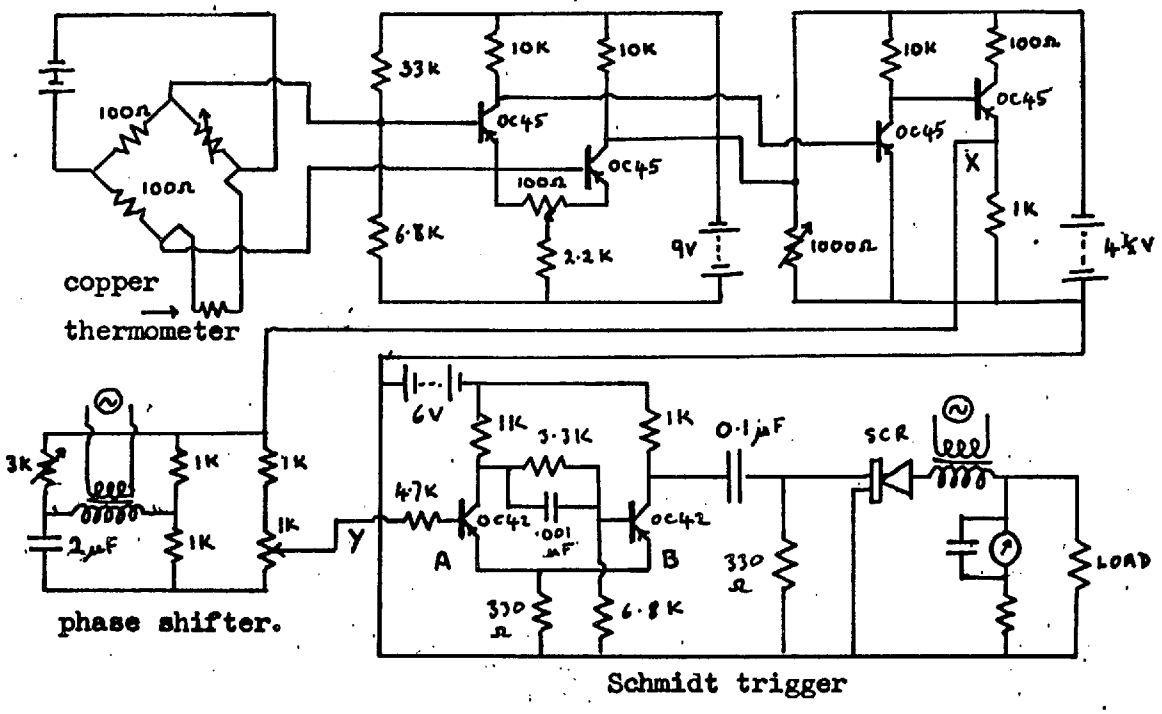

Figure A2.2 Temperature controller circuit diagram.

Figure A2.3

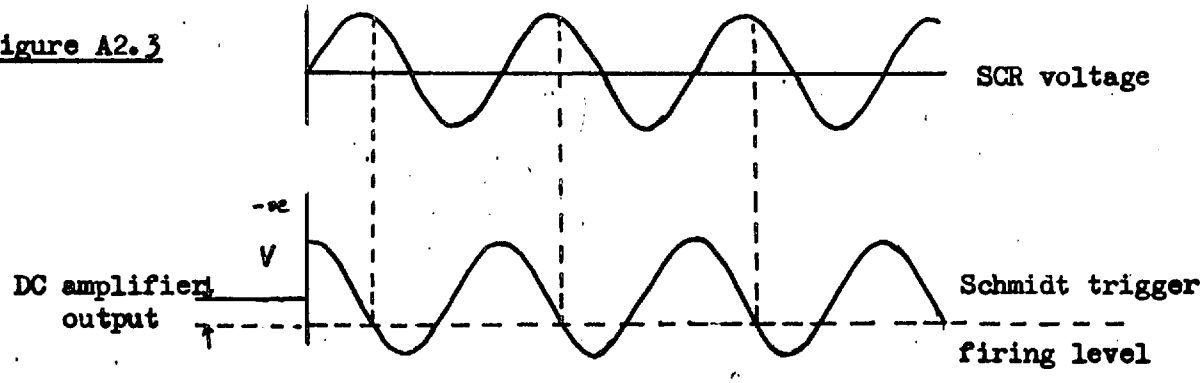

APPENDIX III

The Comparison Program

The aim of this program is to fit the resistance result to Fuchs' theory using the fitting program results (page 126) as a starting point. The input data for each specimen are as follows.

1) $\rho(T)$ from the fitting program with the constants C and ρ_c.
2) $u(T)$ - the points from the universal curve for the dislocation contributions (page 153).
3) The scaling constant for $u(T)$. (D)
4) The residual bulk resistivity (ρ_o).
5) The specimens length width ratio (d/w).

The first stage of the program makes use of only the high temperature results, i.e. those used in the fitting program. Initial values for the specularity coefficient p and the thickness t are obtained from C, d/w, D and ρ_o (pages 128 and 158). At each temperature K is obtained from the total bulk resistivity, and the film resistivity expected from Fuchs' theory obtained (ρ_{th}). It is required that $\rho_f - \rho_{th}$ should be zero at all temperatures. Considered graphically $\rho_f - \rho_{th}$ may appear as in Figure A3.1. The change in C required makes AB horizontal i.e. to A'B'. The distance between A'B' and zero is taken up by changing ρ_c.

$$\Delta C = \frac{x_2 - x_1}{\rho_2 - \rho_1}$$

$$\Delta\rho_c = x_2 - \Delta C\, \rho_2$$

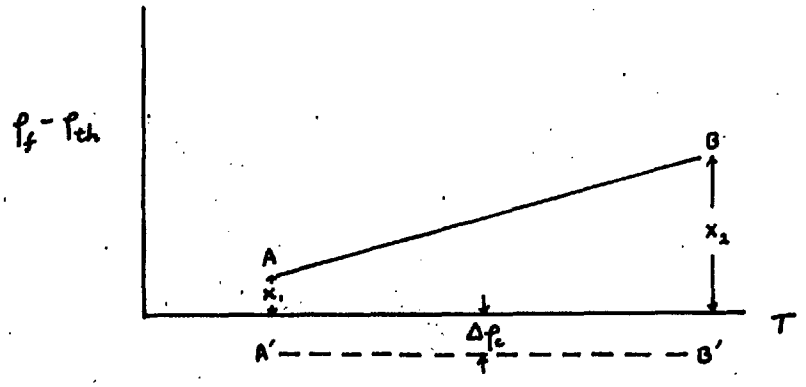

Figure A3.1

The change in ρ_c involves a change of p so the processes must be repeated. The process rapidly converges and two iterations are usually quite sufficient.

The program frequently requires the value of F(K,p). The evaluation of this each time would be very time consuming on the Elliott 803 computer. Tables of F(K,p) obtained by another program (page 54) were included in this program, and particular values are obtained by interpolation.

The final values obtained for C and ρ_c are used to calculate ρ_f and ρ_{th} for all temperature points.

APPENDIX IV

Experimental Results.

Some of the principle results for each specimen are given below, as analysed by the fitting program.

Epitaxial silver films.

Specimen no.	Thickness Å	$\rho_f(4.2)$ μ Ω -cm	ρ_c μ Ω-cm	p(min)
18.1	420	.4601	.501	.33
.2	829	.2412	.288	.25
.3	1004	.1878	.213	.33
.4	1120	.1793	.187	.34
20.1	572	.3134	.327	.41
.2	560	.3617	.362	.36
21.1	525	.3700	.4251	.30
22.1	813	.2564	.3029	.22
.2	910	.2137	.2575	.26
.3	1470	.0784	.1236	.43
.4	1860	.0643	.1024	.40
23.2	635	.3183	.3639	.27
.3	1070	.1207	.1752	.41
26.1	2580	.0398	.0741	.40
.2	2750	.0359	.0689	.40
.3	2970	.0340	.0658	.38
.4	3130	.0392	.0696	.31
27.1	1193	.0949	.1534	.42
.2	893	.1985	.2799	.21
.3	644	.2918	.3833	.22
.4	546	.3719	.4616	.21

continued

no.	t	ρ_f(4.2°K)	ρ_c	p(min)
28.1	2065	.0568	.0952	.38
.2	2550	.0442	.0740	.41
.3	2910	.0402	.0698	.36
31.1	2500	.0978	.1284	-.01
.2	1720	.1138	.1495	.19
.3	1335	.1511	.1937	.18
.4	789	.2417	.3103	.23
33.1	2110	.0651	.1024	.32
.2	1235	.1224	.1716	.33
37.3	1391	.0600	.1073	.53
39.1	596	.2833	.3238	.39
.2	916	.1722	.2021	.41
.3	3005	.0353	.0573	.46
.4	4170	.0309	.0508	.33
48.1	4220	.0400	.0582	.23
.2	5080	.0357	.0505	.19
.3	6100	.0338	.0479	.08
.4	6330	.0395	.0574	-.15
49.1	4020	.0460	.0639	.19
.2	3200	.0591	.0803	.19
.3	2310	.0669	.0963	.30
.4	1340	.1061	.1081	.54
52.1	40800	.0190	.0336	-
.2	43400	.0198	.0328	-
.3	41600	.0208	.0343	-
.4	31800	.0201	.0339	-
54.1	63700	.0151	.0574	-
.2	64500	.0123	.0233	-
57.1	5493	.0206	.0358	.38
.2	3864	.0230	.0446	.46
.3	2407	.0348	.0738	.44
.4	1666	.0535	.1135	.40

continued

no.	t	ρ_f(4.2°K)	ρ_c	p(min)
59.3	4920	.0235	.0458	.29
61.1	1920	.0419	.0923	.44
.2	2730	.0340	.0736	.37
.3	3710	.0266	.0567	.34
63.1	2410	.0795	.1316	.0
.2	2570	.0825	.1294	-.04
.3	3670	.0525	.0897	-.03
.4	4270	.0428	.0755	-.03
65.3	781	.2932	.3411	.16
67.1	2620	.0515	.0848	.30
.2	1750	.0783	.1178	.35
.3	1470	.1247	.1638	.25
.4	1200	.2318	.2868	-.09
69.1	3220	.0461	.0860	.13
.2	1455	.0816	.1416	.35
.3	1020	.1107	.1878	.40
71.1	1645	.0717	.1275	.34
.2	1570	.0702	.1286	.36
.3	1255	.0877	.1569	.38
.4	957	.1209	.2149	.35

Epitaxial silver films with thin aluminium layers.

no.	t	ρ_f(4.2°K)	ρ_c	p (min)
42.2	2810	.0746	.1201	-.07
.3	3260	.0646	.1044	-.07
.4	3460	.0524	.0876	.04
43.1	2190	.0761	.1327	.07
.2	1770	.1384	.1941	-.08
.3	1365	.1914	.2426	-.04
.4	977	.2782	.3412	-.05

continued

no.	t	ρ_f(4.2°K)	ρ_c	p(min)
50.1	4490	.0484	.0793	-.12
.2	5200	.0410	.0666	-.09
.3	5690	.0401	.0631	-.13
.4	5950	.0395	.0652	-.22
51.1	3100	.0746	.1182	-.16
.2	2230	.0924	.1591	-.12
.3	1709	.1255	.2102	-.13
53.2	34000	.0239	.0396	-
.3	35400	.0245	.0390	-
55.1	15140	.0258	.0372	-
.2	17030	.0228	.0325	-
.3	16950	.0207	.0307	-
.4	14300	.0262	.0390	-
56.1	1582	.0834	.1419	.29
.2	2343	.0567	.1007	.25
.3	2790	.0335	.0616	.26
58.1	3330	.0542	.0921	.03
.2	4780	.0374	.0662	.00
.3	7435	.0262	.0476	-.12
.4	9908	.0221	.0387	-.22
60.2	3630	.0375	.0683	.22
.3	2580	.0430	.0836	.32
.4	1810	.0701	.1296	.25
62.1	4256	.0464	.0786	-.03
.2	3640	.0570	.0929	-.06
.3	2590	.0870	.1313	-.07
.4	2420	.0911	.1387	-.06
64.2	599	.5049	.5310	.00
.3	1880	.1353	.1926	-.14
.4	3380	.0921	.1355	-.43
66.1	1135	.2529	.3020	-.08
.2	1235	.2408	.2767	-.07
.3	1560	.1583	.2078	-.02
.4	2460	.0658	.1134	.12

Epitaxial silver films with cold substrate layers

no.	t	ρ_f(4.2°K)	ρ_c	p(min)
36.1	4270	.0452	.0701	.05
.2	1540	.0871	.1462	.29
.3	887	.2828	.3429	.04
38.1	4460	.0398	.0628	.12
.2	3250	.0424	.0658	.33
.3	1208	.1237	.1807	.31
.4	784	.2980	.3453	.15
68.1	740	.2119	.3173	.26
.2	1200	.1060	.1832	.31
.3	1850	.0715	.1295	.25
.4	3420	.0412	.0731	.21
70.1	1275	.1580	.2476	.01
.2	1600	.1129	.1927	.03
.3	1965	.0941	.1575	.02
.4	2000	.0970	.1585	.00

Silver films evaporated on to mica at room temperature.

no.	t	ρ_f(4.2°K)	ρ_c	p(min)
44.3	2300	.509	.642	-
.4	2950	.472	.595	-
45.1	2020	.447	.536	-
.2	1320	.503	.596	-
.3	936	.565	.665	-
.4	706	.604	.682	-

REFERENCES

1. Ziman, J.M. Electrons and Phonons. (Oxford 1960).

2. Mott, N.E. and Jones, H. The Theory and Properties of Metals and Alloys. (Oxford, 1936).

3. Kittel, C. Introduction to Solid State Physics (Wiley, 1956).

4. Pippard, A.B. Rep. Prog. Phys. 23 176 (1960).

5. Shoenberg, D. Phil. Mag. 5 105 (1960).

6. Olsen, J.L. Electrons in Metals. (Wiley 1962).

7. Dekker, A.J. Solid State Physics (Macmillan 1960).

8. Thomson, J.J. Proc. Camb. Phil. Soc. 11 120 (1901).

9. Nordheim, L. Sci. et. Ind. No.133 (Paris 1934).

10. Lovell, A.C.B. Proc. Roy. Soc. A157 311 (1936).

11. Fuchs, K. Proc. Camb. Phil. Soc. 34 100 (1938).

12. Chambers, R.G. Proc. Roy. Soc. A202 378 (1950).

13. Sondheimer, E.H. Adv. in Phys. 1 1 (1952).

14. Mayer, H. Structure and Properties of Thin Films. (New York conference proceedings. Eds. C.A. Neugebauer, J.B. Newkirk and D.A. Vermilyea.) (Wiley 1959).

15. Dingle, R.B. Proc. Roy. Soc. A201 545 (1950).

16. Andrew, E.R. Proc. Phys. Soc. A62 77 (1949).

17. Holland, L. Vacuum Deposition of Thin Films (Wiley 1961).

18. Neugebauer, C.A. Physics of Thin Films II p.1 (1964).

19. Pashley, D.W. Adv. in Phys. 5 173 (1956).

20. Pinsker, Z.G. Electron Diffraction. (Butterworths 1953).

21. Bassett, G.A. Menter, J.W. and Pashley, D.W. New York conference proceedings (ref. 14). (1959).

22. Thun, R.E. Physics of Thin Films I. 187 (1963).

23. Haine, M.E. and Cosslett, V.F. The Electron Microscope. (Spon 1961).

24. Pashley, D.W., Stowell, M.J., Jacobs, M.H., and Law, T.J. Phil. Mag. 10 127 (1964).

25. Pashley, D.W. Advances in Physics 14 327 (1965).

26. Newman, R.C. Phil. Mag. 2 750 (1959).

27. Kehoe, R.B. Phil. Mag. 2 445 (1957).

28. Grunbaum, E. Proc. Phys. Soc. 72 459 (1958).

29. Matthews, J.W. Phil. Mag. 4 1017 (1959).

30. Bailey, J.E. Phil. Mag. 5 833 (1960).

31. Phillips, V.A. Phil. Mag. 5. 571 (1960).

32. Gonzales, C. (Imperial College, London) Private Communication (1965).

33. Appleyard, E.T.S. and Lovell, A.C.B. Proc. Roy. Soc. A158 , 718 (1937).

34. Macdonald, D.K.C. Handb. d. Phys. 14 137 (1956).

35. Chopra, K.L., Bobb, L.C. and Francombe, M.H. J. App. Phys. 34 1699 (1963).

36. Ennos, A.E. Br. J. App. Phys. 8 113 (1957).

37. Reynolds, F.W. and Stillwell, A.R. Phys. Rev. 88 418 (1952).

38. Gillham, E.J. and Preston J.S., Proc. Phys. Soc. B65 649 (1952).

39. Gillham, E.J., Preston, J.S. and Williams, B.J. Phil. Mag. 46 1051 (1955).

40. Bazinski, Z.S., Dugdale, J.S, and Howie, A. Phil. Mag. 8 1989 (1964).

41. Chopra, K.L. and Bobb, L.C. Acta Metallurgica 12 807 (1964).

42. Chopra, K.L. Physics Letters 15 21 (1965).

43. Lucas, M.S.P. App. Phys. Letters 4 73 (1964).

44. Larson, D.C. and Boiko, B.T. App. Phys. Lett. 5 115 (1964).

45. Olsen, J.L. Helv. Phys. Acta 31 713 (1958).

46. Newman, R.C. and Pashley D.W. Phil. Mag. 46 927 (1955).

47. Pashley, D.W., Phil. Mag. 4 316 (1959).

48. White, G.K. Experimental Techniques in Low Temperature Physics. (Oxford 1959).

49. Tolansky, S. Multiple Beam Interferometry of Surfaces and Films (Oxford 1949).

50. Alley, P. and Serin, B. Phys. Rev. 116 334 (1960).

51. Margenau, H. and Murphy, G.M. The Mathematics of Physics and Chemistry. (Van Nostrand, 1956).

52. White, G.K. and Woods, S.B. Phil. Trans. Roy. Soc. A251 273 (1959).

53. Azbel, M. Ya. and Gurzhi, R.N. Soviet Physics JETP 15 1133 (1962).

54. Blatt, F.J. Solid State Physics 4 199 (1957).

55. Crittenden, E.C. and Hoffman, R.W. Rev. Mod. Phys. 25 310 (1953).

56. Blatt F.J. and Satz, H.G. Helva. Phys. Acta 33 1007 (1960).

57. Luthi, B. and Wyder, P. Helv. Phys. Acta. 33 667 (1960).

58. Ittner, W.B. Physics of Thin Films I. 233 (1963).

59. Wolter, A.R. J. App. Phys. 8 2377 (1965).

60. Keesom, P.H. and Pearlman, N. Handb. d. Phys. 14 282 (1956).

61. Ditchburn, R.W. Light. (Blackie 1963).